CODING SCHEMES FOR ENERGY HARVESTING AND MULTI-USER COMMUNICATIONS

A DISSERTATION SUBMITTED TO

THE GRADUATE SCHOOL OF ENGINEERING AND SCIENCE

OF BILKENT UNIVERSITY

IN PARTIAL FULFILLMENT OF THE REQUIREMENTS FOR

THE DEGREE OF

DOCTOR OF PHILOSOPHY

IN

ELECTRICAL AND ELECTRONICS ENGINEERING

By

Mehdi Dabirnia

December 2017

Coding Schemes for Energy Harvesting and Multi-User Communications
By Mehdi Dabirnia
December 2017

We certify that we have read this dissertation and that in our opinion it is fully adequate, in scope and in quality, as a dissertation for the degree of Doctor of Philosophy.

Tolga Mete Duman (Advisor)

Erdal Arıkan

Sinan Gezici

Ali Özgür Yılmaz

Ayşe Melda Yüksel Turgut

Approved for the Graduate School of Engineering and Science:

Ezhan Karaşan
Director of the Graduate School

ABSTRACT

CODING SCHEMES FOR ENERGY HARVESTING AND MULTI-USER COMMUNICATIONS

Mehdi Dabirnia
Ph.D. in Electrical and Electronics Engineering
Advisor: Tolga Mete Duman
December 2017

Many wireless communication and networking applications can benefit from energy harvesting and wireless energy transfer including wireless sensor networks, radio frequency identification systems and wireless body networks. Some of the advantages that energy harvesting provides for such applications include energy self-sufficiency, ability to implement them in hard-to-reach places, reducing the required battery size or even removing the battery completely from the wireless units. In such systems the required energy for the system operation is obtained from a renewable energy source such as solar, thermal or kinetic energy or from a man-made source such as radio frequency (RF) signals, artificial light, etc. While there has been decades of designs and developments of energy harvesting nodes from circuit and device engineering perspectives, only recent studies consider the specific constraints of these systems from a communications point of view, and significant challenges and problems still remain unsolved, particularly, at the physical layer.

With the motivation of addressing some of the above challenges, our main focus in this thesis is the design and analysis of capacity approaching coding schemes for several energy harvesting and multiuser scenarios; in particular, by exploiting nonlinear codes concatenated with low-density parity-check (LDPC) codes for these scenarios. First, novel code design approaches are studied for the joint energy and information transfer specifically, employment of nonlinear trellis codes (NLTCs) in serial concatenation with outer LDPC codes is proposed, and an algorithm is developed to design the NLTCs prior to optimizing the outer LDPC code using the EXIT analysis. The designed codes are shown to improve upon the off-the-shelf point-to-point (P2P) codes and outperform the alternative of utilizing linear codes with time switching and the reference scheme of concatenating LDPC codes with nonlinear memoryless mappers (NLMMs). This coding approach is then examined for the energy harvesting channel (EHC) implementing two decoding approaches at the receiver side wherein the first one ignores the

memory in the battery state, while the second one incorporates this memory into the trellis. Compared with the P2P codes and the reference schemes, the newly designed codes consistently offer better performance. This code design approach is explored for the case of discrete memoryless interference channels (DMICs) implementing the Han-Kobayashi (HK) encoding and decoding strategy as well. A stability condition is derived for the concatenated coding scheme and it is utilized in the process of designing the outer LDPC code employing the EXIT analysis. It is demonstrated that the designed codes achieve rate pairs close to the optimal boundary of the HK subregion and outperform the single user codes with time sharing. Furthermore, code design principles are also investigated for the two-user Gaussian interference channel with fading employing trellis-based codes with short block lengths. Finally, the problem of designing explicit and implementable codes is studied for a two-user interference channel with energy harvesting transmitters, and a design framework is proposed employing similar techniques developed for the DMIC and EHC.

Keywords: Energy harvesting communications, joint energy and information transfer, interference channel, channels with memory, nonlinear trellis codes, low-density parity-check codes, serially concatenated codes, stability condition.

ÖZET

ENERJİ HASADI YAPILAN VE ÇOK-KULLANICILI HABERLEŞME SİSTEMLERİ İÇİN KODLAMA YÖNTEMLERİ

Mehdi Dabirnia
Elektrik ve Elektronik Mühendisliği, Doktora
Tez Danışmanı: Tolga Mete Duman
Aralık 2017

Kablosuz sensör ağları, radyo frekans tanımlama sistemleri ve kablosuz beden ağları dahil olmak üzere birçok kablosuz iletişim ve ağ uygulaması enerji hasadı ve kablosuz enerji transferinden yararlanabilir. Enerji hasadının bu tip uygulamalara getirileri arasında, enerji bakımından kendine yeterlilik, erişimi zor yerlerde kullanım olanağı, daha küçük batarya ile ve hatta bataryasız çalışabilen kablosuz birimler sayılabilir. Böyle sistemler, çalışmak için gerekli enerjiyi güneş, termal ya da kinetik enerji gibi yenilenebilir bir enerji kaynağından veya radyo frekansı sinyalleri, yapay ışık vb. gibi insan yapımı bir kaynaktan elde ederler. Enerji hasadı yapılan ağlarla ilgili devre ve cihaz mühendisliği bakımından uzun süredir tasarım ve geliştirmeler yapılıyor olsa da, bu sistemlerin iletişim açısından belirli kısıtlamalarını ele alan çalışmalar ancak son zamanlarda yapılmaya başlanmıştır. Özellikle fiziksel katmanda olmak üzere, önemli zorluklar ve sorunlar aşılmayı beklemektedir.

Yukarıdaki zorlukların bazılarıyla mücadele etme isteğiyle, bu tezdeki amacımız enerji hasatlı ve çok-kullanıcılı senaryolar için kapasiteye yaklaşan kodlama şemalarının tasarımı ve analizidir. Bu senaryolar için düşük yoğunluklu parite kontrol (LDPC) kodlarıyla sıralanmış doğrusal olmayan kodlardan yararlanılmıştır. Öncelikle, ortak enerji ve bilgi transferi için özel olarak yeni kod tasarım yaklaşımları çalışılmış, dış LDPC kodlarıyla seri sıralanmış doğrusal olmayan kafes kodlayıcı (NLTC) kullanımı sunulmuş ve dış LDPC kodunun dışsal bilgi transferi (EXIT) analizine dayalı optimizasyonu öncesinde NLTC tasarlamak için uygun bir algoritma geliştirilmiştir. Tasarlanan kodların mevcut noktadan-noktaya (P2P) kodlardan daha iyi başarıma sahip oldukları, zaman değişimli doğrusal kod kullanma alternatifini ve LDPC kodlarının doğrusal olmayan belleksiz eşleyicilerle (NLMM) sıralamasıyla elde edilen referans alternatifini performans açısından geride bıraktıkları görülmüştür. Bu kodlama yöntemi, alıcı

kısmında batarya modundaki belleği yok sayan ve bu belleği kafes tabanına dahil eden iki farklı kodçözme varsayımı kullanılarak enerji hasadı kanalı (EHC) için uygulanmıştır. P2P kodlarıyla ve referans şemalarıyla karşılaştırıldığında, yeni tasarlanan kodların tutarlı bir şekilde daha iyi performans sağladığı görülmüştür. Bu kod tasarımı yaklaşımı, hafızasız ayrık girişim kanalları (DMIC) için Han-Kobayashi (HK) kodlama ve çözümleme stratejisi de kullanılarak genişletilmiştir. Sıralanmış kodlama şeması için kararlılık koşulu elde edilmiş ve bu koşul EXIT analizini kullanan dış LDPC kodu tasarlama işleminde kullanılmıştır. Tasarlanan kodların HK alt bölgesinin optimal sınırına yakın oran çiftlerini başardığı ve zaman paylaşımlı tek kullanıcılı kodları geride bıraktığı kanıtlanmıştır. Ayrıca, iki kullanıcılı sönümlenmeli Gauss girişim kanalı için kısa uzunluklu kafes tabanlı kodlar kullanarak kod tasarım prensipleri araştırılmıştır. Sonuç olarak, enerji hasadı yapan vericilere sahip iki kullanıcılı girişim kanalı için açık ve çalıştırılabilir kod tasarlama problemi üzerinde durulmuş, DMIC ve EHC için geliştirilenlere benzer teknikler kullanan bir tasarım yöntemi geliştirilmiştir.

Anahtar sözcükler: Enerji hasadı yapılan haberleşme sistemleri, enerji ve bilgi transferi birleşimi, girişim kanalı, belleklı kanallar, doğrusal olmayan kafes kodlayıcı, düşük yoğunluklu parite kontrol kodları, seri sıralı kodlar, kararlılık koşulu.

Acknowledgement

First of all, I would like to thank my advisor, Dr. Tolga M. Duman, for his valuable guidance and support throughout the course of my Ph.D. His great insight and dedication for research has been of enormous value for this work and also to myself.

I am very grateful to Prof. Sinan Gezici and Prof. Ali Özgür Yılmaz for accepting to be in my thesis committee (TİK) and providing feedback on my research throughout the committee meetings. I would also like to take the opportunity to thank Prof. Erdal Arıkan and Prof. Melda Yüksel for accepting to be in my thesis jury and giving me detailed comments. It has been a great honor to have them in my thesis defense committee.

This work was supported by the Scientific and Technical Research Council of Turkey (TUBITAK) under the grant 114E601 and NPRP Grant 4-1293-2-513 from Qatar National Research Fund (a member of Qatar Foundation). I gratefully acknowledge this support from TUBITAK and NPRP.

I would like to thank the Electrical and Electronics Department of Bilkent University for partially supporting two of my conference trips. I also would like to thank Dr. A. Korhan Tanç for our discussions and collaborations, and also for his feedback on smoothing the Turkish abstract of the thesis.

My sincere thanks also goes to my friend and colleague, Sina Rezaei Aghdam whom I had valuable discussions and memories during these years. I am also grateful to all my colleagues and friends at Bilkent (especially my friends at Bilkent DOST) who made my time enjoyable and rewarding.

Last but not least, I would like to thank my family for their love, support and encouragement.

Contents

List of Figures

List of Tables

Abbreviations

AR	achievable rate
ARR	achievable rate region
AWGN	additive white Gaussian noise
BC	broadcast channel
BCJR	Bahl-Cocke-Jelinek-Raviv
BER	bit error rate
BPSK	binary phase-shift keying
BSC	binary symmetric channel
CDMA	code division multiple access
CND	check node decoder
CSCC	constant subblock-composition code
CSI	channel state information
DC	direct current
DMIC	discrete memoryless interference channel
DPC	dirty paper coding
DPS	dynamic power splitting
EH	energy harvesting
EHC	energy harvesting channel
EHIC	energy harvesting interference channel

EXIT	extrinsic information transfer
FDMA	frequency division multiple access
GIC	Gaussian interference channel
GMAC	Gaussian multiple access channel
HK	Han-Kobayashi
IC	interference channel
ID	information decoding
i.i.d.	independent and identically distributed
INR	interference-to-noise ratio
ISI	inter-symbol interference
IoENT	Internet of Energy Neutral Things
IoT	Internet of Things
JD	joint decoding
JML	joint maximum likelihood
LDPC	low-density parity-check
LLR	log-likelihood ratio
MAC	multiple access channel
MAP	maximum a posteriori
MIMO	multiple-input multiple-output
MISO	multiple-input single-output
NIID	naive i.i.d. Shannon strategy
NLMM	nonlinear memoryless mapper
NLTC	nonlinear trellis code
OIID	optimal i.i.d. Shannon strategy
P2P	point-to-point

PAM	pulse amplitude modulation
PDF	probability density function
PS	power splitting
PSK	phase-shift keying
QAM	quadrature amplitude modulation
R-E	rate-energy
RC	relay channel
RF	radio frequency
RFID	radio frequency identification
RLL	run length limited
SINR	signal-to-interference-plus-noise ratio
SNR	signal-to-noise ratio
SUD	single user decoding
SWIPT	simultaneous wireless information and power transfer
TDMA	time division multiple access
TS	time switching
VND	variable node decoder
WET	wireless energy transfer
WSN	wireless sensor networks

Chapter 1

Introduction

Wireless devices and sensors are expected to form a major portion of the next generation wireless systems making Internet of Things (IoT) one of the main paradigms in 5G and beyond. Ensuring long term operation of these devices is one of the most important challenges for future IoT applications. Ultra-low power technologies and energy efficient communication protocols are frontier techniques towards the energy neutrality of networks of such devices, however, they are not sufficient by themselves and energy harvesting capability is essential towards their perpetual and uninterrupted operation.

Energy harvesting (EH) is a capability of scavenging energy from either a renewable energy source, e.g., solar, wind, sea waves, etc., or from man-made energy sources such as radio frequency (RF) signals and artificial light. EH offers several important benefits for wireless devices including energy self-sufficiency, prolonged functional lifetime and ability to deploy in hard-to-reach places, e.g., remote areas, inside human body, etc. On the other hand, EH from energy sources in the environment imposes significant challenges in realizing such systems due to the stochastic nature of energy arrivals. As an important example of an EH solution, the RF energy transfer and harvesting is a wireless energy transfer (WET) technique where energy is harvested from dedicated RF signals. This approach has the advantages that the energy source is stable and fully controllable. Also,

unlike other wireless energy transfer techniques such as inductive coupling and magnetic resonance coupling that have very limited power transfer distances, the RF energy transfer is a far-field energy transfer technique, which makes it a suitable option for powering wireless networks [1]. Furthermore, information can also be jointly transmitted through the same RF signals, resulting in a scheme referred to as simultaneous wireless information and power transfer (SWIPT).

Many wireless communication and networking applications such as Internet of Energy Neutral Things (IoENT), wireless sensor networks (WSNs), radio frequency identification (RFID) systems and wireless body networks can benefit from energy harvesting. While it offers significant potential benefits, energy harvesting imposes new constraints on the design and implementation of communication systems in a variety of forms. For example, there is a trade-off between energy and information transfer in RF energy harvesting systems. The key goal in such systems is to maximize the information rate while ensuring that the minimum required energy is being delivered, however, these two objectives are conflicting. Another aspect is the randomness of the available energy in ambient energy harvesting communication systems where it is required to maintain reliable communication under random energy arrivals.

Energy harvesting systems have been extensively studied from device and circuit engineering perspective, and many advancements on the energy harvesting mechanisms and devices have been made over the last few decades. However, from a communication and systems engineering perspective, traditionally, the main focus has been on designing energy efficient communication protocols and optimum average-power constrained communications. Only recently, communication schemes with specific energy harvesting constraints have been considered in the literature.

Joint wireless energy and information transfer is studied from an information theoretic point of view in [2, 3]. References [4–6] consider a coding perspective where achievable rates utilizing different constrained codes such as run-length limited (RLL) codes and constant subblock-composition codes (CSCCs) are derived. Communication systems with energy harvesting nodes have been studied from

different perspectives in the literature. For example, an information theoretic view of these systems is considered in [7–15].

Although many recent studies consider communication and information theoretic aspects along with wireless networking challenges of EH communications and SWIPT, there still is a lack of practical coding solutions in this framework. With this motivation, in the first part of this thesis, we study explicit and implementable coding schemes for SWIPT and EH in single user communication systems.

Multi-user channels are general models for many communication scenarios that can be categorized as four basic models, namely, multiple access channels (MACs), broadcast channels (BCs), relay channels (RCs) and interference channels (ICs). Multi-user channels have been extensively studied in the literature from information theoretic and coding perspectives where the characterization of capacity, achievable rates and outer bounds have been the primary goals. Despite many such advances, only limited studies focus on designing practical codes for (some of) these channel models, including the important case of ICs. For example, code design for Gaussian interference channels (GICs) has been investigated in [16–18], and utilizing low-density parity-check (LDPC) codes, rate pairs close to the boundary of the capacity region or the achievable rate region (ARR) have been obtained. With the aim of complementing the existing results in the literature, in the second part of the thesis, we study the design of explicit and implementable codes for discrete memoryless interference channels (DMICs), and investigate short block length code design for GICs with fading.

Another aspect of the EH communication systems that requires a fresh look is the interference treatment in multiuser setups. Although this problem has been investigated for conventional (non-EH) multiuser communication systems, the available approaches do not cope well with the specific constraints of EH. Therefore, in the last part of the thesis, we combine the two settings being investigated, and as a starting point in this line of work, we examine the code design principles for EH two-user ICs.

1.1 Contributions

Our primary goal in this thesis is to address SWIPT and EH communications for both single user and IC setups from a practical and implementable channel coding perspective. We propose using a nonlinear code for all of these problems as a common solution, however, the reason for using nonlinear codes is different for each case. For example, while in SWIPT scenario we employ the nonlinear code for obtaining a wider range of trade-offs between energy and information transmission and delivering the energy in a more regulated way, we utilize this approach for EH communications since the optimal input distribution is nonuniform, or we use it in a DMIC scenario to provide a rate trade-off between users. As a practical solution for these coding problems, we propose a serial concatenation of an inner nonlinear trellis code (NLTC) with an outer LDPC code, wherein the outer LDPC code provides powerful error correction capability.

There are four main contributions of this dissertation as explained below.

Joint RF Energy and Information Transfer: We consider a wireless communication system with joint RF energy and information transfer, and as a practical coding solution, we use the proposed concatenated coding scheme to satisfy the energy and reliable communication constraints. We propose techniques to design the NLTC and to check for its catastrophicity. Furthermore, we use extrinsic information transfer (EXIT) charts and random perturbation to design the outer LDPC code while fixing the inner NLTC. Via examples, we demonstrate that our designed codes operate close to the information theoretic limits, and we show that the proposed scheme outperforms the reference schemes of concatenating LDPC codes with nonlinear memoryless mappers, and using classical linear block codes in a time switching mode.

The results along this line of investigation have been published in [19, 20].

Single User Energy Harvesting Communication Systems: We consider a single user energy harvesting communication system with i.i.d. energy arrivals

where the channel inputs are binary and the transmitter is equipped with a finite battery, and provide achievable rates and design explicit and implementable codes based on the proposed coding scheme for use in this framework. We propose two different decoding methods where the simplified solution ignores the memory in the battery state while the more sophisticated one utilizes it via an extended trellis. The obtained numerical results demonstrate that the designed codes outperform other reference schemes, and the superiority of the improved decoding approach over the naive solution.

The results along this line of investigation have been published in [21].

Interference Channels: First, we consider a two-user DMIC, and utilizing a Han-Kobayashi (HK) type encoding where both public and private messages are used, we design explicit codes based on the proposed concatenated coding scheme. We derive approximate density evolution formulas for the iterative decoding process in the asymptotic regime where the probability of decoding error tends to zero. Based on this approximate analysis, we derive a stability condition for a serial concatenation of an inner NLTC with an outer LDPC code. Via numerical examples, we demonstrate that our designed codes achieve rate pairs close the optimal boundary of the HK subregion, which cannot be obtained without the use of nonlinear codes.

Later, we turn our attention to the case of GICs with fading, and consider short block length code design with the motivation of practical applications with decoding delay and complexity constraints. For this case we deviate from the proposed concatenated scheme and focus on the application of trellis-based codes for this purpose. We derive performance bounds and utilize them for optimal code search.

Our results on these topics are submitted for publication [22, 23].

Two-User Energy Harvesting Communication Systems: In this setting, we consider a two user IC with energy harvesting transmitters with finite batteries and i.i.d. energy arrivals. We consider i.i.d. on-off signaling and for

both cases of DMICs and GICs, and we obtain an ARR based on utilizing the HK scheme with both single-user and joint decoding. We use the proposed practical coding solution and design explicit and implementable codes. We also extend the decoding method exploiting the memory in the system to the two-user joint decoding scenario, and via several numerical examples, we demonstrate that by employing the designed codes, we can achieve rate pairs close to the information theoretic achievable rates.

1.2 Thesis Outline

The rest of the thesis is organized as follows. In Chapter 2, we study the basics of joint RF energy and information transfer, energy harvesting communications and interference channels, and review the existing literature on these subjects. Chapter 3 investigates the code design for wireless communication systems with joint RF energy and information transfer, where we propose a coding scheme based on a serial concatenation of an NLTC with an outer LDPC code. In Chapter 4, we turn our attention to the energy harvesting communication systems with finite battery transmitters over a noisy channel, and design explicit and implementable codes for this setting. In Chapter 5, we examine the code design principles for the two-user DMICs with HK type encoding, and propose a practical coding solution. Design of short block length codes for GICs with and without fading is the focus of Chapter 6. In Chapter 7, we examine the coding principles for a two-user interference channel with energy harvesting transmitters with finite batteries. Finally, we summarize our results, and provide conclusions and directions for future research in Chapter 8.

Chapter 2

Preliminaries and Literature Review

In this chapter, we review the existing literature on information theoretic limits and practical coding schemes for joint RF energy and information transfer, energy harvesting communications and interference channels, and introduce simple models to capture the basics of communications in these settings.

2.1 Joint RF Energy and Information Transfer

RF energy harvesting is a wireless power transfer technique, which relies on collecting energy from the radiated RF signals at the receiver for use in information processing and transmission processes. Potential applications of RF energy harvesting can be found in different areas including WSNs, wireless body networks and wireless charging systems [1].

Along the lines of wireless energy transfer, [24] studies the principals of RF energy harvesting and its application to WSNs. In [25], the authors develop an

RF energy harvesting WSN prototype to demonstrate its effectiveness. Wireless energy transfer and wireless information transmission have previously been considered as separate problems. However, recently a new technique, which is called simultaneous wireless information and power transfer has been proposed in the literature. This scheme has the advantage of delivering wireless energy and information concurrently, on-demand and in a controlled manner, and it has the potential to provide sustainable operation for wireless networks [26].

Recent work on dual use of RF signals for delivering energy and information demonstrates that there is a natural trade-off on the design of such systems [2]. For systems with joint energy and information transfer, it is of interest to increase the received power levels and the information rates at the same time. Using the most energetic symbol all the time is desirable for the first goal, whereas a uniform distribution on the channel input is required to maximize the mutual information over a symmetric noisy channel. Consequently, there is a natural trade-off and the amount of transmitted information and transferred energy cannot generally be maximized at the same time. Understanding this trade-off and investigating techniques to achieve different trade-off points is a major goal of this thesis.

2.1.1 Basic Model

Let us consider a single user communication system where the receiver completely relies on the energy that it harvests from the RF signals that it receives from the transmitter. We consider an ideal receiver which can harvest energy from the received signal and perform information decoding at the same time. We assume that the only randomness in the channel is due to the noise in the receiver circuitry, which does not affect the harvested energy. For the purposes of providing the basic model, we further assume that the channel between the modulator at the transmitter and the information decoder at the receiver is noiseless.

Let $b(x)$ denote the received energy when x is transmitted, hence using ideal receiver we have $b(x) = |x|^2$. Let us also assume that the transmitter can only transmit two signals with zero or one unit of energy, namely, on-off signaling with

the input alphabet $\mathcal{X} = \{0, 1\}$. If the transmitter transmits the symbol 1 with probability p, i.e., $P(X = 1) = p$, then the average amount of received energy B is

$$B = E[b(X)] = \sum_{x \in \mathcal{X}} b(x)P(x) = p,$$

and the rate of information transmission is

$$R = I(X; Y) = H_2(p),$$

where H_2 is the binary entropy function. Fig. 2.1 shows the average received energy and the average transmission rate utilizing this scheme, which demonstrates that there is a trade-off between transmission of energy and information, that is, a larger p value results in a higher average energy while $p = \frac{1}{2}$ (uniform distribution) maximizes the information rate.

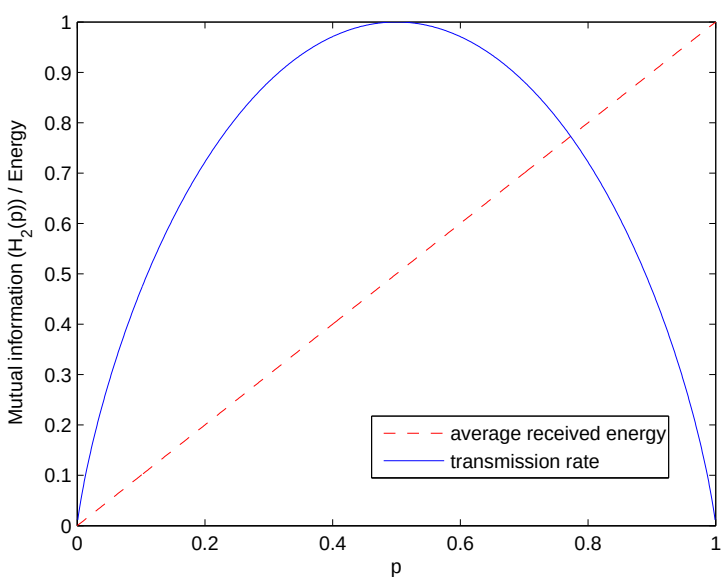

Figure 2.1: Average received energy and transmission rate for a communication system with an energy harvesting receiver over a noiseless channel.

Classical linear codes only achieve single trade-off point on the curve shown in Fig. 2.1, which maximizes the information rate, however, in order to achieve

different trade-offs, we need to provide a nonuniform distribution at the channel input. Also, classical linear codes can have bursty sequences of zeros in their codewords, which causes energy depletion in the energy harvesting receiver or discontinuity in the operation of the receiver, so by utilizing constrained codes which have energy constraint over a sliding window or each subblock of the codewords, we can deliver the energy in more regulated manner. In order to provide an input distribution, which satisfies the average and subblock energy constraints at the receiver, we propose utilizing nonlinear codes in this thesis. As another simpler solution one can use a memoryless mapper combined with a linear code to shape the input distribution, which we also use as a reference scheme for comparing our results.

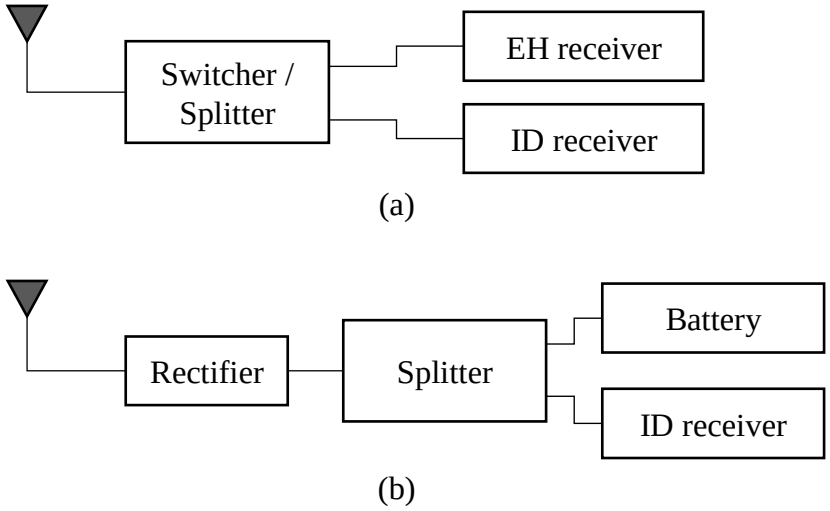

Figure 2.2: Practical receiver architectures for SWIPT.

In order to understand the rationale behind on-off signaling, we need to look at the practical receiver structures for SWIPT. Fig. 2.2 shows two different receiver architectures, namely, time-switching (TS) or power splitting (PS) receiver architecture and integrated receiver architecture. The first receiver consists of co-located EH and information decoding (ID) receivers where the ID receiver is a conventional information decoder and the EH receiver has a rectifier to convert the incoming RF signal into a direct current (DC) used for charging the battery. In case of time switching, the energy and information signal are transmitted over

orthogonal timeslots and the receiver switches its operation accordingly to perform one of the operations at each time slot. For power switching, the receiver splits the received signal into two streams, one for EH and the other one for ID. Different rate-energy (R-E) trade-offs can be obtained by changing the switching or splitting ratio for this receiver. Unlike the TS/PS receiver, that switches/splits the signal in the RF band, the integrated receiver, uses a (passive) rectifier for RF-to-baseband conversion and splits the signal after converting it into DC. Hence, it saves the power consumed by active circuits used in the conventional approach of the TS/PS receiver. When the first architecture is employed, any conventional modulation scheme such as phase-shift keying (PSK) may potentially be utilized, however, by considering the integrated architecture, energy modulation is required. A typical example of such modulations is the classic on-off signaling.

2.1.2 Recent Developments

Varshney in [2] describes the fundamental trade-off between transmission of energy and information through the same signal. He proves that the capacity-energy function is a nonincreasing concave function, and obtains closed form expressions for it for several channels such as the noiseless and noisy binary symmetric channel and the Z-channel. He also shows that for an additive white Gaussian noise (AWGN) channel with a given minimum received energy and maximum input amplitude constraint, the capacity achieving input distribution consists of a finite number of mass points [2]. Authors in [3] extend this framework to AWGN channels with frequency-selective fading and characterize the optimal trade-off between the achievable rate (AR) and the power transferred given the total available power. SWIPT on a point-to-point fading channel subject to time-varying co-channel interference is considered in [27] where interference was utilized as a source of energy harvesting as well. The optimal mode switching rule to achieve various (R-E) trade-offs are derived and outage-energy and (R-E) regions are characterized. Reference [28] investigates robust precoder designs for systems with SWIPT capabilities under a stochastic Rician fading framework.

The concept of SWIPT is considered in multiple antenna communication systems extensively for different scenarios of broadcast, relay and interference channels as well. In [29], a three node multiple-input multiple-output (MIMO) broadcast system is studied and the (R-E) region for the case of separate energy and information receivers is derived. For the case of co-located receivers an outer bound for the achievable R-E region is calculated and achievable R-E regions for two practical designs, namely, time switching and power splitting are characterized. Authors in [30] study optimal beamforming design for a multiuser multiple-input single-output (MISO) broadcast system in which the weighted sum of the powers harvested by EH receivers is maximized subject to individual signal-to-interference-plus-noise ratio (SINR) constraints at the ID receivers. Beamforming problems are studied in [31] and [32] for a two-way relay system with the objective of maximizing the weighted sum-rate with the transmit power limit and energy harvesting constraints. [33] studies linear precoder design and [34–36] investigate optimal transmission strategies for SWIPT in multi-antenna ICs. Concept of secrecy in wireless information and power transfer systems is explored in [37–40]. References [41, 42] address some practical imperfections, namely, non-ideal transmitter hardware and nonlinear behavior in energy conversion efficiency in SWIPT systems. The concept of energy cooperation in energy harvesting communications over relay, two-way relay and multiple access channels are in [43–48]. The works in [49, 50] consider interactive exchange of energy and information in a two-way communication system.

A general receiver operation, namely, dynamic power splitting (DPS), and also two practical receiver architectures, namely, separated and integrated information and energy receivers are proposed in [51] for SWIPT. For both architectures (R-E) performance taking the circuit power consumption into account is characterized, and the optimal transmission strategy is derived to achieve different R-E tradeoffs.

Noticing the fundamental trade-off between the transmission of energy and information in SWIPT systems, we infer that widely used traditional channel codes, which are designed with the goal of maximizing the information rate, are not optimal. Hence, several recent studies consider alternative schemes with the aim of addressing this problem. Along these line of investigations, energy usage

of the receiver is modelled stochastically and battery overflow and underflow probabilities are computed using classical codes and constrained RLL codes in [4]. The results show that the RLL codes are better suited for the receiver's energy utilization pattern compared to the classical unconstrained ones. Binary code design for simultaneous energy and information transfer is studied in [5] where achievable rates using RLL codes over binary input noisy channels are investigated. Authors in [6], study CSCCs, where all the subblocks in every codeword have the same fixed composition, and this subblock composition is chosen to maximize the rate of the information transfer while meeting the energy requirement. Considering a discrete memoryless channel, they characterize the ARs and the error exponents using CSCCs. They also present a tight lower bound on the average energy per symbol within a sliding time window. We emphasize that, while addressing practical channel coding related issues, none of the previous studies provide any explicit and implementable code designs for SWIPT.

2.2 Energy Harvesting Communications

Energy harvesting is a process in which the energy is obtained from a renewable energy source such as solar, thermal or kinetic energy, or from man-made sources such as RF signals, artificial light, etc. Application of the energy harvesting has been considered in different technologies, and more recently, in the field of communications as well. An important application of EH is in WSNs where the sensor nodes utilize the harvested energy to transmit their data.

2.2.1 Basic Model

An energy harvesting communication system is defined as a system in which the transmitter derives the required energy for information transmission from an external source (Fig. 2.3). The transmitter transmits a symbol through the channel with respect to the availability of energy in its battery. It also harvests energy and stores it for subsequent transmissions. In order to explain the difference compared

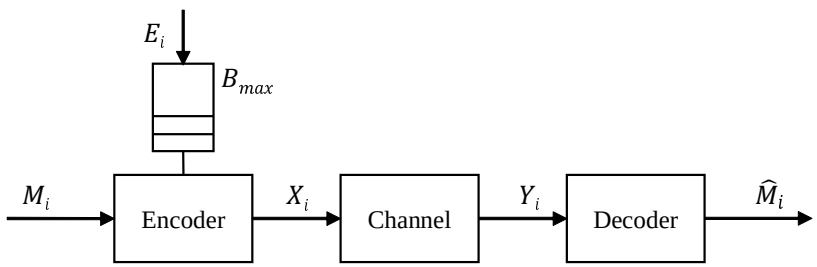

Figure 2.3: A single user energy harvesting communication system with finite battery.

to the conventional communication systems, we consider a simple single user energy harvesting communication system for which the amount of harvested energy at time instant i (E_i), required energy for a symbol transmission, and also the size of the battery B_{max} are multiples of a predetermined unit. We normalize these values and consider it to be 1. We assume i.i.d. binary energy arrivals ($E_i \sim$ Bernoulli(q)) and consider utilizing on-off signaling, i.e., $X_i \in \{0, 1\}$. By observing the battery state S_i, for each channel use, the transmitter first transmits a symbol X_i, and then it harvests energy E_i and stores it in the battery if there is space. If the battery is empty, regardless of what the input bit is, $X_i = 0$ is transmitted. The battery state evolves as

$$S_{i+1} = \min\{S_i - X_i + E_i, B_{max}\},$$

and it is causally known at the transmitter only. For this simple example we consider a noiseless channel model and utilize the methods developed in [9, 14] to investigate the information theoretic limits with different assumptions on the battery size. First, we consider the zero battery case where the encoder is allowed to transmit symbol 1 only if energy is harvested within the same channel use. Hence, a harvest first model is considered. Using i.i.d. on-off signaling with a ones' density p, the capacity for this case C_{ZB} becomes [14]

$$C_{ZB} = \max_p H_2(pq) - pH_2(q).$$

The capacity for the infinite battery case is derived in [14], where it is shown that using the save-and-transmit scheme implies the achievability of the derived capacity. The capacity for this case C_{IB} is

$$C_{IB} = \begin{cases} H_2(q) & \text{if } q \leq 0.5, \\ 1 & \text{if } q > 0.5, \end{cases}$$

Calculation of the AR for finite battery cases is more involved and will be described in detail in Chapter 4.2. Here we provide two AR results with unit and two-unit batteries ($B_{max} = 1, 2$) for illustration. Fig. 2.4 shows the capacity and AR results, where one can observe that increasing the battery size significantly improves the ARs. Also, having a larger energy arrival probability increases the AR for finite battery sizes.

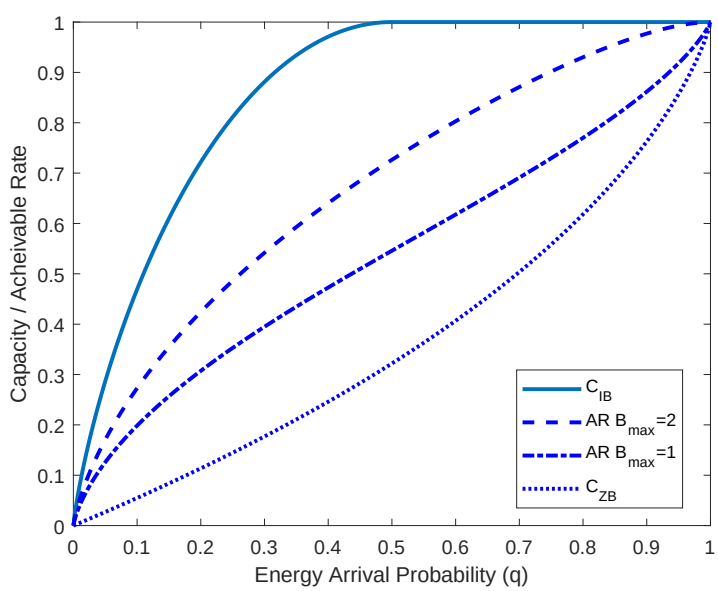

Figure 2.4: Capacity and ARs for a single user EH system over a noiseless channel.

We note that the input distributions that achieve the capacity in zero or infinite battery case or the ARs in finite battery cases are nonuniform in most cases. For example, the ones' density that result in the two ARs in Fig. 2.4 for $q < 1$ is always less than 0.5, i.e., $0 \leq p < 0.5$. Hence, in order to provide the required

nonuniform input distributions and to obtain a good error correction performance, we propose utilizing a concatenation of nonlinear codes with an outer linear code as a practical approach for energy harvesting communication systems, paralleling our proposal for SWIPT.

2.2.2 Existing Results

Energy harvesting communication systems have been studied from an information theoretic point of view in the recent literature. It is shown in [7] that for the case of infinite battery, the capacity of an AWGN channel with the average power constraint equal to the average recharge rate can be achieved. The case with no battery over an AWGN channel is considered in [8], and an analysis of the channel capacity is performed. Finite battery case is the focus of several studies [9–13], however, the capacity for this case is still open. The references [9, 10] study discrete EH channels with two different transmitter side energy information assumption, i.e., causal battery information vs. causal harvested energy information, and derive capacity formulas for arbitrary energy harvesting processes. For the special case of a finite-order Markov energy arrival process, they also obtain computable upper and lower bounds.

The capacity for the case of Gaussian channels with finite sized battery transmitters and deterministic energy arrivals is determined as the maximum of an n-letter mutual information expression in [12]. Furthermore, a lower bound on the capacity by exploiting the volume of the energy feasible vectors is obtained. Authors in [13] consider an energy harvesting AWGN channel with an i.i.d. energy harvesting process, and characterize the capacity of this channel as an n-letter mutual information expression under various assumptions on the availability of energy arrival information, namely, causal and noncausal knowledge of the energy arrivals at the transmitter with and without their knowledge at the receiver. They derive lower and upper bounds on the capacity that are computable and within a constant gap of each other. Authors in [14, 15] consider binary energy harvesting noiseless channels with unit-sized battery, derive a channel capacity

formula by utilizing an equivalent timing channel, and provide computable upper and lower bounds.

In the context of data scheduling and transmit power optimization, several recent studies consider the energy harvesting constraints [52–56], in which the assumption is a monotonically increasing concave rate-power relation. They optimize the transmit power sequence subject to energy causality and no battery overflow constraints. The references [52, 53] consider this problem in a non-fading channel in which the solution turns out to be the tightest curve through the energy feasibility tunnel, and it is invariant to the form of the objective function, as long as it is concave and monotonically increasing. In [54], the problem is extended to the case of fading channels and solved by a directional water-filling algorithm. The incoming energy is allocated to the interval until the next energy arrival and it is allowed to flow causally from past to the future, but the amount of the flow is limited by the battery size. The energy flows until the levels are balanced. The references [57–68] extend these ideas for multi-user channels.

While many advancements on energy harvesting communication systems have been made from information theoretic perspective, much less is achieved on the practical coding solutions to facilitate a reliable communication for this scenario. Although some ideas from the literature of joint energy and information transfer can be applied for this scenario as well, to the best of our knowledge, there is no previous study considering directly the (practical, explicit and implementable) coding solutions for energy harvesting communication systems making our study in this thesis the first one in the literature.

2.3 Interference Channels

An interference channel is a communication medium shared by several sender-receiver pairs. Transmission of information from each sender to its corresponding receiver interferes with the communication among the other sender and receiver pairs. Therefore, in such communication scenarios, besides the channel noise,

there are further disturbances on the transmitted signal due to unwanted interfering signals.

2.3.1 Basic Model

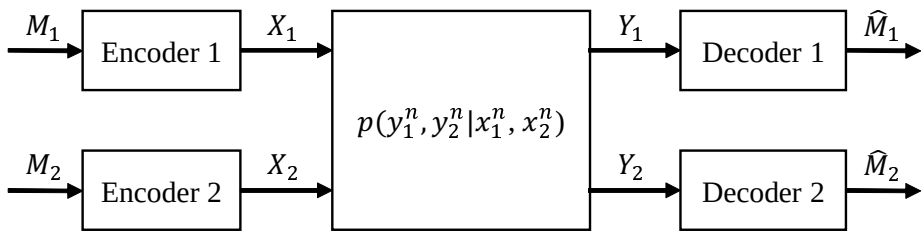

Figure 2.5: Block diagram of the two-user interference channel.

Two-user DMIC model, as depicted in Fig. 2.5, consists of two finite input alphabets $\mathcal{X}_1$ and $\mathcal{X}_2$, two finite output alphabets $\mathcal{Y}_1$ and $\mathcal{Y}_2$, and the channel transition probabilities $p(y_1 y_2 | x_1 x_2)$. The full mathematical definition of a two-user DMIC can be found in [69]. One of the fundamental results on two-user IC is an ARR due to Han-Kobayashi [69, 70], which is the best known inner bound on the capacity region. In order to illustrate the basics, we consider an example of two-user DMIC with one-sided interference binary inputs and outputs for which the input-output relationship is

$$\begin{cases} Y_1 = (X_1 \otimes X_2) \oplus Z_1, \\ Y_2 = X_2 \oplus Z_2, \end{cases}$$

where $\oplus$ and $\otimes$ represent the "XOR" and the "OR" operations, respectively, with Z_1 and Z_2 being the noise samples at receiver 1 and 2 drawn from a Bernoulli distribution with parameters $\epsilon_1 = 0.21$ and $\epsilon_2 = 0.25$, respectively. We utilize a simple HK encoding scheme of sending the messages of both users as private and compute a subregion of the HK ARR for this example as shown in Fig. 2.6. The achievable subregion by employing only uniform input distribution and time sharing between rate points is also illustrated on the same figure, which suggests

that by considering a nonuniform input distribution a wider range of trade-offs between the rates of the two users can be attained. In other words, there is a need for designing nonlinear codes for this communication setting as well.

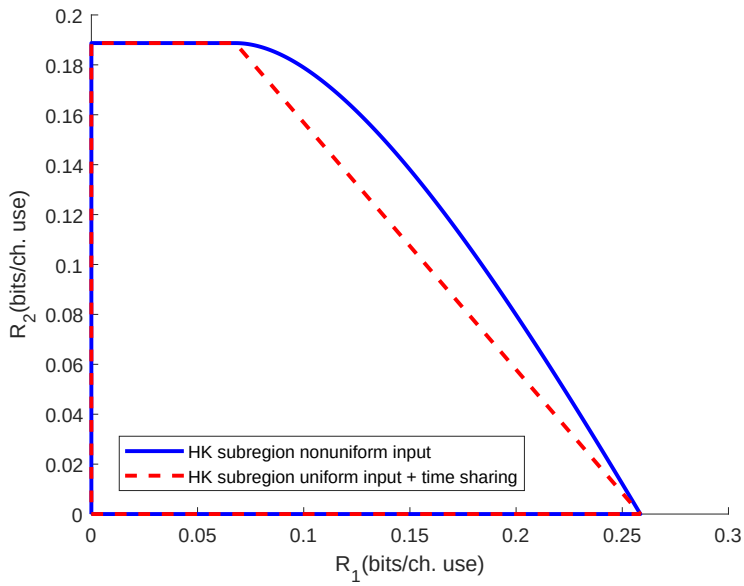

Figure 2.6: Achievable HK subregions.

2.3.2 Brief Literature Review

Despite decades of research and many advancements, characterization of the capacity of ICs is still an open problem for the general case. The capacity is known for some special cases, e.g., strong ICs [71,72], classes of degraded ICs [73,74], and classes of deterministic and semi-deterministic ICs [75, 76]. Han and Kobayashi in [70] establish an inner bound on the capacity region, which is still the best known ARR for the general case. In this scheme, each user splits its data into private and public messages, which are decoded at the intended receivers and both receivers, respectively. The decoding of the interfering signal helps the receivers recover their desired messages. More recently, the authors in [77] derive the sum rate capacity of a DMIC with one-sided weak interference, and show that in order

to achieve this sum rate, both users should transmit their information as private messages only, and the receivers decode the desired messages while treating the interference as noise. Several genie-aided outer bounds are also derived for the GICs in the literature, e.g., see [78–81].

In conventional communication systems, a practical solution for interference management is to avoid interference by orthogonalization methods such as time division multiple access (TDMA), frequency division multiple access (FDMA) or code division multiple access (CDMA) where by separating the users' channels over time, frequency or code domains the interference is avoided at the cost of a lower spectral efficiency. More recently, the concept of interference alignment has been introduced in [82, 83], where by properly designing the transmitted signals and aligning the interference, more resources can be left for the transmission of information. However, in order to realize this scheme, perfect global channel state information (CSI) is needed at all the transmitters, which may not be very practical and may limit its application.

Different coding schemes exploiting LDPC codes, superposition coding and dirty paper coding (DPC) are developed for MACs, BCs and RCs in the literature, and performances close to the theoretical limits have been obtained. For instance, [84, 85] study design of LDPC codes for the two-user Gaussian MAC. An efficient coding scheme based on LDPC codes is proposed for MIMO MAC in [86]. Authors in [87] present a superposition based turbo-coding scheme for degraded BC while the reference [88] studies LDPC code design for the two-user Gaussian BC. Code design for MIMO BC based on LDPC codes and DPC is studied in [89, 90], respectively. Authors in [91] design turbo-based coding/decoding schemes for MIMO RCs and extend it to half-duplex relay systems in [92]. LDPC code design for full duplex RCs with fading is studied in [93]. In another study, LDPC codes are optimized for two-way relay systems with physical-layer network coding [94].

Despite the developments on some multi-user communication scenarios, very limited studies focus on practical code design approaches for ICs. For instance, [16–18] consider code design for GICs where LDPC codes with very large block lengths are considered for the two-user case, and it is shown that rate pairs close

to the capacity or ARR boundaries are attainable. In another study, lattice codes along with underlying spatially coupled LDPC codes are shown to provide excellent performance for the three user symmetric GIC [95]. A coding scheme based on concatenation of a Kite code with a convolutional code is recently proposed in [96], and rate pairs close to the theoretical ARs are obtained, and it is shown that a decoding gain can be achieved by considering the structure of the interference.

2.4 Chapter Summary

In this chapter, we have reviewed the existing literature on the topics of joint RF energy and information transfer, energy harvesting communications and interference channels related to the work in this dissertation. In addition, we have summarized the existing results on the coding schemes for these scenarios. We notice that although there are extensive information theoretic studies for these settings, only a very limited amount of work is available on practical (explicit and implementable) coding solutions motivating us to study this problem further, as detailed in the rest of the thesis.

We emphasize that despite the differences in the considered problems and settings, a common solution for explicit and implementable code design for SWIPT, EH and ICs can be based on utilizing a nonlinear code. That is, while in each problem, there are different constraints and requirements, they all require a nonuniform distribution at the channel input. In order to provide the nonuniform input distribution while achieving a good error correction performance, we propose concatenation of nonlinear codes with powerful outer linear block codes as an effective approach throughout the thesis (except for the case of trellis-based short block length designs for ICs).

Chapter 3

Code Design for Joint Energy and Information Transfer

Harvesting energy from radio frequency signals along with transmitting data through them is appealing for different wireless communication scenarios such as RFID systems and implantable devices. In this chapter, we propose a technique to design nonlinear codes for use in such systems taking into account both energy transmission and error rate requirements. Specifically, we propose using concatenation of an NLTC with an outer LDPC code. We design the NLTC based on maximization of its free distance. We give necessary and sufficient conditions for its catastrophicity; and, in order to avoid catastrophic codes we connect each designed NLTC to a corresponding linear convolutional code allowing for use of simpler conditions for verification. Furthermore, we use EXIT charts to design the outer LDPC code while fixing the inner NLTC. Via examples, we demonstrate that our designed codes operate at about 0.8 dB away from the information theoretic limits, and they outperform both regular LDPC codes and optimized irregular LDPC codes for AWGN channels. In addition, we show that the proposed scheme outperforms the reference schemes of concatenating LDPC codes with nonlinear memoryless mappers and using classical linear block codes

Part of this work was presented at IEEE ICC 2015 [19] and a full version is published in IEEE Transactions on Communications in June 2016 [20].

in a time switching mode.

The rest of the chapter is organized as follows. In Section 3.1, we describe the joint energy and information transfer idea and review some related work. In Section 3.2, the channel model is described, information theoretic limits for the considered scenario are given and the proposed scheme of concatenation of an outer linear block code with a nonlinear trellis code is presented. The design of nonlinear trellis codes for our purposes is then introduced in Section 3.3. Ways of avoiding catastrophic codes are discussed in Section 3.4. EXIT charts and LDPC code optimization are detailed in Section 3.5. In Section 3.6, several numerical examples are provided, and finally, the chapter is concluded in Section 3.7.

3.1 Introduction

As we reviewed in Section 2.1, most of the existing research in the area of joint energy and information transfer is either on communication theoretic or information theoretic approaches, specifically on capacity energy functions for different channels [2], on performance achievable with RLL codes [4], and achievable rates over some noisy binary channels using RLL codes [5]. Our focus in this chapter is on the design of practical codes for simultaneous energy and information transfer complementing these existing results.

A trade-off between transmission of energy and information emerges when the amount of received energy differs for different channel input symbols (which is not the case for binary phase shift keyinf (BPSK) modulation). A simple model that makes this trade-off clear is using on-off signaling which has already been studied in some information theoretic works [2, 4]. For a more general case one might consider transmission of any set of symbols with different energy levels (amplitudes) such as quadrature amplitude modulation (QAM). Here, we consider the case of on-off signaling in which only two symbols "0" and "1" are used, and with the primary objective to complement the existing information theoretic results, we investigate the joint energy and information transfer from a

communication theoretic perspective.

We note that a traditional information receiver architecture designed for information reception is not able to harvest energy from the received RF signals. Motivated with this, there are ongoing efforts on designing receivers for joint energy and information transfer. These include separated receiver architectures [29], co-located receiver architectures [29, 51] which can further be categorized into two models, i.e., time-switching and power-splitting architectures, integrated receiver architectures [51], and ideal receiver architectures. The assumption for an ideal receiver is that it can harvest energy from the same signals used for information decoding without any energy loss, however, as mentioned in [51], this assumption is not practical. In this chapter, we assume an ideal receiver as also done in several other recent related papers in the literature [2, 4, 5], and investigate the achievable reliable transmission rates using the proposed coding scheme. While an ideal receiver is adopted in this study, the same scheme and designed codes can be used with separated receivers, power-splitting architectures and integrated receivers to provide gains over the schemes using classical linear codes. Specifically, for the integrated receiver architecture which is the only proposed receiver with a single front-end that can perform both energy harvesting and information decoding at the same time, one needs to consider energy modulation [51] such as on-off signaling and design nonlinear codes with the required ones density to satisfy both the energy and reliable transmission requirements.

Linear codes such as convolutional codes and LDPC codes have equal density of ones and zeros [97]. Hence, in order to transmit more than $\frac{1}{2}$ (normalized) energy per symbol, there is a need to design nonlinear codes with a desired ones' density which provide good error correction capabilities. With this motivation, we propose a coding scheme based on concatenation of an NLTC with an outer linear block code, specifically an LDPC code. We describe an algorithm for the inner NLTC design based on maximization of the minimum distance of the code. Then, we fix the designed NLTC and optimize the outer LDPC code using EXIT charts. Via several examples, we observe that the designed codes based on the proposed solution offer excellent performance in terms of operating near information theoretic limits, for instance, a particular design is only about 0.8

dB away.

3.2 Proposed Coding Scheme

3.2.1 Channel Model

We consider an additive white Gaussian noise channel for which the input-output relationship is

$$Y = X + Z, \tag{3.1}$$

where $X \in \{0, 1\}$ and Z is independent and identically distributed (i.i.d.) Gaussian noise with zero mean and variance $\frac{N_0}{2}$. In order to model the trade-off between simultaneous energy and information transfer we need to consider signals with different energy levels. Here, we consider using on-off signaling where "1" (resp. "0") corresponds to the presence (resp. absence) of a signal. Using such a representation enables us to transmit more energy through the channel by using a code with a higher ones' density. Signal to noise ratio (SNR) at the receiver side with average ones' density p is defined as $\frac{E_b}{N_0} = \frac{p}{N_0}$. We assume that the receiver needs to harvest at least a certain amount of energy on average. In order to provide this required energy at the receiver side, we place a constraint on the average ones' density p at the channel input, i.e., on the coded symbols. Therefore, our aim is to design practical codes with a predetermined constraint on the average ones' density of the transmitted codewords.

3.2.2 Information Theoretic Limits

Assuming that the required ones' density is p and i.i.d. channel input symbols are used, the mutual information between the input and the output of an AWGN channel with a predetermined input distribution (in this case (i.i.d.) Bernoulli(p)

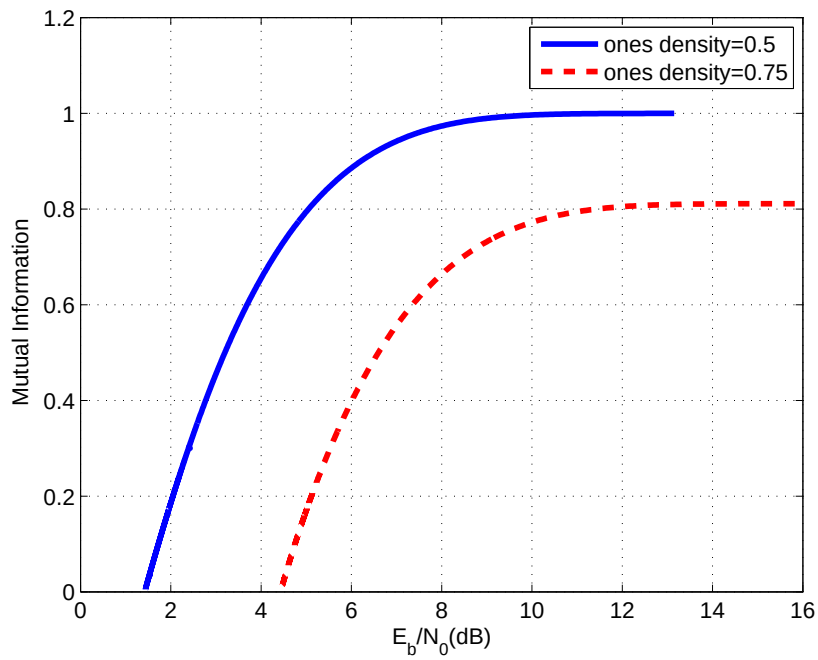

Figure 3.1: Maximum transmission rate over an AWGN channel with on-off signaling for $p = \frac{1}{2}$ and $p = \frac{3}{4}$.

probability mass function) is given by [98]

$$I(X;Y) = h(Y) - \frac{1}{2}log(\pi e N_0), \tag{3.2}$$

where

$$h(Y) = \int_{-\infty}^{\infty} f_Y(y) log\left(\frac{1}{f_Y(y)}\right) dy, \tag{3.3}$$

$$f_Y(y) = \frac{1}{\sqrt{\pi N_0}}\left((1-p)e^{-\frac{y^2}{N_0}} + pe^{-\frac{(y-1)^2}{N_0}}\right). \tag{3.4}$$

As an illustration, (3.2) is computed for $p = \frac{1}{2}$ and $p = \frac{3}{4}$, and the results are shown in Fig. 3.1 which clearly illustrates that there is a trade-off between the ones' density and the maximum possible transmission rate through the channel. That is, by choosing a ones' density of $p = \frac{3}{4}$, we can send more energy compared to the uniform input case, however, we sacrifice some data rate.

3.2.3 Concatenation of LDPC and Nonlinear Trellis Codes

We propose using concatenation of an outer linear block code such as an LDPC code with a nonlinear trellis code as a practical coding solution for joint energy and information transfer. The transmitter side shown in Fig. 3.2 consists of concatenation of an outer LDPC encoder and an inner NLTC encoder, which is directly connected to the channel. As shown in Fig. 3.2, binary message sequence $\{m_i\}$ is first encoded by a rate R_1 LDPC code into a binary sequence $\{x_j\}$. The binary symbols $\{x_j\}$ are then encoded with a rate R_2 and ones' density p NLTC to channel input symbols $\{c_k\}$ which results in an overall code rate of R_1R_2.

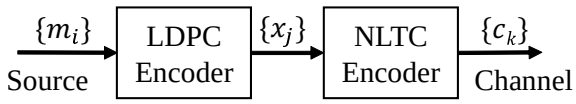

Figure 3.2: Block diagram of the transmitter.

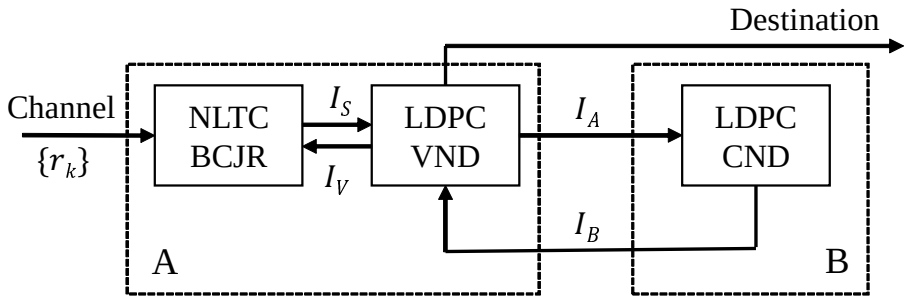

Figure 3.3: Iterative decoder.

The receiver is depicted in Fig. 3.3. The sequence of channel observations $\{r_k\}$ are the input of the receiver. We follow the scheme that is described in [99] and partition the receiver into two blocks, denoted as Block A and Block B. LDPC variable node decoder and LDPC check node decoder is represented as LDPC VND and LDPC CND subblocks in Fig. 3.3, respectively. Block A includes following subblocks:

- A Bahl-Cocke-Jelinek-Raviv (BCJR) decoder which is matched to the NLTC and the channel. This subblock computes a posteriori log-likelihood ratio (LLR) values of the binary symbols $\{x_j\}$ based on the channel observations $\{r_k\}$ and the relevant apriori information from the subblock "LDPC VND".

- An LDPC VND that computes the LLR values of the binary symbols $\{x_j\}$ using LLR values from NLTC-BCJR and the information received from Block B based on the LDPC code constraints.

Block B includes the LDPC CND which computes the extrinsic LLR of binary symbols $\{x_j\}$ using a priori information received from Block A based on LDPC code constraints.

We note that only extrinsic LLR values are passed between component decoders and they are interpreted as a priori information by the recipient block. The overall decoding algorithm can be described as follows:

1. For initialization, the a priori LLRs of binary symbols $\{x_j\}$ at the input of Block A (from Block B) is set to zero (complete uncertainty).

2. Inside Block A the VND computes the a priori input for NLTC-BCJR by summing all the incoming messages from check nodes at each variable node.

3. NLTC-BCJR computes extrinsic LLRs of binary symbols $\{x_j\}$ based on the channel input and the input from the VND and passes it to VND as a priori input.

4. The VND computes the messages to be sent to Block B according to standard LDPC decoding, but using, as a priori input, the messages from NLTC-BCJR.

5. The CND computes the extrinsic LLRs to be passed to Block A according to the standard LDPC decoding.

6. The VND computes total LLRs and checks if the obtained codeword is valid. The algorithm iterates from step (2) until a valid codeword is obtained or the maximum number of allowed iterations is reached.

3.3 Nonlinear Trellis Code Design

In this section, we present a design technique for nonlinear trellis codes for use over an AWGN channel with the purpose of joint energy and information transfer. Our goal is to maximize the minimum Hamming distance between the codewords through the trellis while keeping a certain ones' density. Specifically, we use a finite-state shift register which consists of K (k-bit) stages and input data is shifted into and along the shift register (from the left) k bits at a time. The contents of the shift register (Kk previous input bits) specify the state of the encoder, and the state transitions and corresponding branches are determined by the previous state of the encoder and the input data at that time instant. A nonlinear look-up table is used to assign encoder outputs for each branch. Encoder outputs are chosen to provide the required ones' density p. An example of a trellis with memory $M = 3$ and $k = 1$ is shown in Fig. 3.5. We note that although we do not consider all types of trellises, the specific class that we consider is rich enough to obtain good results for our purposes as will be illustrated later.

3.3.1 Generating and Partitioning the Labels

In this step, considering the desired ones' density p and code rate $R = \frac{k}{n_0}$, we generate labels with length n_0 and average Hamming weight $\omega = pn_0$. We assume that all the labels are used with the same frequency, hence the average Hamming weight of the selected subset of binary labels should be equal to ω. For the rest of the chapter, we consider NLTC of rate $R = \frac{1}{n_0}$ and simply note that one can carefully generalize these ideas to the case with $R = \frac{k}{n_0}$, $k > 1$.

Given the selected subset of binary labels, with the goal of maximizing the

minimum distance between the codewords, we perform set partitioning. In order to do this, we first partition the labels into pairs in such a way that the minimum pairwise Hamming distance between labels in each pair ($d_{min}^{(1)}$) is maximized. Then, we partition the pairs into groups of two pairs such that the minimum pairwise distance between the quadruples ($d_{min}^{(2)}$) is maximized and continue partitioning in this manner. We denote the minimum pairwise Hamming distance of groups of 2^i labels as ($d_{min}^{(i)}$). Assuming that the subset of labels has size 2^h, we obtain a partition tree with h levels. There may be many ways to accomplish this, however, we select one of the possibilities that maximizes $\sum_{i=1}^{h} d_{min}^{(i)}$. Using the partitioned labels and applying the extended Ungerboeck's rule (which will be further discussed in Section 3.3.2), we can generate a nonlinear trellis code of memory M, where $M + 1 \geq 2h$, with a lower bound on its minimum distance given by

$$\text{min-distance} \geq 2 \sum_{i=1}^{h} d_{min}^{(i)}. \tag{3.5}$$

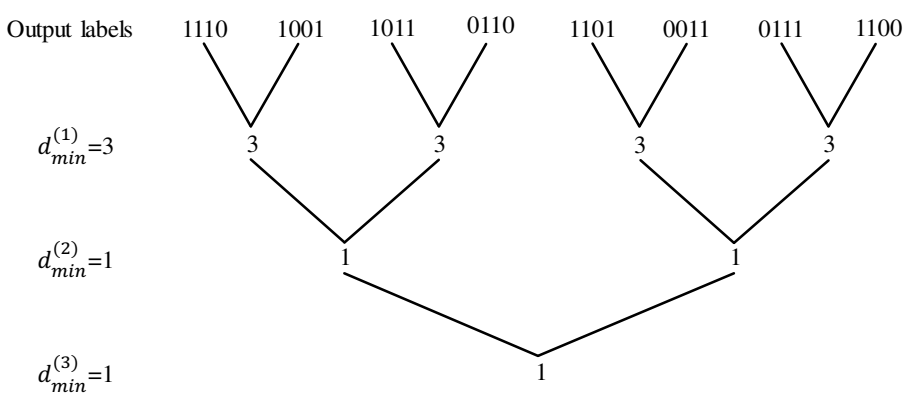

Figure 3.4: Generated labels and their partition tree for $R = \frac{1}{4}$ and $p = \frac{5}{8}$ and the "within-distance" at different levels.

Assigning 2^i labels that have a distance of at least d_{min}^{i} in the i-th level of the partition tree with the branches emanating from (combining at) a split (merge) i sections before (later), we add d_{min}^{i} to the distance between two corresponding paths. One should note here that the first merge after any split from a given path will be at least $M + 1$ trellis sections later, and we need h trellis sections

after split and before merge without overlap between them to include every $d_{min}^{(i)}$, $\forall i$ s.t. $1 \leq i \leq h$ in calculating the lower bound. The paths merging in a larger number of steps than $M+1$ will also have at least the same minimum distance. If $M+1 < 2h$, there are not a sufficient number of trellis sections until the first merge after any split to include all the distance levels d_{min}^{i}, $i = 1, 2, ..., h$, in other words, the distances can be included until $d_{min}^{\lfloor \frac{M+1}{2} \rfloor}$ after each split and before each merge plus one more level with distance $d_{min}^{\lceil \frac{M+1}{2} \rceil}$ on either split or merge side if M is even. Hence, the lower bound on minimum distance for the case of $M+1 < 2h$ can be rewritten as,

$$\text{min-distance} \geq 2 \sum_{i=1}^{\lfloor \frac{M+1}{2} \rfloor} d_{min}^{(i)} + \mathbb{1}_{even}(M) d_{min}^{(\lceil \frac{M+1}{2} \rceil)}, \tag{3.6}$$

where $\mathbb{1}_{even}(M)$ is the indicator function defined as,

$$\mathbb{1}_{even}(M) \triangleq \begin{cases} 1 & \text{if } M \text{ is even,} \\ 0 & \text{otherwise.} \end{cases} \tag{3.7}$$

In the case where more than one such subset of labels are available, we select the one that results in the largest lower bound on the minimum distance.

As an example, we consider a design with rate $R = \frac{1}{4}$ and ones' density $p = \frac{5}{8}$. Generated labels, a partition tree with three levels and minimum distance at each level are shown in Fig. 3.4. For this example, the minimum distance of the code with memory $M \geq 5$ using these labels satisfies min-distance ≥ 10.

3.3.2 General Rules for Label Assignment

The main step in the NLTC design is to assign output values to the branches of the trellis to maximize the minimum distance of the code while keeping the desired ones' density. In our design, assignment of output labels to branches is performed according to the extended Ungerboeck's rule [100] which maximizes the

minimum Hamming distance of the code. Ungerboeck noted that every incorrect codeword, in its trellis representation, departs from the correct path (split) and returns to it (merge) at least once, so he maximized the distance between splits and merges. One can extend the Ungerboeck's rule further into the trellis and maximize the Hamming distance between the branches emanating from a split h trellis sections before, where h is a natural number that can be at most M. The same procedure can be followed for the branches that merge h sections later. Having the set of 2^h distinct labels partitioned in the previous sections for a rate $\frac{1}{n_0}$ code, we can assign the labels according to the extended Ungerboeck's rule as follows:

- 2^i labels in the same partition at level i of the partition tree are assigned to 2^i branches emanating from (merging at) the same state i trellis sections before (later).
- All the labels are used equally often.

The main difference between our approach for NLTC design and the earlier work of [100] is in the target code rates. That is, the codes designed in [100] are of small rates and are intended for use over a multiple access channel, therefore the sum rate is important for their goal. However, here we design codes of high rates with a specified ones' density. One of the design constraints used in [100] is to ensure that all the branches produced by the same input to have different output labels which cannot be satisfied for codes of high rates with large memories. However, we know that in order to obtain large minimum distances for higher rate codes we should use trellises with large memories. Note that as the memory of the trellis increases, assignment of the labels to branches becomes more complicated, hence we need to have a systematic algorithm to apply the design rules.

In order to design higher rate codes, one needs to consider codes of rate $\frac{k}{n_0}$, with $k > 1$. In the following we provide a sketch of how the NLTC code design principles can be generalized to the case of rate $\frac{k}{n_0}$, however, due to the space limitations, we do not give any specific code design examples. The required modifications are as follows:

- selecting a subset of size 2^h from binary sequences of length n_0 where $h \geq k+1$ that satisfies the desired ones density p,
- organizing the selected labels in a partition tree as the case of rate $\frac{1}{n_0}$ with the only difference of partitioning in groups of size 2^k at the first level of the partition tree,
- assigning the partitioned labels to the branches of trellis in such a way to satisfy Ungerboeck's rule for branches emanating from (merging at) each state.

3.3.3 Grouping of Branches for a Specific Trellis

The aim of this section is to describe an algorithm to arrange the trellis branches in 2^h groups (where h is the number of trellis sections for which the Ungerboeck's rule will be extended after each split and before each merge) and to assign partitioned labels to these groups with the same order in which they appear in the partition tree. First, we number the states in natural order starting from zero and assign indexes to outgoing branches from each state as follows: for state number $i \in \{0, 1, ..., 2^M - 1\}$

$$\text{branch-index} = \begin{cases} 2i & \text{if input } u = 0, \\ 2i+1 & \text{if input } u = 1. \end{cases} \tag{3.8}$$

Then, we arrange each set of four branches with consecutive indexes (first one starting with branch with index zero) in two subgroups and represent them using two blocks A_l and A_l^* as follows

(I) A_l

(0)	(1)
$4l$	$4l+1$
$4l+3$	$4l+2$

(II) A_l^*

(0)	(1)
$4l+1$	$4l$
$4l+2$	$4l+3$

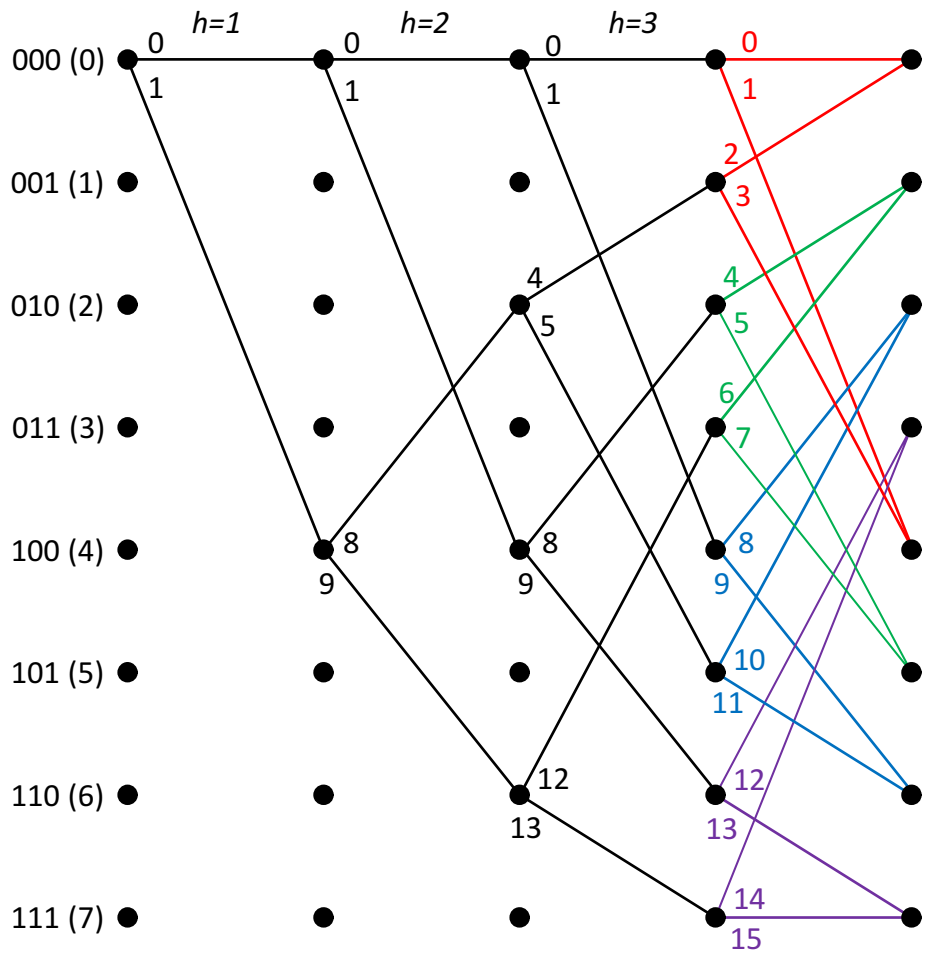

Figure 3.5: 8-state trellis diagram and extension of the Ungerboeck's rule.

$\forall l = 0, 1, ..., 2^{M-1} - 1$. The columns of these blocks represent two different subgroups (0) and (1). We define the star operation (*) above as exchanging the branches between subgroup (0) and subgroup (1). A trivial observation is that $(A^*)^* = A$. Two branches emanating from each split and two branches combining at each merge are placed in different subgroups inside these blocks, hence assigning different labels to subgroup (0) and subgroup (1) of each block ensures that the Ungerboeck's rule is satisfied for the first section of splits and merges. Using these blocks simplifies grouping of the branches. Hence, we need to arrange these blocks in 2^{h-1} groups for which, each of these groups have two subgroups

(0) and (1). We define the group operator $G(.)$ over blocks (and branches) which specifies the group index for the input block (branch), i.e., $G(A_i)$ is the group index of block A_i and $G(S = 2i)_{u=0}$ is the group index of branch corresponding to state $2i$ with input $u = 0$. Placing block A_i in group j which can be shown by $G(A_i) = j$ means that $G(S = 2i)_{u=0} = j(0)$, $G(S = 2i)_{u=1} = j(1)$, $G(S = 2i+1)_{u=0} = j(1)$ and $G(S = 2i+1)_{u=1} = j(0)$. Accordingly if $G(A_i^*) = j$ then $G(S = 2i)_{u=0} = j(1)$, $G(S = 2i)_{u=1} = j(0)$, $G(S = 2i+1)_{u=0} = j(0)$ and $G(S = 2i+1)_{u=1} = j(1)$. After completing grouping of these blocks we will need to assign the ith pair of labels from the partition tree to the group with index i to complete the label assignment process.

In the following we go on with an example to illustrate the grouping step and then we extend the rules to the general case. We consider the 8-state trellis shown in Fig. 3.5 with $h = 3$ and rate $\frac{1}{n_0}$. Considering the second stage, four branches with indexes $\{0, 1, 8, 9\}$ at the second section of the trellis in Fig. 3.5 emanating from a split at first section needs to be arranged in different groups, i.e., blocks A_0 and A_2 should be placed in different groups. Extended rule for the third section after a split forces to arrange eight branches with indexes $\{0, 1, 4, 5, 8, 9, 12, 13\}$ in 8 different groups, i.e., blocks A_0, A_1, A_2 and A_3 should be placed in different groups. Note that applying the rule to the third section after splits also satisfies the rule for the first and the second sections. The same idea can be applied to the merges. Following these rules for this example and using the partitioned labels in Fig. 3.4 result in Table 3.2.

Table 3.2: Assignment of labels for the example of 8-state trellis.

Output label	1110	1001	1011	0110	1101	0011	0111	1100
Group index	0(0)	0(1)	1(0)	1(1)	2(0)	2(1)	3(0)	3(1)
Blocks	A_0		A_1		A_2		A_3	

The design rules can be generalized for any h as follows:
Split Rule: Place 2^{h-1} blocks with indexes $\left\{i, \frac{2^M}{2^h}+i, \frac{2\times 2^M}{2^h}+i, ..., \frac{(2^{h-1}-1)\times 2^M}{2^h}+i\right\}$, $\forall i = 0, 1, ..., \frac{2^M}{2^h} - 1$ in different groups.
Merge Rule: Place 2^{h-1} blocks with indexes $\left\{2^{h-1}i + l | l \in \{0, 1, ..., 2^{h-1} - 1\}\right\}$,

$\forall i = 0, 1, ..., \frac{2^M}{2^h} - 1$ in different groups.

One should note that for the trivial case of $h > M$ which corresponds to the case where the number of distinct labels are greater than or equal to the number of branches, these rules will not apply and one can easily assign distinct output labels to each of the branches.

According to the above rules we propose the following algorithm for the grouping step:

1. Decide about h (number of trellis sections for which the Ungerboeck's rule will be extended) and memory of the trellis M (number of blocks will be 2^{M-1}).

2. Place each block with index j, $\forall j = 0, 1, ..., 2^{h-1} - 1$, in the group with index j as A_j, and assign $i = h$.

3. Considering the split rule, put the block with index 2^{i-1} in one of the admissible groups as $A_{2^{i-1}}$ or $A^*_{2^{i-1}}$ (split rule may restrict these admissible placements), then place blocks with indexes $2^{i-1}+j$, $\forall j$ s.t. $1 \leq j \leq 2^{i-1}-1$ in the group with index $g \oplus g'$, and place it as $A^*_{2^{i-1}+j}$ if only one of the $A_{2^{i-1}}$ and A_j is placed as A^* otherwise place it as $A_{2^{i-1}+j}$, where g and g' are binary group indexes of $A_{2^{i-1}}$ and A_j respectively, and $\oplus$ is bitwise XOR operation.

4. If there are blocks that are not placed inside any groups yet, increment i by one and repeat step 3.

To make this more clear we give an example of trellis with memory $M = 8$ in which we have 128 blocks and we want to arrange these blocks in 2 different groups $h = 2$. We start by placing blocks with indexes 0 to 1 in groups with the same indexes. Then, at the second step there is no restriction for placing block with index 2 regarding the split rule and blocks that are already placed inside groups so we can select either block A_2 or A^*_2 and place it in one of the groups

$\{0, 1\}$. For instance, here we select the block A_2^* and place it in group 0, Then according to the third step of the algorithm we should place block A_3^* in group 1. A sample result after completing the grouping for this trellis is shown in Table 3.3 in which the group indexes are shown in the first row.

Table 3.3: Grouping result of trellis of memory $M = 8$ for $h = 2$.

0	1	0	1	0	1	0	1
A_0	A_1	A_{32}^*	A_{33}^*	A_{65}	A_{64}	A_{97}^*	A_{96}^*
A_2^*	A_3^*	A_{34}	A_{35}	A_{67}^*	A_{66}^*	A_{99}	A_{98}
A_5^*	A_4^*	A_{37}	A_{36}	A_{68}^*	A_{69}^*	A_{100}	A_{101}
A_7	A_6	A_{38}^*	A_{39}^*	A_{71}	A_{70}	A_{103}^*	A_{102}^*
A_8^*	A_9^*	A_{40}	A_{41}	A_{73}^*	A_{72}^*	A_{105}	A_{104}
A_{10}	A_{11}	A_{42}^*	A_{43}^*	A_{75}	A_{74}	A_{107}^*	A_{106}^*
A_{13}	A_{12}	A_{44}^*	A_{45}^*	A_{77}	A_{76}	A_{109}^*	A_{108}^*
A_{15}^*	A_{14}^*	A_{47}	A_{46}	A_{78}^*	A_{79}^*	A_{110}	A_{111}
A_{17}^*	A_{16}^*	A_{49}	A_{48}	A_{80}^*	A_{81}^*	A_{112}	A_{113}
A_{19}	A_{18}	A_{50}^*	A_{51}^*	A_{83}	A_{82}	A_{115}^*	A_{114}^*
A_{20}	A_{21}	A_{52}^*	A_{53}^*	A_{85}	A_{84}	A_{117}^*	A_{116}^*
A_{22}^*	A_{23}^*	A_{54}	A_{55}	A_{87}^*	A_{86}^*	A_{119}	A_{118}
A_{25}	A_{24}	A_{56}^*	A_{57}^*	A_{89}	A_{88}	A_{121}^*	A_{120}^*
A_{27}^*	A_{26}^*	A_{59}	A_{58}	A_{90}^*	A_{91}^*	A_{122}	A_{123}
A_{28}^*	A_{29}^*	A_{60}	A_{61}	A_{93}^*	A_{92}^*	A_{125}	A_{124}
A_{30}	A_{31}	A_{62}^*	A_{63}^*	A_{95}	A_{94}	A_{127}^*	A_{126}^*

At the end, after completing the grouping of the blocks, we assign distinct labels to each group. We use the partitioned labels obtained previously and assign them to the groups with the same order in which they appear in the partition tree.

3.4 Avoiding Catastrophic Codes

We refer to an NLTC that is prone to catastrophic error propagation as a catastrophic code for which a finite number of channel errors may cause an infinite number of decoder errors. With this reference, we derive the necessary and sufficient conditions for catastrophicity of nonlinear trellis codes which is stated in

Theorem 1.

Theorem 1. *A nonlinear trellis code for which the trellis is defined based on sequence of shift registers is catastrophic if and only if one of these two conditions occur: 1) there is a cycle in its state diagram such that starting from at least two different states of the cycle and traversing around results in the same output sequences corresponding to different input sequences, 2) there are at least two different cycles in its state diagram with different input sequences giving rise to the same output sequence.*

Proof. The sufficiency part is straightforward. We assume that either one of these two conditions is true and then we find two different paths of infinite length with finite number of differences in the output and infinite number of differences in the input sequence. First note that starting from any state one can find a path of length M to any other state in the state diagram (due to the specific structure of the evolution of memory). Next if condition 1 is true then we consider the two different states of the cycle as state a and b, or if condition 2 is true we consider state a from the first cycle and state b from the second one. We can find two different paths with starting part of length M from state zero to state a or b and final state transitions the other way around, the middle part can be arbitrarily long consisting of traversing around the cycle corresponding to state a or b. The starting and ending parts will result in finite number of differences in the output, and for the middle part which is arbitrarily long the output sequence is the same for both paths but the input sequences have arbitrarily large number of differences.

For the necessity part we know that we have two input sequences with infinite number of differences with corresponding output sequences of finite number of differences. We separate the parts in which two input sequences are different but their corresponding outputs are the same. Two situations can occur: 1- There are infinite number of such finite-length subsequences of different inputs that have same corresponding output. 2- There is at least one infinite length subsequence of different inputs for each sequence that have same corresponding output. For each case we can argue that at least one of the catastrophicity conditions must

be satisfied.

Case 1: Since the trellis has a finite number of states and a finite number of branches, the number of different paths with the same output in the state diagram is finite, this means that at least one of them must repeat infinitely many times in each sequence, and in order to repeat a path we need to go back to its starting point which means we have traversed around separate cycles infinitely many times with each one of the two sequences and these separate cycles having different input sequences but the same output sequence.

Case 2: The infinite length subsequence needs to contain cycles (since trellis has finite number of branches) that are repeating infinitely many times and have different inputs, hence, there are separate cycles in each subsequence with different inputs but same output (separate cycles can be due to a single sequence of paths starting from different states). □

Catastrophic codes clearly need to be avoided to achieve good error correction capabilities, however, checking for the conditions mentioned in Theorem 1 when the memory of the trellis grows can be very complicated. We already know catastrophicity conditions for linear convolutional codes [97], that is a convolutional code is catastrophic if and only if its corresponding state diagram contains a circuit in which a nonzero input sequence corresponds to an all-zero output sequence. Therefore, checking for catastrophicity of convolutional codes and avoiding such codes is much simpler compared to a nonlinear trellis code. Fortunately, for the specific design (grouping) that we introduced in the previous section, we can show that checking for the code being catastrophic can be performed in an easy and systematic manner by connecting the design to that of standard convolutional codes. In the following, we introduce two theorems and one corollary in order to detect and avoid catastrophic codes in our specific design in Section 3.3.3.

Theorem 2. *For the design in Section 3.3, there exists a one-to-one mapping (which is not necessarily unique) from the full set of binary labels with h bits to the group indexes such that assignment of the corresponding binary labels to the branches inside the group results in a linear convolutional code. The resulting*

convolutional code is called the corresponding convolutional code of the original NLTC.

Proof. The proof is constructive. We will show that if we assign binary values of $(2j, (2^h - 1) - 2j)$ to groups with indexes $(j(0), j(1))$, $j \in 0, 1, ..., 2^{h-1} - 1$, respectively, the following will be the generator polynomials for the resulting convolutional code (note that two labels are one's complement of each other):

$$\begin{aligned}
G_1(D) &= 1 + \sum_{i=h}^{M-1} a_{1,i} D^{M-i} + D^M, \\
G_2(D) &= 1 + \sum_{i=h}^{M-1} a_{2,i} D^{M-i} + D^{M-1} + D^M, \\
... &= \qquad\qquad ... \\
G_h(D) &= 1 + \sum_{i=h}^{M-1} a_{h,i} D^{M-i} + D^{M-h+1} + D^M,
\end{aligned}$$

where $a_{h,i}...a_{1,i}$ and its one's complement are, respectively, the corresponding outputs for subgroup (0) and (1) of the block with index 2^{i-1}. Note that the coefficient of D^M in multiplication of polynomials $G_i(D)$ by $u_k D^M + u_{k-1} D^{M-1} + ... + u_{k-M}$ (where u_k is the current input and $u_{k-1}...u_{k-M}$ is the binary value of the current state) gives the i-th bit of the output.

In the following, in two parts, we will show that for any branch both generator polynomials and the look-up table from the proposed grouping algorithm give the same output.

First we show that if the claim is true for the first branch inside a block then it will also be true for the rest of the branches inside that block. The second and third branches inside a block have the same output which is one's complement of the first branch's output. The same will be obtained by generator polynomials since the only change for second branch is that the input is changed from zero to one for the same state and for the third branch s_1 (least significant bit of state value) is changed from zero to one for the same input. The fourth branch and the first branch have the same output which can again be obtained by generator polynomials since now both input and s_1 are changed from zero to one and they

cancel each other at every bit of the output. Hence, without loss of generality, we can check the claim for the first branch inside each block (which corresponds to even states with input zero) and make sure that the rest will be correct if the first one is correct.

The second part of the proof follows using induction. For the first step of induction, we select a branch corresponding to an even state $0 \leq S \leq 2^h - 1$ with input $u = 0$, so $S = \underbrace{s_M s_{M-1} ... s_{h+1}}_{\text{all are zero}} s_h ... s_2 \underbrace{s_1}_{\text{zero}}$ and $G(S)_{u=0} = s_h s_{h-1} ... s_2(0)$ (according to second step of the grouping algorithm) and the output for this branch is $Output(S_i)_{u=0} = s_h s_{h-1} ... s_2 0$ (according to the assumed label assignment) which can be exactly obtained by the generators given that $u = 0$, $s_1 = 0$ and s_{h+1} to s_M are all zeros. For the kth bit: $G(D).U(D) = (1 + \sum_{i=h}^{M-1} a_{2,i} D^{M-i} + D^{M-k+1} + D^M).(\underbrace{uD^M + s_M D^{M-1} + ... + s_{h+1} D^h}_{0} + s_h D^{h-1} + ... + s_k D^{k-1} + ... + s_2 D + \underbrace{s_1}_{0}) = s_k D^M$ for all $k = 2, ..., h$.

For the second step, assuming that for all the branches corresponding to the states $0 \leq S \leq 2^i - 1$ the claim is true, then we will show that it is true for all the branches corresponding to states $2^i \leq S \leq 2^{i+1} - 1$. Hence, we select a branch corresponding to an even state S with input $u = 0$ where $2^i \leq S \leq 2^{i+1} - 1$, so $S = \underbrace{s_M s_{M-1} ... s_{i+2}}_{\text{all are zero}} \underbrace{s_{i+1}}_{\text{one}} s_i ... s_2 \underbrace{s_1}_{\text{zero}}$. For $S = 2^i$ by the assumption $Output(S = 2^i)_{u=0} = a_{h,i} a_{h-1,i} ... a_{1,i}$ which can be exactly obtained by the generator polynomials since s_{i+1} is one and all the other bits are zero. Also

$$G(S = 2^i)_{u=0} = \begin{cases} a_{h,i} a_{h-1,i} ... a_{2,i}(a_{1,i}) & \text{if } a_{1,i} = 0, \\ \overline{a_{h,i} a_{h-1,i} ... a_{2,i}}(a_{1,i}) & \text{if } a_{1,i} = 1. \end{cases}$$

$$G(A_{2^{i-1}}) = a_{h,i} a_{h-1,i} ... a_{2,i} \text{ if } a_{1,i} = 0,$$

$$G(A^*_{2^{i-1}}) = \overline{a_{h,i} a_{h-1,i} ... a_{2,i}} \text{ if } a_{1,i} = 1$$

where $\overline{()}$ is the one's complement operator.

Now we want to prove the case for $S = 2^i + 2j$ where $1 \leq j \leq 2^{i-1} - 1$. If $G(A_j) = g' = g'_{h-1} ... g'_1$ then $Output(S = 2j)_{u=0} = g'_{h-1} ... g'_1 0$, following the rule

in step 3 of grouping algorithm we can see that

$$G(A_{2^{i-1}+j}) = (g'_{h-1} \oplus a_{h,i})...(g'_1 \oplus a_{2,i}) \text{ if } a_{1,i} = 0,$$

$$G(A^*_{2^{i-1}+j}) = (g'_{h-1} \oplus \overline{a_{h,i}})...(g'_1 \oplus \overline{a_{2,i}}) \text{ if } a_{1,i} = 1,$$

and hence the output will be

$$\begin{aligned} Output(S = 2^i + 2j)_{u=0} &= (g'_{h-1} \oplus a_{h,i})...(g'_1 \oplus a_{2,i})a_{1,i} \\ &\qquad \text{if } a_{1,i} = 0, \end{aligned}$$

$$\begin{aligned} Output(S = 2^i + 2j)_{u=0} &= \overline{(g'_{h-1} \oplus \overline{a_{h,i}})...(g'_{h-1} \oplus \overline{a_{2,i}})}a_{1,i} \\ &= (g'_{h-1} \oplus a_{h,i})...(g'_1 \oplus a_{2,i})a_{1,i} \text{ if } a_{1,i} = 1, \end{aligned}$$

which is consistent with the output obtained by generator polynomials. If $G(A^*_j) = g' = g'_{h-1}...g'_1$ then $Output(S = 2j)_{u=0} = \overline{g'_{h-1}...g'_1}1 = \overline{g'_{h-1}}...\overline{g'_1}1$, Now following the rule in step 3 of grouping algorithm we can see that

$$G(A^*_{2^{i-1}+j}) = (g'_{h-1} \oplus a_{h,i})...(g'_1 \oplus a_{2,i}) \text{ if } a_{1,i} = 0,$$

$$G(A_{2^{i-1}+j}) = (g'_{h-1} \oplus \overline{a_{h,i}})...(g'_1 \oplus \overline{a_{2,i}}) \text{ if } a_{1,i} = 1,$$

and hence the output will be

$$\begin{aligned} Output(S = 2^i + 2j)_{u=0} &= \overline{(g'_{h-1} \oplus a_{h,i})...(g'_1 \oplus a_{2,i})a_{1,i}} \\ &= (\overline{g'_{h-1}} \oplus a_{h,i})...(\overline{g'_1} \oplus a_{2,i})\overline{a_{1,i}} \text{ if } a_{1,i} = 0, \end{aligned}$$

$$\begin{aligned} Output(S = 2^i + 2j)_{u=0} &= (g'_{h-1} \oplus \overline{a_{h,i}})...(g'_{h-1} \oplus \overline{a_{2,i}})\overline{a_{1,i}} \\ &= (\overline{g'_{h-1}} \oplus a_{h,i})...(\overline{g'_1} \oplus a_{2,i})\overline{a_{1,i}} \text{ if } a_{1,i} = 1, \end{aligned}$$

which is consistent with the output obtained by generator polynomials. □

We give a specific example of constructing corresponding convolutional code for a designed grouping. Let the trellis memory be $M = 4$ and $h = 3$. For the grouping in Table 3.4 obtained earlier, we can assign the outputs (as stated in the proof of Theorem 2) and obtain the generating polynomials as $G_1 = 1 + D + D^4$,

$G_2 = 1 + D^3 + D^4$, $G_3 = 1 + D + D^2 + D^4$.

Table 3.4: Assignment of labels for the corresponding convolutional code.

Output label	000	111	010	101	100	011	110	001
Group index	0(0)	0(1)	1(0)	1(1)	2(0)	2(1)	3(0)	3(1)
Blocks	A_0 A_5^*		A_1 A_4^*		A_2 A_7^*		A_3 A_6^*	

Theorem 3. *An NLTC is catastrophic if and only if the corresponding convolutional code is catastrophic.*

Proof. First assume that the corresponding convolutional code is catastrophic, by definition there is a cycle in its state diagram with a nonzero input sequence which corresponds to the all-zero output sequence. We also know that every convolutional code has a cycle from state zero to itself with zero input and all-zero output. Due to the one-to-one mapping between labels, the NLTC will have two different cycles with different input sequences but the same output sequence which means that NLTC is catastrophic. Conversely if NLTC is catastrophic, from the definition at least one of the following conditions is true, 1) there is a cycle in its state diagram such starting from at least two different states of the cycle and traversing around, results in the same output sequence, 2) there are at least two different cycles in its state diagram with same input sequence but different output sequences. Again because of the one-to-one mapping in either one of these cases, the same condition for the convolutional code will also be true which show that the corresponding convolutional code is prone to catastrophic error propagation. □

Corollary 1. *All non-recursive NLTCs of rate $\frac{1}{n_0}$ designed using less than four distinct output labels by our algorithm are catastrophic.*

Proof. We already showed in Theorem 2 that our designed NLTCs are combinations of a non-recursive convolutional code and a one-to-one mapping, hence we can use the theorem in Section 4.2 of [101] which states that if the encoder of

a rate $\frac{1}{n_0}$ constraint length K fixed binary convolutional code is initially in any nonzero state and $K-1$ input symbols are shifted into the shift register, then all $n_0(K-1)$ output symbols can be zero only if the code exhibits catastrophic error propagation. We consider that only two distinct output labels are used in NLTC design which are mapped into 0 and 1 in corresponding convolutional code, also we know that by our design algorithm we make sure that two branches of each split have different labels, so, the corresponding convolutional code at each split in the trellis has one branch with output label 0. Using the mentioned theorem from [101] it is obvious that the corresponding convolutional code and hence the NLTC is catastrophic. □

In a convolutional code with two distinct labels, if we map one of the output labels (0 or 1) to two different output labels (each one-half of the time), then we will obtain an NLTC with three distinct labels in which one of the labels is used with twice the frequency of the other two. It is straightforward to show that the resulting NLTC will again be a catastrophic code. The above two theorems and the corollary allow us to avoid catastrophic codes in a simple way, and they are utilized in the next section for our specific design examples.

3.5 Outer LDPC Code Optimization

3.5.1 EXIT Chart-Based Analysis

In this section, we use EXIT charts to characterize the iterative decoder's operation. In order to do this we need to draw the EXIT curve for each subblock in the iterative decoder. Following the notation in [99], we denote the mutual information terms at the output of block A and B as I_A and I_B, respectively. Also, mutual information at the input and output of the NLTC-BCJR subblock is shown by I_V and I_S (Fig. 3.3). We follow the iterative update of mutual information as the measure of decoding performance. When the mutual information converges to 1 it shows that the probability of error will converge to zero. By

combining the EXIT curve of LDPC VND with that of the NLTC-BCJR, we can obtain the exit curve for block A. EXIT curve of block B is simply the EXIT curve of LDPC CND. By assuming the Gaussian distribution for exchanged messages between these subblocks we can use analytical formulas for I_A, I_B and I_V. In order to calculate the I_S at the output of the NLTC-BCJR, we use Monte Carlo simulations. We have

$$I_A = \sum_i \lambda_i J\left(\sqrt{(i-1)(J^{-1}(I_B))^2 + (J^{-1}(I_S))^2}\right), \tag{3.9}$$

$$I_B = 1 - \sum_j \rho_j J\left(\sqrt{(j-1)}J^{-1}(1-I_A)\right), \tag{3.10}$$

$$I_V = \sum_i \tilde{\lambda}_i J\left(\sqrt{i}J^{-1}(I_B)\right), \tag{3.11}$$

where $\tilde{\lambda}(x) = \frac{\int_0^x \lambda(z)dz}{\int_0^1 \lambda(z)dz}$ is the variable node degree distribution from the node perspective and $J(.)$ is defined as

$$J(\sigma) = 1 - \int_{-\infty}^{\infty} \frac{1}{\sqrt{2\pi}\sigma} e^{-\frac{(l-\frac{\sigma^2}{2})^2}{2\sigma^2}} \log_2(1+e^{-l})dl. \tag{3.12}$$

3.5.2 Degree Distribution Optimization using EXIT Charts

As it is studied previously in [99], using powerful off-the-shelf LDPC codes designed for AWGN channels is not sufficient to achieve near channel capacity performance for all possible inner codes or modulation schemes. In general, the LDPC code has to be optimized for the specific coding and modulation scheme, and EXIT analysis is a powerful tool that can be exploited for this purpose.

In order to perform the LDPC code optimization we fix the inner NLTC and do the optimization over the LDPC degree distribution. Inspired by the results of [99] which suggest that using multiple degrees at both the variable node and the check node sides could result in lower thresholds for the concatenated scheme, we

select an initial degree distribution with multiple degrees at both sides satisfying the required code rate. Using the analytical formulas at VND and CND, and performing Monte Carlo simulations for sufficiently long block-lengths for NLTC-BCJR, we calculate the threshold for this initial degree distribution. We track the evolution of the mutual information at the output of blocks A and B, and stop and call the degree distribution admissible if I_B (MI at the output of check nodes) evolves to 0.995.

At the NLTC-BCJR decoder, we consider a random input sequence of length 10^6 and based on input mutual information I_v, we generate Gaussian distributed intrinsic LLRs with the same MI for the random input sequence and apply it as input to the soft-input soft-output BCJR decoder. We calculate the MI at the output of this subblock by estimating the probability density functions $P_L(l|0)$, $P_L(l|1)$ from the obtained extrinsic LLRs and using the following formula

$$\begin{aligned} I(X;L) &= 1 - E\Big[\log_2\Big(\frac{1}{P_{X|L}(x|l)}\Big)\Big] \\ &= 1 - \sum_{x=0,1} \frac{1}{2} \int_{-\infty}^{\infty} P_L(l|x) \log_2\Big(\frac{P_L(l|0)+P_L(l|1)}{P_L(l|x)}\Big) dl. \end{aligned} \tag{3.13}$$

We employ a specific implementation of differential evolution [102] for designing the LDPC code. We use perturbing vectors to generate new instances of degree distributions with lower thresholds following the approach utilized in [99] in an iterative fashion. Both variable and check node degree distributions are perturbed as $\widetilde{\lambda_i} = \lambda_i + e_{1i}$, $\widetilde{\rho_j} = \rho_j + e_{2j}$ where e_{1i} and e_{2j} denote the ith and the jth elements of perturbing vectors. For the degree distribution to be valid the following equations should be satisfied

$$\textstyle\sum_{i=2}^{d_v} \lambda_i + e_{1i} = 1, 0 \leq \lambda_i + e_{1i} \leq 1, 2 \leq i \leq d_v, \tag{3.14}$$

$$\textstyle\sum_{j=2}^{d_c} \rho_j + e_{2j} = 1, 0 \leq \rho_j + e_{2j} \leq 1, 2 \leq j \leq d_c. \tag{3.15}$$

Also we keep the rate of the code unchanged during the optimization, i.e., we

take

$$1 - \frac{\sum_{j=2}^{d_c} \frac{\rho_j + e_{2j}}{j}}{\sum_{i=2}^{d_v} \frac{\lambda_i + e_{2i}}{i}} = r. \tag{3.16}$$

We draw all the elements of the perturbing vectors except three from a normal distribution $\mathcal{N}(0, \sigma^2)$ where σ is a design coefficient. The remaining three elements are obtained by solving linear equations in (3.14)-(3.16). The perturbed degree distribution will replace the current one if it has a lower threshold, otherwise it is dismissed and new perturbation is performed. The procedure is terminated if no improvement can be obtained after a predetermined number of iterations.

3.6 Numerical Examples

In this section, we present several examples of the designed codes (both inner NLTC and outer LDPC codes) for joint information and energy transfer, and evaluate their performance over an AWGN channel. As a first example, we consider an NLTC of rate $\frac{1}{3}$ with memory $M = 4$ and ones' density $p = \frac{3}{4}$. Label assignment table for the trellis of this NLTC is shown in Table 3.5 (note that the branches are represented by the branch number introduced in (3.8)). As the outer LDPC code, we consider three different codes all of rate $\frac{1}{2}$: the first one is the regular (3,6) LDPC code, the second one is an optimized irregular LDPC code for AWGN channel with maximum variable degree 50 obtained from [103], and the third one is the optimized LDPC code specifically for the inner NLTC employed by the algorithm developed in the previous section with

$$\rho_3 = 0.48052, \quad \rho_4 = 0.00315, \quad \rho_8 = 0.01327, \quad \rho_{15} = 0.50306,$$
$$\lambda_2 = 0.55833, \quad \lambda_3 = 0.03322, \quad \lambda_4 = 0.40845.$$

We evaluate the performance of the optimized code ensemble through finite block-length simulations and computation of decoding thresholds. The overall rate of the coding scheme is $R = \frac{1}{6}$. The information theoretic results indicate that we need about 4.99 dB for reliable communication at this transmission rate for

the specified ones' density of $p = \frac{3}{4}$ (Fig. 3.1). Considering that the decoding threshold for the optimized degree distribution is at 5.8 dB (which is obtained by Monte Carlo simulations and without any Gaussian approximation), we observe that the proposed coding scheme has a performance about 0.8 dB away from this limit. To study the performance of specific codes from the designed ensemble, parity check matrices for a block-length of 100k are obtained using the tools in [104] where the length-4 cycles are removed for improved performance. The resulting bit error rates (BERs) are depicted in Fig. 3.6. We observe that the optimized LDPC code for an AWGN channel has the worst performance, and even the regular (3,6) code performs better when concatenated with the NLTC. The optimized code for the specific NLTC performs the best with a gain of about 1.65 dB compared to the regular (3,6) code at an error rate of 10^{-3}.

Table 3.5: Label assignment to the branches of 16-state trellis ($M = 4$) using the proposed algorithm.

Branch index								Output label (rate $\frac{1}{3}/\frac{1}{4}$)
0	3	9	10	20	23	29	30	011/0111
1	2	8	11	21	22	28	31	101/1011
4	7	13	14	16	19	25	26	110/1101
5	6	12	15	17	18	24	27	111/1110

Table 3.6: Nonlinear memoryless mapper of rate $R = \frac{1}{3}$ and ones' density $p = \frac{3}{4}$.

Mapper input	Mapper output
00	011011
01	101101
10	110111
11	111110

For comparison purposes, we also consider a reference scheme of using a nonlinear memoryless mapper (NLMM) instead of an NLTC, concatenated with an outer LDPC code. For the ongoing example, we use the NLMM shown in Table 3.6 and design a rate $\frac{1}{2}$ outer LDPC code using the optimization method

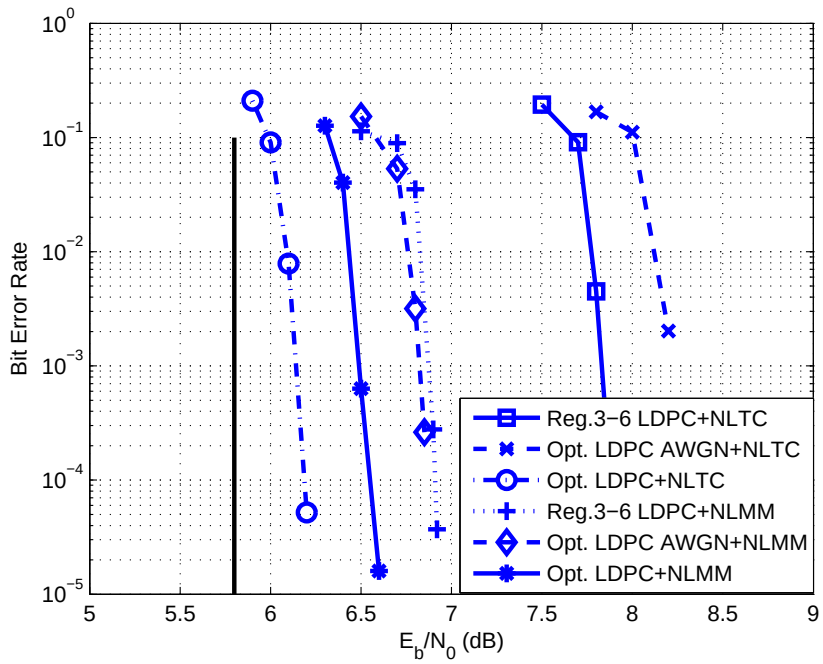

Figure 3.6: BER performance of three LDPC codes concatenated with the NLTC of rate $R = \frac{1}{3}$, memory ($M = 4$), and ones' density $p = \frac{3}{4}$. Outer LDPC codes are of rate $R = \frac{1}{2}$ and block-length 100k.

described in the previous section. The resulting degree distribution is

$$\rho_7 = 0.94397, \quad \rho_8 = 0.05603,$$
$$\lambda_2 = 0.33052, \quad \lambda_3 = 0.21239, \quad \lambda_4 = 0.01314, \quad \lambda_{10} = 0.44395.$$

BER results for codes (of length 100k) picked from this ensemble, along with two other reference codes are also reported in Fig. 3.6. We observe that the proposed scheme using NLTCs yields a gain of about 0.4 dB in terms of the BER performance over the reference scheme with NLMMs.

As another example, we consider an NLTC of rate $R = \frac{1}{4}$ with memory $M = 4$ and ones' density $p = \frac{3}{4}$. The label assignment for this code is based on the look-up table shown in Table 3.5. Again as the outer codes, we consider three different LDPC codes of rate $\frac{1}{2}$, of which the first and the second ones are the

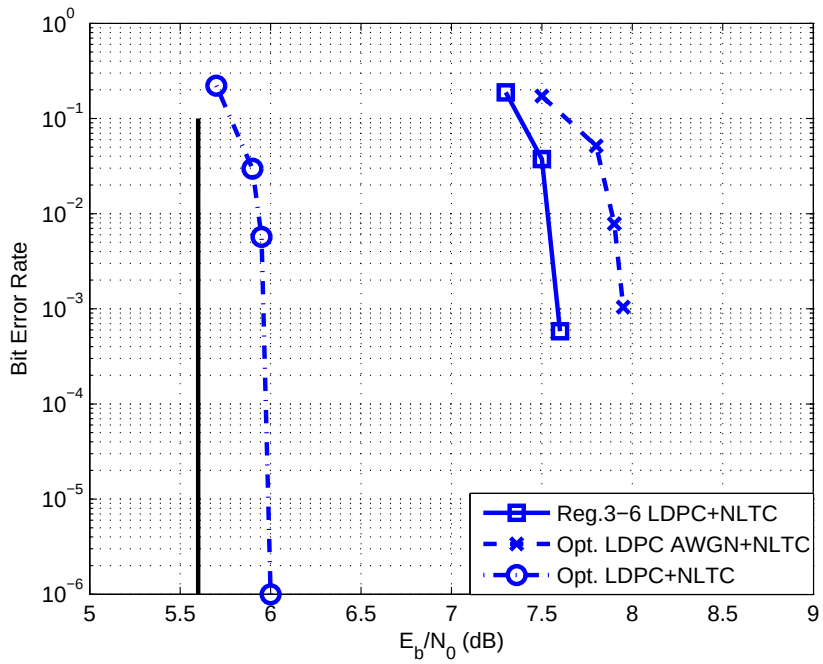

Figure 3.7: BER performance of three LDPC codes concatenated with the NLTC of rate $R = \frac{1}{4}$, memory ($M = 4$), and ones' density $p = \frac{3}{4}$. Outer LDPC codes are of rate $R = \frac{1}{2}$ and block-length 100k.

regular (3,6) LDPC code and the optimized irregular LDPC code for an AWGN channel, respectively. The third one is an optimized LDPC code for the specific NLTC used in this example with

$$\rho_3 = 0.46241, \quad \rho_4 = 0.03137, \quad \rho_8 = 0.00871, \quad \rho_{15} = 0.49751,$$
$$\lambda_2 = 0.55613, \quad \lambda_3 = 0.04170, \quad \lambda_4 = 0.40217.$$

The overall rate of the coding scheme is $R = \frac{1}{8}$. The information theoretic limit for this transmission rate with ones' density $p = \frac{3}{4}$ is at about 4.84 dB and the threshold for the optimized degree distribution is at 5.6 dB (which is obtained without any Gaussian approximation). We observe that the proposed scheme operates at about 0.8 dB from the information theoretic limit. Parity check matrices for the outer LDPC codes are generated using the tools in [104] and also optimized by removing length-4 cycles. Fig. 3.7 shows the decoding results

for concatenation of these three different LDPC codes with the inner NLTC. We observe that the optimized LDPC code beats the two other alternatives as expected. It has gain of about 1.65 dB compared to the regular (3,6) code and of about 2 dB over the AWGN-optimized LDPC code at an error rate of 10^{-3}.

The examples above show the importance of the LDPC code optimization for the specific inner NLTC, and illustrate that large performance improvements can be obtained by using optimized degree distributions for each inner code.

Table 3.7: Optimized degree distributions of LDPC codes of rate $R = 0.823$ for concatenation with NLTCs of Table 3.5.

NLTC rate	$\frac{1}{3}$	$\frac{1}{4}$		$\frac{1}{3}$	$\frac{1}{4}$
λ_2	0.53462	0.52982	ρ_3	0.01075	0.00467
λ_3	0.02631	0.00838	ρ_4	0.02634	0.03621
λ_7	0.0004	0.01381	ρ_9	0.21403	0.17650
λ_8	0.06054	0.03963	ρ_{10}	0.04209	0.06318
λ_{11}	0.09629	0.02539	ρ_{39}	0.32566	0.39733
λ_{12}	0.28184	0.38297	ρ_{40}	0.38113	0.32211

Table 3.8: Optimized degree distributions of LDPC codes of rate $R = \frac{3}{4}$ for concatenation with NLTC of rate $\frac{1}{3}$ of Table 3.5.

λ_2	0.35789	ρ_3	0.02806
λ_3	0.12842	ρ_4	0.07483
λ_7	0.03020	ρ_9	0.15047
λ_8	0.04853	ρ_{10}	0.04484
λ_{11}	0.03455	ρ_{39}	0.54824
λ_{12}	0.40041	ρ_{40}	0.15356

As another example, we consider both NLTCs from the two previous examples, and optimize an outer LDPC code of rate $R = 0.823$ for each. The optimization procedures for these two cases result in the degree distributions which are given in Table 3.7. Using Monte Carlo simulations, the threshold for the concatenation of the optimized codes with NLTCs of rate $\frac{1}{3}$ and $\frac{1}{4}$ are calculated as 6.6 dB and 6.4 dB, respectively, while the information theoretic limits are 5.42 dB and 5.14

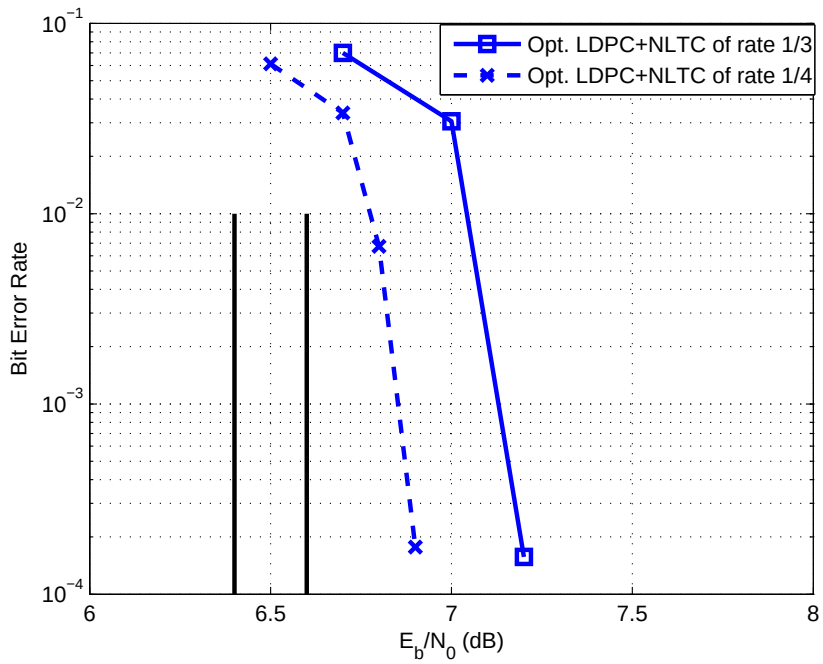

Figure 3.8: BER performance of optimized LDPC code of table 3.7 concatenated with NLTCs of rate $R = \frac{1}{3}\&\frac{1}{4}$, memory ($M = 4$) and ones' density $p = \frac{3}{4}$. Outer LDPC code is of rate $R = 0.823$ and block-length $100k$.

dB. Hence the proposed scheme operates at about 1.2 dB from the limit in both cases. We also generate sample parity check matrices and report the resulting BER performances in Fig. 3.8. We observe that the gap to the information theoretic limits are larger in this example compared to the previous ones. We attribute this to the following: for high rate LDPC codes, there are check nodes of large degrees and the Gaussian approximation for the outgoing messages of these check nodes may be less accurate, and since we use the Gaussian approximation in the EXIT chart analysis for the code design, the larger gaps to the information theoretic limits result.

Finally, we compare the performance of the designed codes for joint energy and information transfer with that of classical linear codes used with time switching (TS). For the time switching alternative, sending both information and energy half the time using on-off signaling, and sending only "1" for the other half will

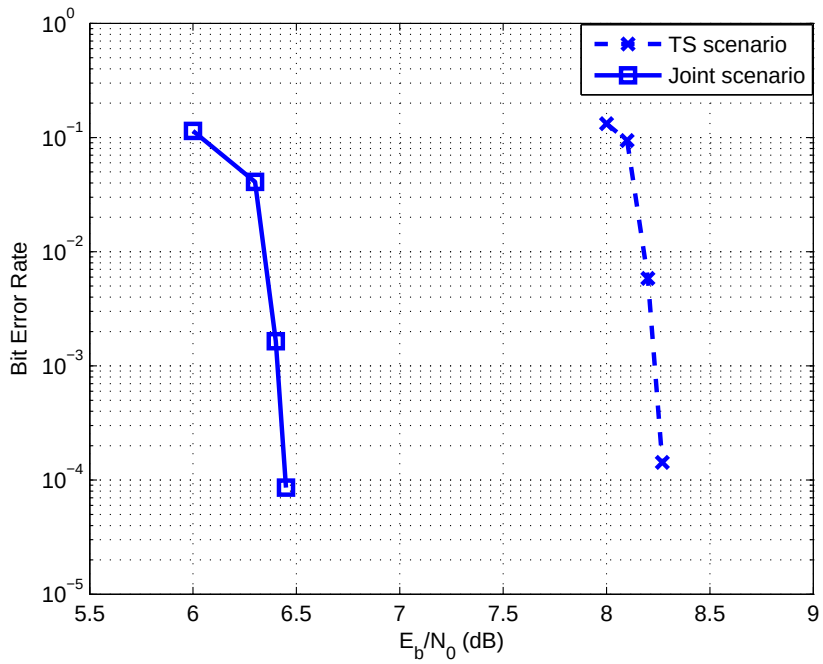

Figure 3.9: Comparison of BER performance between joint transfer and time switching scenarios.

result in a ones' density of $p = \frac{3}{4}$. In this example, for the TS scenario, the degree distribution of the outer LDPC code is obtained from [103], and the parity check matrices are obtained with tools in [104]. An irregular LDPC code of rate $\frac{1}{2}$ with block-length 100k is used for the TS option, hence the overall information transfer rate is $\frac{1}{4}$. As an example of the proposed design, a nonlinear code realized with concatenation of the NLTC of rate $\frac{1}{3}$, memory $m = 4$ and ones' density $p = \frac{3}{4}$ from the first example with an optimized outer LDPC code of rate $\frac{3}{4}$ (with the degree distribution in Table 3.8) and block-length 100k (resulting in the same overall rate of $\frac{1}{4}$) is used for joint energy and information transfer. Fig. 3.9 shows the BER performance results which clearly show that using the designed nonlinear codes for joint energy and information transfer provides significant SNR benefits compared to linear codes in a time switching mode.

3.7 Chapter Summary

In this chapter, a coding scheme based on concatenation of a nonlinear trellis code with an outer LDPC code for joint energy and information transfer is proposed. In order to design the NLTCs, an algorithm based on maximizing the minimum distance of the code is provided. Also, necessary and sufficient conditions for catastrophicity of nonlinear trellis codes are obtained; and, in order to avoid such catastrophic codes, each designed NLTC is connected to a corresponding linear convolutional code. This allows for the use of simpler conditions for checking for the catastrophicity of the designed NLTC. Furthermore, we employ EXIT charts to design the outer LDPC codes while fixing the inner NLTCs. Several design examples are provided, and their performances are evaluated. The results indicate that the designed codes operate at about 0.8 dB away from the information theoretic limits, and they outperform both regular LDPC codes and optimized irregular LDPC codes for AWGN channels when used with NLTCs for joint energy and information transfer. In order to have a practical code design, we employ small degrees in both check and variable nodes, however, we expect that by using larger degrees the gap to the information theoretic limits can be decreased. Furthermore, our results also show that the designed codes outperform the alternative of using classical linear block codes with time switching and the reference schemes of concatenating LDPC codes with nonlinear memoryless mappers considerably.

Chapter 4

Code Design for Energy Harvesting Communication Systems

In this chapter, we consider a binary energy harvesting communication system with a finite battery transmitter over a noisy channel, and design explicit and implementable codes based on concatenation of an NLTC with an outer LDPC code. We propose two different decoding methods where the simplified one ignores the memory in the battery state while the more sophisticated one utilizes the memory. Numerical results demonstrate that the designed codes outperform other reference schemes. The results also show the superiority of the improved decoding approach over the naive solution.

The chapter is organized as follows. In Section 4.1 we review the previous studies on energy harvesting communications. In Section 4.2, we introduce the system model for a binary energy harvesting communication system, and provide achievable rates and optimal ones' densities for different channel models. Proposed encoding and decoding schemes are presented in Section 4.3 along with the

This work was presented at IEEE ISIT 2017 [21].

code design procedure. We provide several design examples and decoding performance results in Section 4.4, and finally, we conclude the chapter in Section 4.5.

4.1 Introduction

We consider a single user communication system in which the transmitter derives the required energy for information transmission from an external source. The transmitter transmits a symbol through the channel with respect to the availability of energy in the battery. It also harvests energy and stores it in a battery for subsequent transmissions. Energy harvesting communication systems have been studied recently from an information theoretic point of view in the literature. While the capacity has been obtained for the case of infinite battery and no battery in [7] and [8], respectively, it is still open for the finite sized battery case. Authors in [14,15] consider binary energy harvesting noiseless channels with unit-sized battery, derive a channel capacity formula by utilizing an equivalent timing channel, and provide computable upper and lower bounds.

While many advancements have been made from an information theoretic perspective, explicit code design for the binary energy harvesting noisy channel has not been studied previously. With this motivation, we consider this model with finite battery and design explicit and implementable codes based on a serially concatenated coding scheme. We consider using i.i.d. on-off signaling and derive the optimal ones' density for different energy arrival probabilities and battery capacities. Observing that the optimal input distribution is nonuniform we propose an encoding scheme based on concatenation of an inner NLTC with an outer LDPC code. The inner nonlinear code is used to provide the optimal ones' density while the outer linear code offers strong error correction capabilities. We note that, other approaches, e.g., based on "probabilistic shaping" [105] or "constrained coding" [4] can be employed for this problem. At the receiver side, as a simple decoding approach, we ignore the memory in the battery state and consider a channel with i.i.d states. We calculate the stationary probability of the zero battery state (π_0) and consider a memoryless Z channel with $1 \to 0$

crossover probability π_0 connected to the corresponding channel model. The receiver performs iterative decoding over the equivalent memoryless channel. Due to its simplicity, this decoding scheme is utilized for code design purposes, i.e., for finding the optimal LDPC code ensembles. The scheme obtained by this simple strategy is called the naive i.i.d. Shannon strategy (NIID) and the corresponding achievable rates are obtained in [14]. This scheme is clearly sub-optimal because it ignores the memory in the system.

Another main contribution of this study is the development of an improved alternative decoding scheme for the system model under consideration. In order to take advantage of the memory in the battery state at the decoder side, we build an extended trellis representing both the NLTC and battery states, and perform BCJR decoding on this extended trellis. The scheme obtained by this modified decoding strategy is called optimal i.i.d. Shannon strategy (OIID) and the corresponding achievable rates are obtained in [9, 14]. Through several numerical examples, we demonstrate that the proposed decoder is highly superior to the simple decoding approach.

4.2 System Description

We consider the model introduced in [14] for an energy harvesting channel in which the energy arrivals (E_i) are binary (i.e., either zero or one unit of energy arrives, $E_i \in \{0, 1\}$). The channel inputs are binary as well, i.e., $X_i \in \{0, 1\}$ (with zero or one unit energy cost). Battery size is a multiple of the fixed unit of energy harvests (denoted by B_{max}). We assume an i.i.d. energy arrival process ($E_i \sim \text{Bernoulli}(q)$), however, the specific coding scheme proposed in Section 4.3 can be extended easily to other energy arrival models such as those incorporating Markov arrivals as well.

By observing the battery state S_i, for each channel use, the transmitter first transmits a symbol X_i, and then it harvests energy E_i and stores it in the battery if there is space. If the battery is empty, regardless of what the input bit is, $X_i = 0$

is transmitted. The battery state evolves as $S_{i+1} = \min\{S_i - X_i + E_i, B_{max}\}$, and it is causally known at the transmitter only. In this model, we have a state dependent channel for which the channel state S_{i+1} depends on the channel input X_i, energy arrival E_i and previous battery state, hence it has memory. Since the channel state is not i.i.d. over time, i.i.d. Shannon strategy does not give the capacity for this channel, however, it can provide an achievable rate [9].

We compute achievable rates based on the i.i.d. Shannon strategies for binary symmetric channel (BSC) and AWGN channel for illustration. We consider the encoding scheme with i.i.d. on-off signaling and ones' density ($P(X_i = 1) = p$). Since energy arrivals are i.i.d., the battery state process can be modelled as a Markov chain shown in Fig. 4.1. The stationary probabilities of the battery states are given as

$$P(S = 0) = \pi_0 = \frac{(1-q)p}{(1-q)p + q \sum_{i=0}^{B_{max}-1} (\frac{q(1-p)}{p(1-q)})^i} \tag{4.1}$$

$$P(S = i) = \pi_i = \frac{1}{1-q}(\frac{q(1-p)}{p(1-q)})^i \pi_0, \ i = 1, ..., B_{max}. \tag{4.2}$$

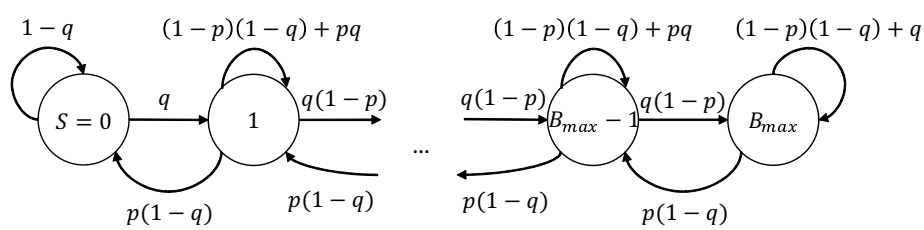

Figure 4.1: Markov chain model of the battery state with battery capacity B_{max}.

If the receiver ignores the memory in the model and considers a channel with i.i.d. states with the state probabilities given above, namely, using NIID [14], the achievable rate over a BSC with crossover probability ϵ and an AWGN channel

with noise variance $\frac{N_0}{2}$ are given as

$$R_{NIID-BSC} = \max_{p\in[0,1]} H_2\Big(p((1-\pi_0)(1-\epsilon)+\pi_0\epsilon)+(1-p)\epsilon\Big)$$
$$- pH_2\Big((1-\pi_0)(1-\epsilon)+\pi_0\epsilon\Big) - (1-p)H_2(\epsilon), \tag{4.3}$$
$$R_{NIID-AWGN} = \max_{p\in[0,1]} I(Y;M) = \max_{p\in[0,1]} h(Y) - h(Y|M), \tag{4.4}$$

respectively, where $H_2(.)$ is the binary entropy function, and

$$Y \sim \Big((1-p)+p\pi_0\Big)\mathcal{N}(0,N_0/2) + p(1-\pi_0)\mathcal{N}(1,N_0/2),$$
$$Y|M \sim \begin{cases} \mathcal{N}(0,N_0/2) & \text{if } M=0, \\ \pi_0\mathcal{N}(0,N_0/2)+(1-\pi_0)\mathcal{N}(1,N_0/2) & \text{if } M=1, \end{cases}$$

and $\mathcal{N}(0,N_0/2)$ represents the zero mean Gaussian distribution with variance $\frac{N_0}{2}$. Note that in both (4.3) and (4.4) the parameter π_0 depends on the ones' density p. For the AWGN case, the signal to noise ratio is defined as the ratio of energy arrival rate to the noise power, namely, SNR= $\frac{q}{N_0}$.

The optimal ones' density p to achieve $R_{NIID-BSC}$ over a BSC(0.1) is depicted in Fig. 4.2. Clearly, the optimal ones' density in most cases is not uniform which suggests that using linear block codes which induce a uniform input distribution of "0"s and "1"s, by themselves is not optimal, namely, one can obtain higher rates by using nonlinear codes for reliable information transmission.

When the battery capacity increases, the optimal ones' density approaches the energy arrival probability for the interval $0 < q < 0.5$, and it becomes uniform for $0.5 \leq q \leq 1$. Another interesting observation from Fig. 4.2 is that when the battery capacity is small and energy arrival probability is also very small, e.g., $q = 0.12$ or lower, the optimal ones' density is larger than the energy arrival probability.

Fig. 4.3 depicts the achievable rates for the special case of $q = 0.4$ over an AWGN channel for which the ones' density $p = 0.25$ is optimal for high SNRs. As it is shown in this figure, by using a ones' density of $p = 0.25$, higher rates

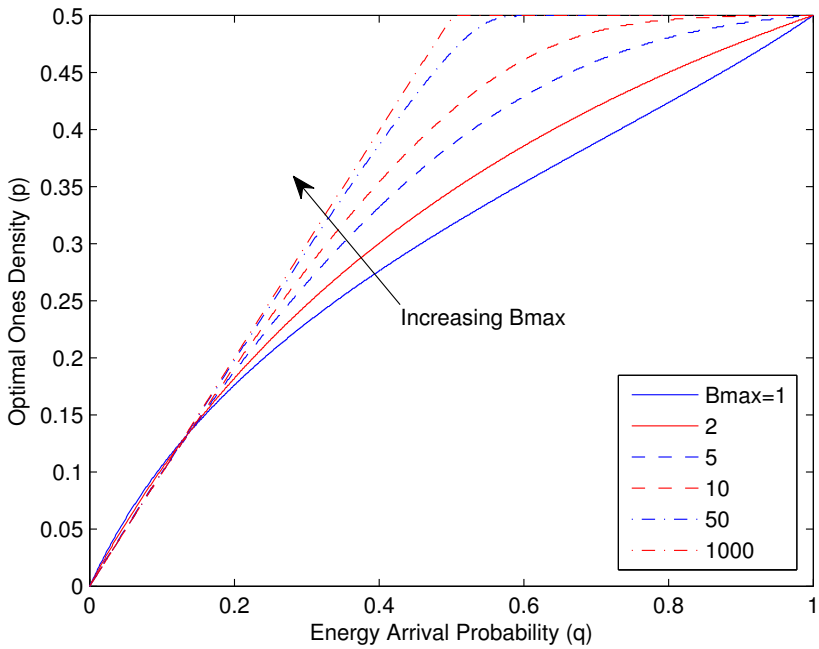

Figure 4.2: Optimal ones' density for the NIID scheme for binary input energy harvesting BSC(0.1).

compared to those of uniform inputs can be achieved.

4.3 Proposed Coding Scheme

As described in the previous section, in order to achieve R_{NIID}, a specific input distribution at the channel input (which is usually nonuniform) needs to be employed. To generate the required nonuniform input distribution and also to obtain good error correction performance, in this chapter, we propose concatenation of an outer linear block code such as an LDPC code with an inner nonlinear trellis code as a practical approach.

Fig. 4.4 depicts the block diagram of the proposed coding scheme. The transmitter side consists of concatenation of an outer LDPC encoder with an inner nonlinear trellis encoder with a battery state conditioner, which is then connected

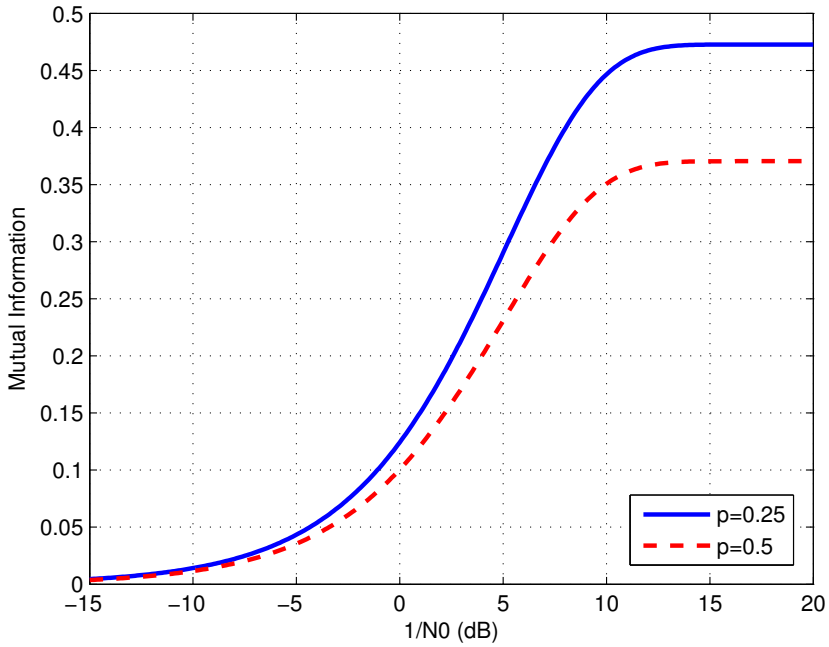

Figure 4.3: Achievable rates with the NIID scheme over an AWGN channel with $q = 0.4$.

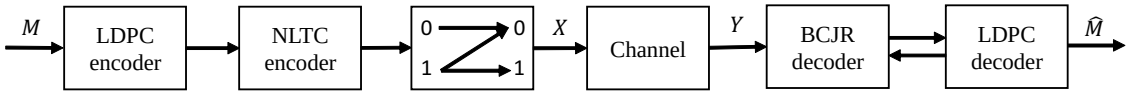

Figure 4.4: Block diagram of the proposed coding scheme.

to the channel. Battery state conditioner simply applies the battery outage effect which is nothing but transmitting symbol 0 when the battery is empty. Considering an LDPC code of rate R_1 and an NLTC of rate R_2, the overall code rate is equal to $R_1 R_2$. The goal of the inner NLTC is to induce the desired nonuniform distribution at the channel input while providing error protection against channel noise. The outer LDPC code is intended to provide error correction capabilities.

At the receiver side, as a simple approach, we first ignore the memory in the channel state and consider a channel with i.i.d. states with stationary probabilities given in (4.1)-(4.2). As a result we have a memoryless Z channel with crossover $1 \to 0$ probability π_0 connected to the memoryless noisy channel (which

is either a BSC or an AWGN channel in our setting). Then a BCJR algorithm based decoder is adopted for the two step memoryless channel computing the LLRs of the encoded bits to be fed to the LDPC decoder. To improve the decoding performance, the soft outputs of the LDPC decoder are fed back to the BCJR decoder in an iterative fashion as also illustrated in Fig. 4.4. The decoding scheme described above is used for the code design purposes in the next section, however, we introduce another (improved) iterative decoding solution in Section 4.3.3 which exploits the memory in the battery state as well.

4.3.1 Inner NLTC Design

To design the inner NLTC, we utilize the algorithm developed in 3.3 which maximizes the minimum distance of the code while keeping a desired ones' density. As it will be stated in Section 5.4, having a larger minimum distance helps with the stability of the iterative decoding process. Also, it is a valid criterion for designing trellis-base codes for P2P scenarios. The output of the design algorithm is a lookup table which assigns specific labels to the branches of the trellis in such a way that ensures the specific distribution of ones and zeros, and provides a large minimum distance.

4.3.2 Outer LDPC Code Design

Off-the-shelf LDPC codes that are optimized for P2P communication scenarios (e.g., for AWGN channels) are not optimal for the case of energy harvesting communication systems, that is, one needs to optimize the degree distribution of the LDPC ensemble (for each specific energy harvesting scenario). To accomplish this, we fix the inner NLTC (which is specifically designed to provide the optimal ones' density for the particular energy harvester parameters, e.g., battery size, energy arrival probability), and perform optimization of the LDPC degree distribution. LDPC code optimization can be done based on different objectives such

as decoding threshold optimization or rate maximization. In this chapter, we employ the latter approach. Among different algorithms and techniques available, we utilize the EXIT analysis [106] to measure the iterative decoding threshold of the concatenated coding scheme, and employ the random perturbation algorithm to generate new instances of the LDPC degree distribution.

We assume symmetry of the probability density function (PDF) of the exchanged LLRs between the component decoders, and perform the EXIT analysis by using Monte Carlo simulations without any assumption on the Gaussianity of the exchanged LLRs [20]. We follow the approach taken in [107] and compute the extrinsic mutual information using

$$I(L;X) \approx 1 - \frac{1}{N}\sum_{n=1}^{N} \log_2(1+e^{-L_n}) \tag{4.5}$$

with L_n denoting the LLR corresponding to the nth coded bit of the all-zero codeword. We utilize i.i.d. channel adaptors introduced in [108] with common randomness at the transmitter and the receiver sides for each message to validate the all-zero codeword transmission assumption. Using Monte Carlo simulations for sufficiently long block lengths (taken as 10^6 in this study) for the iterative decoder, and tracking the evolution of the mutual information at the output of the component decoders, we check for convergence. We use perturbing vectors to generate new instances of the degree distributions with the goal of maximizing the rate of the code. Then, we check the convergence of the iterative decoding for the new degree distribution ensemble using the EXIT analysis. We terminate the optimization procedure if no improvement can be obtained after a predetermined number of iterations. Further details about the LDPC code design by using random perturbation technique will be given in Section 5.3.3.

4.3.3 An Improved Iterative Decoding Algorithm

As a second decoding approach, we propose building an extended trellis by including the battery state at the beginning of each trellis section along with the

NLTC states which expands the size of the trellis by a factor of $B_{max} + 1$, i.e., for each NLTC state, there are $B_{max} + 1$ corresponding states in the extended trellis, namely, one for each battery state in $\{0, 1, ..., B_{max}\}$. Each transition in the NLTC trellis corresponds to $(B_{max} + 1)^2$ transitions in the extended trellis, however, some of these transitions might be invalid depending on the current and the next battery states and the output label in the NLTC.

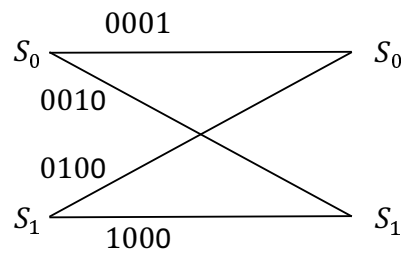

Figure 4.5: The 2-state NLTC.

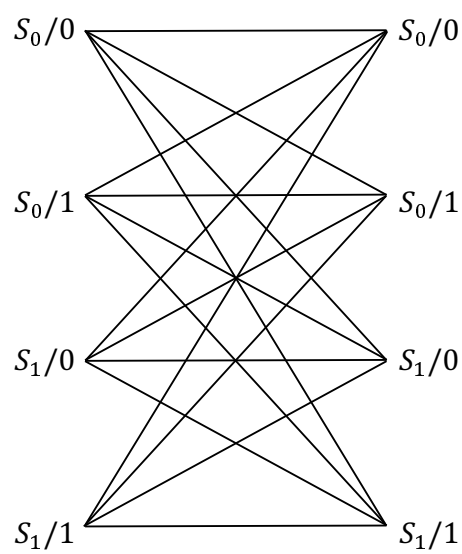

Figure 4.6: The extended trellis section for 2-state NLTC and unit-sized battery.

Let us illustrate this idea by a simple example. Consider a simple two state NLTC given in Fig. 4.5. Assuming that the energy harvester is equipped with a unit-sized battery, a section of the extended trellis diagram for this code is

Table 4.1: Labels corresponding to the transitions of the extended trellis and their probabilities.

Current State	Next State	Output Label	Probability
$S_0/0$	$S_0/0$	0000	$\bar{q}^4$
		0001	$(1-\bar{q}^3)\bar{q}$
$S_0/0$	$S_0/1$	0000	$\bar{q}^3 q$
		0001	$(1-\bar{q}^3)q$
$S_0/1$	$S_0/0$	0001	$\bar{q}$
$S_0/1$	$S_0/1$	0001	q
$S_0/0$	$S_1/0$	0000	$\bar{q}^4$
		0010	$(1-\bar{q}^2)\bar{q}^2$
$S_0/0$	$S_1/1$	0000	$\bar{q}^2(1-\bar{q}^2)$
		0010	$(1-\bar{q}^2)^2$
$S_0/1$	$S_1/0$	0010	$\bar{q}^2$
$S_0/1$	$S_1/1$	0010	$1-\bar{q}^2$
$S_1/0$	$S_0/0$	0000	$\bar{q}^4$
		0100	$q\bar{q}^3$
$S_1/0$	$S_0/1$	0000	$\bar{q}(1-\bar{q}^3)$
		0100	$q(1-\bar{q}^3)$
$S_1/1$	$S_0/0$	0100	$\bar{q}^3$
$S_1/1$	$S_0/1$	0100	$1-\bar{q}^3$
$S_1/0$	$S_1/0$	0000	$\bar{q}^4$
$S_1/0$	$S_1/1$	0000	$1-\bar{q}^4$
$S_1/1$	$S_1/0$	1000	$\bar{q}^4$
$S_1/1$	$S_1/1$	1000	$1-\bar{q}^4$

shown in Fig. 4.6. The state S_i/x corresponds to the case where the NLTC state is S_i and the battery state is x. The labels corresponding to each transition of the extended trellis along with their probabilities are given in Table 4.1 where $\bar{q} = 1 - q$. In this approach, the BCJR decoder operates on the extended trellis and exchanges the soft extrinsic LLRs with the LDPC decoder in an iterative manner. Complexity increase for the improved decoder compared to the simple decoding scheme is at most quadratic which can be tolerated even for code design purposes, however, we do not use this scheme for designing codes in this chapter. We demonstrate the superior performance of this approach via finite block length BER simulations using the specific codes taken from the designed ensembles of the

previous subsection. We also note that, reduced complexity trellis-based decoders can also be employed to obtain computationally simpler decoding solutions while still utilizing the extended trellis.

4.4 Numerical Examples

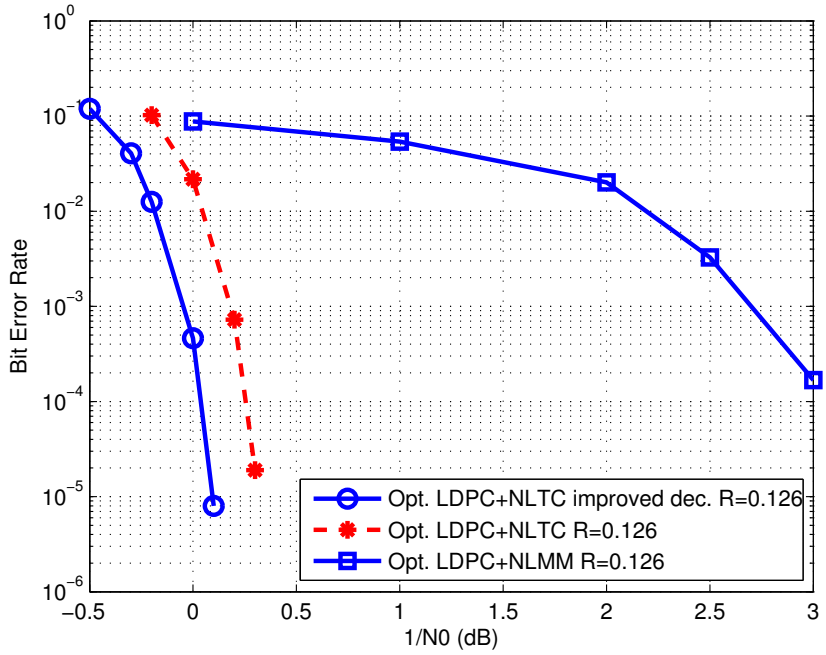

Figure 4.7: BER performance of the proposed concatenated coding scheme with simple and improved decoding compared to that of the reference scheme ($q = 0.4$).

As a first example, we consider an energy harvester with a unit-sized battery and energy arrival probability of $q = 0.4$ over an AWGN channel for which the achievable rates using ones' density of 0.25 and 0.5 are shown in Fig. 4.3. We consider a ones' density $p = 0.25$ which is the optimal ones' density for this energy arrival probability at high SNRs and design an NLTC satisfying this constraint while maximizing the minimum distance of the code. Details of the designed trellis code are given in Table 4.2. In the next step, by fixing the inner NLTC, the outer

LDPC code is designed by maximizing the rate of the code for a convergence threshold of 0 dB for which the result is given in Table 4.3. Also concatenation of a nonlinear memoryless mapper (NLMM) (of the same rate and ones' density as the designed NLTC) with an optimized outer LDPC code is considered as reference.

Table 4.2: Label assignment to the branches of 16-state trellis ($M = 4$) for the designed NLTC.

State/Input								Output
0000/0	0001/1	0100/1	0101/0	1010/0	1011/1	1110/1	1111/0	0001
0000/1	0001/0	0100/0	0101/1	1010/1	1011/0	1110/0	1111/1	0010
0010/0	0011/1	0110/1	0111/0	1000/0	1001/1	1100/1	1101/0	0100
0010/1	0011/0	0110/0	0111/1	1000/1	1001/0	1100/0	1101/1	1000

Table 4.3: Optimized degree distribution of the outer LDPC code for the proposed coding scheme.

	λ_2	λ_3	λ_4	λ_5		
Ex.1 (AWGN)	0.492561	0.106999	0.399260	0.001180		
Ex.2 (BSC)	0.568342	0.067598	0.351750	0.012310		
	ρ_2	ρ_3	ρ_4	ρ_8	ρ_14	ρ_15
Ex.1 (AWGN)	0.012700	0.405182	0.034768	0.027342	0.025157	0.494851
Ex.2 (BSC)	0.000208	0.088826	0.004891	0.067288	0.254800	0.583986

To study the performance of the specific codes from the designed ensemble, parity check matrices for a block-length of 10k are obtained using the tools in [104] where the length-4 cycles are removed for improved performance. The resulting BERs are depicted in Fig. 4.7. The overall code rate for both schemes are 0.126. We observe that the designed codes via the proposed coding solution outperform the reference scheme by about 2.5 dB at a BER of 10^{-3}. Furthermore the superior performance of the improved decoding scheme compared to the simple one (by about 0.25 dB at the same BER value) can be observed from the simulations.

As a second example, we consider an energy harvester with a unit-sized battery

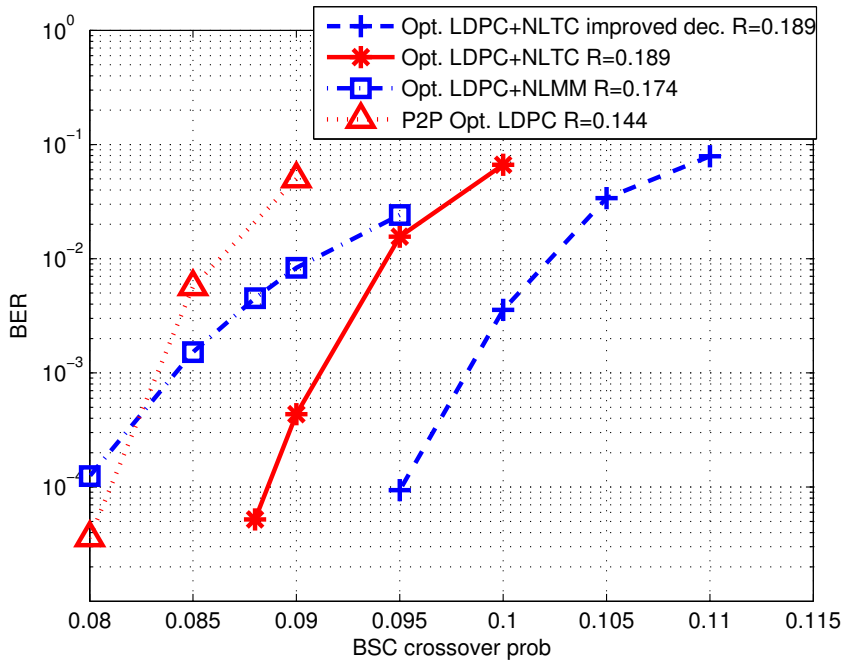

Figure 4.8: BER performance of the proposed concatenated coding scheme and reference scheme ($q = 0.34$).

and an energy arrival probability of $q = 0.34$ over a BSC with crossover probability $\epsilon = 0.1$. The optimal ones' density for this setup is $p = 0.25$, hence we use the same NLTC as the one in the previous example. We optimize the outer LDPC code for this channel by fixing the inner NLTC and maximizing the rate of the LDPC code ensemble (see Table 4.3 for the resulting degree distributions). The achieved rates by using the proposed scheme and reference scheme are 0.1892 and 0.1741, respectively. We note that the achieved rate of 0.1892 has a very small gap (of only 0.009) with the achievable information theoretic limit by using the NIID strategy.

We also construct specific LDPC codes with block lengths of 10k using the optimized degree distributions employing the tools in [104], and perform BER simulations. The results are illustrated in Fig. 4.8. It can be observed that the newly designed codes provide clear rate and error rate benefits compared to the reference scheme of using nonlinear memoryless mappers with optimized outer

LDPC codes, and P2P optimal codes. In addition, simulation results show that, for example, at a crossover probability of $\epsilon = 0.095$, an improvement of about two orders of magnitude in the BER can be obtained by using the improved iterative decoding solution compared to the simple approach in Section 4.3. Note that since the capacity is unknown for these examples, we do not provide a comparison with the information theoretic limits.

4.5 Chapter Summary

In this chapter, we have considered a binary energy harvesting communication system over noisy channels, and designed explicit and implementable codes based on a concatenated coding solution consisting of an inner NLTC and an outer LDPC code. At the receiver side, two decoding approaches are studied. The first one ignores the memory in the battery state, while the second one incorporates this memory into the trellis resulting in an extended trellis. For both cases, the BCJR decoder iteratively exchanges soft information with the LDPC decoder. To design the outer LDPC code, we utilize the first decoding scheme which is simpler. Through several numerical examples for different channel models, we illustrate that the newly designed codes outperform the alternatives of using P2P optimal codes and the reference scheme of utilizing nonlinear memoryless mappers with specifically optimized LDPC codes.

Chapter 5

Code Design for Discrete Memoryless Interference Channels

In this chapter, we study design of explicit and implementable codes for the two-user DMICs. We consider an HK type encoding where both public and private messages are used, and propose coding techniques utilizing a serial concatenation of an NLTC with an outer LDPC code. Since exact analytical treatment of the BCJR decoder for the inner trellis-based code appears infeasible, we analytically investigate the iterative decoding process in the asymptotic regime where the probability of decoding error tends to zero. Based on this approximate analysis, we derive a stability condition for this type of a concatenated coding scheme for the first time in the literature. Furthermore, we use an extrinsic information transfer (EXIT) analysis to design the outer LDPC code while fixing the inner NLTC, and utilize the derived stability condition to accelerate the design process and to avoid code ensembles that potentially produce high error floors. Via numerical examples, we demonstrate that our designed codes achieve rate pairs close to the optimal boundary of the HK subregion, which cannot be obtained

The material in this chapter has been submitted to IEEE Transactions on Communications [22].

without the use of nonlinear codes. Also we verify the estimated thresholds of the designed codes via finite block length simulations, and show that our designs significantly outperform the point-to-point optimal codes, hence demonstrating the need for designs specifically tailored for DMICs.

The rest of the chapter is organized as follows. In Section 5.1 we review the information theoretic results in the literature for DMICs and some recent works on code design for interference channels. In Section 5.2, we describe the system model for a two user DMIC. We explain the proposed coding scheme and elaborate the code design process in Section 5.3. We provide an asymptotic analysis of the concatenated coding scheme over both symmetric and asymmetric channels, and derive the stability condition for the convergence of the iterative decoder in Section 5.4. Section 5.5 includes three different sets of DMIC examples with several newly designed codes for each case. Concluding remarks are provided in Section 5.6.

5.1 Introduction

As we reviewed in Section 2.3, interference channels have been studied mostly from information theoretic perspective and only a few works have been reported on designing practical and implementable codes. In this chapter, our objective is to consider the case of generic DMICs, and design explicit and implementable codes for different scenarios as a complementary work to [16–18, 95, 96] which focus on the case of GICs.

Recent studies have investigated optimal transmission strategies for some instances of multi-user channel models. The authors in [109] present an optimal transmission strategy for the broadcast Z channel with independent encoding and successive decoding. They employ nonlinear turbo codes with a desired distribution of ones and zeros in their codebook to operate close to the optimal rate region boundary. A capacity-achieving encoding scheme is designed for a general degraded binary broadcast channel in [110]. The designed scheme uses simple

logical operators (i.e., XOR, OR and AND) at the output of independent binary encoders to achieve the capacity boundary. In [111], a relatively simple encoding scheme which is called natural encoding is shown to achieve the capacity of several classes of discrete memoryless degraded broadcast channels. Design of NLTCs for binary-input binary-output MACs has been investigated in [100] where a non-uniform distribution of ones and zeros is required. A polar coding scheme for the two user DMIC is introduced in [112] which achieves the HK inner bound and generalizes to interference networks. The authors in [113] propose a simplified design of polar codes to achieve the HK region for the two-user DMIC which does not require mapping functions from auxiliary random variables to channel inputs. While these studies on the use of polar codes over DMICs show the asymptotic achievability of the HK inner bound, they do not provide explicit and implementable codes, which motivates our approach in this chapter.

In this chapter, we consider practical code design for different instances of DMICs. We employ an HK type encoding by considering private and public messages for both users and decoding both intended messages and public message of the other user at each decoder. As a practical coding scheme we propose a serial concatenation of a trellis based code (which can be an NLTC or a convolutional code depending on the required distribution for each message) with an outer LDPC code. In order to design the inner trellis based code we adopt the algorithm proposed in [20], which is based on maximizing the minimum distance of the code. Motivated by their excellent performance over various channels, we use irregular LDPC codes as the outer codes in the concatenated coding scheme. At the receiver side, we utilize an iterative decoder composed of a BCJR decoder over the extended trellis for the inner codes, and a component belief propagation decoder for each of the outer LDPC codes. Furthermore, we optimize the degree distribution of the outer LDPC codes via an instance of differential evolution [102], namely, the random perturbation technique armed with the extrinsic information transfer (EXIT) analysis. In some special cases, we also consider a simpler version of the proposed coding scheme by utilizing only private messages, or one user's message as public while the other is private.

Another main contribution of this chapter is the development of a general stability condition for the concatenated coding scheme (over symmetric and asymmetric channels), which is applicable more broadly than the present set-up. We utilize the derived stability condition to accelerate the LDPC code design process, and to avoid code ensembles that potentially produce high error floors. Through several examples, we explicitly show that our designed codes operate at rates close to the optimal rate region boundaries and significantly outperform the single user codes with time sharing. Additionally, we demonstrate that by utilizing the concatenated coding scheme with the inner NLTC, one can achieve rate pairs that cannot be obtained by linear codes alone.

5.2 System Model

A two sender-receiver pair communication system is depicted in Fig. 5.1, where each sender wishes to communicate a message to its corresponding receiver over a shared interference channel. The discrete IC is specified by its finite input alphabets $\mathcal{X}_1$ and $\mathcal{X}_2$, finite output alphabets $\mathcal{Y}_1$ and $\mathcal{Y}_2$, and the channel transition probabilities

$$p(y_1|x_1x_2) = \sum_{y_2\in\mathcal{Y}_2} p(y_1y_2|x_1x_2), \tag{5.1}$$

$$p(y_2|x_1x_2) = \sum_{y_1\in\mathcal{Y}_1} p(y_1y_2|x_1x_2). \tag{5.2}$$

We also assume that the IC is memoryless, i.e.,

$$p(y_1^n y_2^n|x_1^n x_2^n) = \prod_{i=1}^{n} p(y_{1i}y_{2i}|x_{1i}x_{2i}) \tag{5.3}$$

where the subscript i denotes the time instant. The HK ARR for this channel can be found in [69, 70, Page 143].

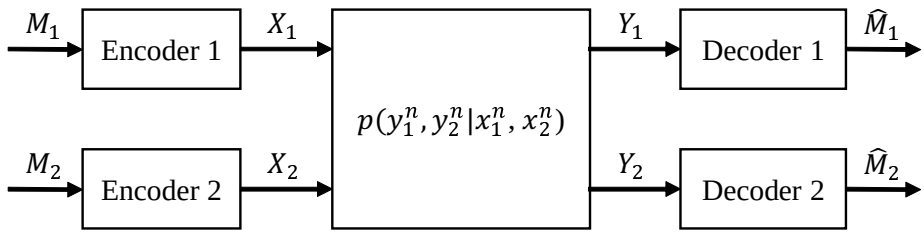

Figure 5.1: Block diagram of the two-user interference channel.

5.3 Proposed Coding Scheme

5.3.1 Encoding and Decoding

We consider practical code design for different instances of DMICs in which, we restrict ourselves to the case of binary inputs and binary outputs. We employ an HK type encoding which assumes transmitting private and public messages for each user, and decoding three messages (both intended messages and the public message of the other user) at each decoder. Since communication takes place over an IC, there is a tradeoff between the rates at which both users can reliably communicate. Because of this reason, one may use different input distributions and obtain different optimal rate pairs on the boundary of the achievable rate region. In order to operate at one of these points, a specific input distribution is required for each message which is usually nonuniform. On the other hand, linear codes (e.g., LDPC codes) induce a uniform distribution of 0's and 1's, hence new solutions are needed for implementable coding solutions over ICs.

In order to obtain good error correction performance and to generate the required nonuniform input distributions, we propose employing concatenation of an outer LDPC code with an inner nonlinear trellis code as a practical and implementable solution. Fig. 5.2 depicts the block diagram of the proposed coding scheme for a two-user IC. The transmitter side consists of concatenation of an outer LDPC code and an inner trellis based code for either one of the public and private messages of each user, which are then connected to the channel after

superposition. The objective of the inner trellis based code is to introduce the required distribution at the channel input while also providing further protection against channel noise. For the cases where the optimal input distribution is uniform, we can remove the trellis based code, and employ only an LDPC code. At the receiver sides, BCJR algorithm based decoders operating over the product trellises of the NLTCs are adopted to compute the LLRs of the encoded bits which are then iteratively exchanged with the respective LDPC decoders to improve the decoding performance.

While the general HK type encoding can be implemented using the proposed scheme, it is not necessary for certain special cases and one may use simpler versions, e.g., by utilizing only private messages, or only public messages. We note that for the case of using only private messages and treating interference as noise at both decoders, the problem becomes similar to transmitting over a point-to-point asymmetric channel which has been studied in several papers, e.g., in [114], which introduces three different approaches to achieve the capacity of asymmetric channels. We emphasize, however, that this work does not provide any explicit code design. We also note that the proposed scheme in this chapter is more general than the problem of code design over asymmetric channels as it provides a practical HK type coding solution for DMICs.

5.3.2 Inner NLTC Design

An NLTC design algorithm is developed in [20] with the goal of maximizing the minimum distance of the code while keeping a desired ones' density. The result of the design algorithm is a lookup table which determines the assignment of the labels to the branches of the trellis. As we will discuss later in Section 5.4, having a larger minimum distance helps with the stability of the iterative decoding process and provides a lower error floor for the concatenated coding scheme. Therefore, we utilize the approach in [20] to design the inner NLTC needed in our set-up.

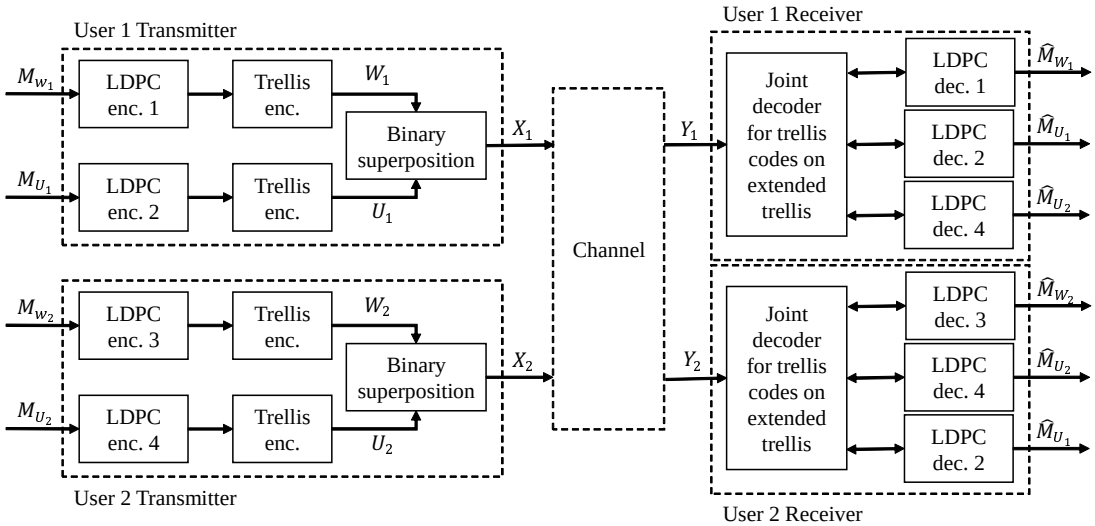

Figure 5.2: Block diagram of the proposed coding scheme.

5.3.3 Outer LDPC Code Design

Due to the use of an inner code and the presence of interference, off-the-shelf LDPC codes that are optimized for P2P communications may not be optimal in our set-up. That is, we need to design new LDPC codes for each specific scenario. After we fix the inner NLTC (as in the previous subsection), we optimize the degree distribution of the LDPC code ensemble for which we can utilize different algorithms such as linear programming or random perturbation, and various analysis techniques such as density evolution or EXIT analysis. Density evolution, which is introduced in [103], is a method to track the probability density functions (PDFs) of the exchanged LLRs in the belief propagation decoder analytically. However, the analytical treatment of the BCJR decoder is not feasible [106], and hence, it is not a reasonable choice for analyzing the behavior of the iterative decoding process for the proposed concatenated scheme.

EXIT analysis is a method developed to track the evolution of the mutual information between the transmitted bits and the corresponding LLRs [106], which

requires a significantly lower computational complexity. In this chapter, we utilize an EXIT analysis without making any assumptions on the Gaussianity of the PDFs of the exchanged LLRs within the decoder. The only assumption is the symmetry of the PDFs of the exchanged LLR values between the component decoders defined as the condition $f(x) = e^x f(-x)$ for $x \in \mathbb{R}$ where f denotes a PDF. As we will discuss in detail in Section 5.4, the LLR symmetry property is satisfied for the exchanged LLRs in the iterative decoding of the proposed class of concatenated codes, hence our approach is valid. However, the channel output symmetry, which enables us to consider transmission of the all-zero codeword is not valid for multi-user scenarios; and, in order to overcome this problem, we utilize independent and identically distributed (i.i.d.) channel adaptors with common randomness at the transmitter and receiver sides for each message [108]. We note that the i.i.d. channel adaptors are utilized for the sake of analysis only and they are neither needed nor utilized for the actual communication system. Then, we follow the approach taken in [107] and compute the extrinsic mutual information as

$$I(L;X) \approx 1 - \frac{1}{N}\sum_{n=1}^{N} \log_2(1 + e^{-L_n}) \tag{5.4}$$

with L_n denoting the LLR corresponding to the nth coded bit of the all-zero codeword.

Inspired by the results of [99], in order to get lower decoding thresholds, we select an initial degree distribution with multiple degrees at both variable and check node sides with a rate lower than the final goal such that it satisfies the stability condition. Using the Monte Carlo simulations for sufficiently long block lengths (taken as 10^6 for the LDPC codeword length in this study), and running the iterative decoding algorithm, we check the admissibility of the initial degree. More precisely, we track the evolution of the mutual information at the output of the variable node decoder and the check node decoder, and stop and call the degree distribution admissible if; first the mutual information at the output of the check nodes evolves to 0.99, which corresponds to converging to a very small bit error probability [18], second if the stability condition is satisfied for the degree distribution ensemble, which verifies the convergence to zero error probability

after decoding to a very small probability of error. In case the selected degree is not admissible, we choose another degree distribution (satisfying the stability condition) until we obtain an admissible initial degree.

We employ a specific implementation of differential evolution [102] for designing the outer LDPC code. Having obtained the admissible initial degree distributions, we use perturbing vectors to generate a new instance with the goal of maximizing the rate of the code. Both variable node and check node degree distributions are perturbed as $\hat{\lambda}_i = \lambda_i + e_{1i}$, $\hat{\rho}_j = \rho_j + e_{2j}$ where e_{1i} and e_{2j} denote the ith and the jth elements of the perturbing vectors. For the degree distribution to be valid the following equations should be satisfied

$$\sum_{i=2}^{d_v} \lambda_i + e_{1i} = 1, 0 \leq \lambda_i + e_{1i} \leq 1, 2 \leq i \leq d_v, \tag{5.5}$$

$$\sum_{j=2}^{d_c} \rho_j + e_{2j} = 1, 0 \leq \rho_j + e_{2j} \leq 1, 2 \leq j \leq d_c. \tag{5.6}$$

At each iteration of the perturbation, we increase the current rate (r) by ΔR, which enforces,

$$1 - \frac{\sum_{j=2}^{d_c} \frac{\rho_j + e_{2j}}{j}}{\sum_{i=2}^{d_v} \frac{\lambda_i + e_{1i}}{i}} = r + \Delta R. \tag{5.7}$$

We draw all the elements of the perturbing vectors except three from a normal distribution $\mathcal{N}(0, \sigma^2)$ where σ is a design coefficient [18]. The remaining three elements are obtained by solving (5.5)-(5.7). The perturbed degree distribution will replace the current one if it is admissible, otherwise it is dismissed and new perturbation is performed. The procedure is terminated if no improvement can be obtained after a predetermined number of iterations.

5.4 Asymptotic Analysis of the Iterative Decoder

In this section, we derive a stability condition for the iterative decoder which specifies its convergence behavior when the probability of the decoding error is very small, namely, it shows whether the probability of error will converge to zero or not. Another important consequence of the stability condition is that the implied upper bound on the threshold, in some cases, is tight. Stability condition has been derived for different cases before, e.g., LDPC codes in P2P scenarios, Gaussian broadcast channels and GICs, also parallel and serially concatenated turbo codes in [18,88,103,115], respectively. On the other hand, it is not available for concatenation of LDPC codes with inner trellis-based codes, which motivates us to derive it for the concatenated coding scheme in a general form, and utilize it in the design of the outer LDPC codes for the specific scenario.

We first go over some definitions and state several propositions that will help in our presentation later in this section. In the following definitions, the term "mapper" refers to a memoryless one-to-one mapper.

Definition 1. *The distance spectrum of a codeword is the set of all Hamming distances from that specific codeword to all other codewords.*

Definition 2. *A code is called symmetric if the distance spectrum of all of its codewords are the same.*

All binary linear codes, specifically, convolutional codes are instances of such symmetric codes.

Definition 3. *A one-to-one mapper for which the input labels are the set of all binary sequences of length m_i, and the Hamming distance between each pair of the output labels are the same is called* pairwise symmetric.

An example of pairwise symmetric mapper is $\{00, 11, 01, 10\} \rightarrow \{100, 010, 001, 111\}$.

Proposition 1. *Combination of a convolutional code with a pairwise symmetric mapper is a symmetric code.*

The proof is straightforward and follows from the Definitions 2 and 3.

Definition 4. *Directional Hamming distance* $d_D(c_1, c_2) = (d_{01}, d_{10})$ *is a pair of distance values for which* d_{01} (d_{10}) *is the number of positions at which* c_1 *has a 0 (or 1) and* c_2 *has a 1 (or 0), respectively.*

Note that $d_D(c_1, c_2)$ is not necessarily equal to $d_D(c_2, c_1)$.

Definition 5. *A one-to-one mapper for which the input labels are the set of all binary sequences of length* m_i *and the directional Hamming distance between each pair of the output labels are the same is called* pairwise directional symmetric.

An example of pairwise directionally symmetric mapper is $\{00, 11, 01, 10\} \rightarrow \{1000, 0100, 0010, 0001\}$.

Definition 6. *A code for which the directional distance spectrum of all of the codewords are the same is called* directionally symmetric.

One may note that the directional symmetry of a code is a stronger property than symmetry.

Proposition 2. *Combination of a convolutional code with a pairwise directional symmetric mapper is a directionally symmetric code.*

The proof is straightforward and follows from the Definitions 4, 5 and 6.

5.4.1 LLR Symmetry Property

It is shown in [103] that for an output-symmetric channel[1], the PDFs of the LLRs passed between variable and check node decoders of an LDPC code are

[1]By an output symmetric channel we mean that $p(y|x = 1) = p(-y|x = -1)$ where $p(y|x = i)$ is the conditional probability of the channel output y given that channel input $x = i$.

symmetric. On the other hand, an exact analytical investigation of the BCJR decoder regarding the densities of the extrinsic LLRs seems infeasible. However, for parallel concatenated turbo codes, the symmetry property for the exchanged extrinsic LLRs between the component decoders is stated as an observation in [106]. Similarly, our extensive large block length simulations show that the symmetry property holds for the proposed concatenated scheme as well (at least approximately), i.e.,

$$\langle f_e(m) \rangle = \frac{f_{e,0}(m) + f_{e,1}(-m)}{2} \tag{5.8}$$

is symmetric, where $f_{e,0}$ and $f_{e,1}$ denote the codeword averaged LLR densities corresponding to transmitting input bit 0 and 1, respectively.

For the cases of symmetric trellis codes over a symmetric channel or directionally symmetric codes over an asymmetric channel, it is sufficient to use the codeword corresponding to the all-zero message to obtain the average LLR density $\langle f_e(m) \rangle$ which will be equal to $f_{e,0}$. For all other cases, one can take an average over a large block length typical codeword with a uniform 0 and 1 distribution to estimate $\langle f_e(m) \rangle$.

Considering that the density evolution equations at the variable and check nodes of the LDPC code preserve the symmetry property [103], the LLR densities at the output of each component decoder will be symmetric as well.

5.4.2 Asymptotic Density Evolution for Trellis-Based Codes

An approximate asymptotic density evolution analysis for recursive systematic convolutional codes has been performed in [115]. Inspired by this approach, we analyze the asymptotic behavior of the BCJR decoder for other classes of trellis-based codes on a general asymmetric channel. We consider the case of a non-recursive non-systematic convolutional code plus a one-to-one memoryless mapper as the trellis-based code in this analysis. We focus on the case of an asymmetric channel case since in multi-user communications, specifically for ICs,

users (often) experience asymmetric channels. We will specialize this analysis to the case of a symmetric channel later in this section.

We denote the PDF of the channel LLRs, a priori LLRs from the VND to the BCJR decoder, extrinsic LLRs at the output of the BCJR decoder, and the LLRs from VND to CND (at the lth iteration) as f_r, f_a, f_e and P_l, respectively, in which for the first three, the subscript l is dropped, as shown in Fig. 5.3. We consider the regime where the bit error probability $\mathcal{P}(f_a) \to 0$. Assuming that the all zero sequence is transmitted [2], the bit error probability is obtained as follows

$$\mathcal{P}(f) = \int_{-\infty}^{0} f(x)dx. \tag{5.9}$$

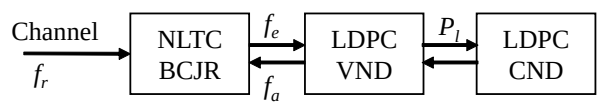

Figure 5.3: Iterative decoder for concatenated code.

The LLR at the output of the BCJR decoder for the trellis-based code which is a bitwise maximum a posteriori (MAP) decoder can be expressed as

$$L_k = \log \frac{P(c_k = 0|\mathbf{y})}{P(c_k = 1|\mathbf{y})} = \log \frac{\sum\limits_{\mathbf{x}, c_k(\mathbf{x})=0} P(\mathbf{x}|\mathbf{y})}{\sum\limits_{\mathbf{x}, c_k(\mathbf{x})=1} P(\mathbf{x}|\mathbf{y})} \tag{5.10}$$

where $\mathbf{x}$ is the codeword at the input of the channel and $c_k(\mathbf{x})$ is the kth bit of the message corresponding to the codeword $\mathbf{x}$. With the assumption that $\mathcal{P}(f_a) \to 0$, the probability term $P(\mathbf{x}) \to 1$ for the correct codeword and $P(\mathbf{x}) \to 0$ for all other codewords. In other words, the summations can be approximated by maximum operations, i.e.,

$$L_k \simeq \max_{\mathbf{x}, c_k(\mathbf{x})=0} \log P(\mathbf{x}|\mathbf{y}) - \max_{\mathbf{x}, c_k(\mathbf{x})=1} \log P(\mathbf{x}|\mathbf{y}). \tag{5.11}$$

[2]This assumption is valid for the LDPC code by utilizing an i.i.d. random channel adaptor between the outer and the inner code

We assume the transmission of a random codeword $\mathbf{x}^*$ with a uniform probability over the codebook and define a modified LLR L_k^* as follows

$$L_k^* = \log \frac{\sum_{\mathbf{x}, c_k(\mathbf{x})=c_k(\mathbf{x}^*)} P(\mathbf{x}|\mathbf{y})}{\sum_{\mathbf{x}, c_k(\mathbf{x})=1-c_k(\mathbf{x}^*)} P(\mathbf{x}|\mathbf{y})} \tag{5.12}$$

$$= (-1)^{c_k(\mathbf{x}^*)} L_k \simeq \max_{\mathbf{x}, c_k(\mathbf{x})=c_k(\mathbf{x}^*)} \log P(\mathbf{x}|\mathbf{y}) - \max_{\mathbf{x}, c_k(\mathbf{x})=1-c_k(\mathbf{x}^*)} \log P(\mathbf{x}|\mathbf{y}) \tag{5.13}$$

Note that L_k^* is the LLR value if the corresponding bit is 0, and it is the negative of the LLR value if the corresponding bit is 1. The first term in the last expression (asymptotically) delivers the correct codeword $\mathbf{x}^*$ as $\mathcal{P}(f_a) \to 0$, hence we can write

$$\begin{aligned} L_k^* &\simeq \log P(\mathbf{x}^*|\mathbf{y}) - \max_{\mathbf{x}, c_k(\mathbf{x})=1-c_k(\mathbf{x}^*)} \log P(\mathbf{x}|\mathbf{y}) \\ &= \min_{\mathbf{x}, c_k(\mathbf{x})=1-c_k(\mathbf{x}^*)} \log \frac{P(\mathbf{x}^*|\mathbf{y})}{P(\mathbf{x}|\mathbf{y})} \\ &= \min_{\mathbf{x}, c_k(\mathbf{x})=1-c_k(\mathbf{x}^*)} \left\{ \log \prod_i \frac{P(y_i|x_i^*)}{P(y_i|x_i)} \prod_j \frac{P(c_j(\mathbf{x}^*))}{P(c_j(\mathbf{x}))} \right\}, \end{aligned} \tag{5.14}$$

where we assume that a priori probabilities of the message bits are independent of each other, i.e., $P(\mathbf{x}^*) = \prod_j P(c_j^*)$.

The space of all the codewords $\mathbf{x}$ with $c_k(\mathbf{x}) = 1 - c_k(\mathbf{x}^*)$ is described by the error paths in the trellis diagram diverging from the $\mathbf{c}(\mathbf{x}^*)$ path at $k' \leq k$, merging with it at a later time instant $k'' \geq k$, and having a corresponding input bit error at time index k. Let these paths be denoted by $\mathbf{X}^{(w_0,w_1,h_0,h_1)}$ where for any $\mathbf{x} \in \mathbf{X}^{(w_0,w_1,h_0,h_1)}$ we have the input directional distance $d_D(\mathbf{c}(\mathbf{x}^*), \mathbf{c}(\mathbf{x})) = (w_0, w_1)$ and output directional distance $d_D(\mathbf{x}^*, \mathbf{x}) = (h_0, h_1)$, by which we can rewrite the last equation as, $\forall x \in \{0, 1\}$

$$\begin{aligned} L_k^*(x) \simeq \min_{\mathbf{x} \in \mathbf{X}^{(w_0,w_1,h_0,h_1)}} \Bigg\{ & \sum_{i: x_i \neq x_i^* = 0} L_{c,i}^*(0) + \sum_{i: x_i \neq x_i^* = 1} L_{c,i}^*(1) \\ & + \sum_{j: c_j(\mathbf{x}) \neq c_j(\mathbf{x}^*) = x} L_{a,j}^*(x) + \sum_{j: c_j(\mathbf{x}) \neq c_j(\mathbf{x}^*) = 1-x} L_{a,j}^*(1-x) \Bigg\} \end{aligned} \tag{5.15}$$

where $L^*_{c,i}$ and $L^*_{a,j}$ denote the modified channel LLRs and a priori LLRs of information bits.

The modified extrinsic LLR $L^*_{e,k}$ corresponding to the kth information bit is given by $L^*_{e,k}(x) = L^*_k(x) - L^*_{a,k}(x)$, hence

$$\begin{aligned} L^*_{e,k}(x) &\simeq \min_{\mathbf{x}\in\mathbf{X}^{(w_0,w_1,h_0,h_1)}} \Bigg\{ \sum_{i:x_i\neq x_i^*=0} L^*_{c,i}(0) + \sum_{i:x_i\neq x_i^*=1} L^*_{c,i}(1) + \sum_{j:c_j(\mathbf{x})\neq c_j(\mathbf{x}^*)=x, j\neq k} L^*_{a,j}(x) \\ &\qquad\qquad + \sum_{j:c_j(\mathbf{x})\neq c_j(\mathbf{x}^*)=1-x} L^*_{a,j}(1-x) \Bigg\} \\ &= \min_{\mathbf{x}\in\mathbf{X}^{(w_0,w_1,h_0,h_1)}} \tilde{L}^*(\mathbf{x}), \end{aligned} \tag{5.16}$$

where $\tilde{L}^*(\mathbf{x})$ is defined as the summation term.

The asymptotic PDF of the $L^*_{e,k}(x)$ can be obtained using the union bound as

$$\begin{aligned} f^*_{e,x} &= \sum_{\mathbf{x}\in\mathbf{X}^{(w_0,w_1,h_0,h_1)}} f_{\tilde{L}^*(\mathbf{x})} \\ &= \sum_{(w_0,w_1,h_0,h_1)} w_x D_{w_0,w_1,h_0,h_1} f_{r,0}^{*\otimes h_0} \otimes f_{r,1}^{*\otimes h_1} \otimes f_{a,x}^{*\otimes (w_x-1)} \otimes f_{a,1-x}^{*\otimes (w_{1-x})} \end{aligned} \tag{5.17}$$

where D_{w_0,w_1,h_0,h_1} is the number of error paths with input directional distance (w_0, w_1) and output directional distance (h_0, h_1) diverging at a specific trellis section from the $\mathbf{c}(\mathbf{x}^*)$ path. Note that there are w_x times as many paths that have a corresponding information bit error at time index k. (5.17) refers to the PDF of $L^*_{e,k}(x)$ (corresponding to the bit x for an arbitrary but fixed codeword $\mathbf{x}^*$).

The set of error paths $\mathbf{X}^{(w_0,w_1,h_0,h_1)}$ in (5.16) are exactly the same for an arbitrary codeword of a directionally symmetric code, however, they may be different for distinct codewords of other trellis codes. Therefore, we may obtain different PDFs, $f^*_{e,x}$, by considering different codewords being transmitted. Here, as an approximation, we note that using a large block length typical codeword (with a uniform distribution of 0's and 1's at the input), the resulting PDF $f^*_{e,x}$ can be

treated as the average of the PDFs over all codewords. Applying this averaging, the updated expression for the PDF of the modified extrinsic LLRs becomes

$$f^*_{e,x} = \sum_{i,(w_0,w_1,h_0,h_1)_i} p_i w_x D_{(w_0,w_1,h_0,h_1)_i} f^{*\otimes h_0}_{r,0} \otimes f^{*\otimes h_1}_{r,1} \otimes f^{*\otimes (w_x-1)}_{a,x} \otimes f^{*\otimes (w_{1-x})}_{a,1-x} \tag{5.18}$$

where p_i is the probability of observing the set of error paths $\mathbf{X}^{(w_0,w_1,h_0,h_1)_i}$.

Assuming transmission of the all-zero codeword for the LDPC code and introducing i.i.d. (random) channel adaptors between the LDPC and trellis-based codes (both at the encoder and decoder sides), the PDF of the modified LLRs at the output of the BCJR decoder becomes the average of $f^*_{e,x}$ for $x = 0, 1$, i.e., $\langle f_e \rangle = \frac{f^*_{e,0}+f^*_{e,1}}{2}$. As a result, the extrinsic LLRs from the LDPC decoder to the BCJR decoder will have the same PDF for $x = 0, 1$, i.e., $f_a = f^*_{a,0} = f^*_{a,1}$.

Performing extensive numerical simulations, we observed that if the corresponding convolutional code of the trellis-based code is nonsystematic (which is the case in this chapter), and if $\mathbf{x}^*$ is a typical codeword with a large block length, then the density of $L^*_{e,k}(x)$ for $x = 0$ and $x = 1$ are approximately the same, i.e., $\langle f_e \rangle = f_{e,0} = f^*_{e,0} = f^*_{e,1}$ even without using channel adaptors. Furthermore, if the trellis-based code is directionally symmetric then the previous argument is exact and it is valid for any arbitrary codeword not only for typical codewords.

5.4.3 Asymptotic Density Evolution for the Concatenated Coding Scheme

Assuming that the all-zero codeword for the LDPC code is transmitted, we combine the density evolution expressions for the LDPC code over a symmetric channel [103] with the average asymptotic density of $\langle f_e \rangle$, and obtain the approximate

asymptotic density evolution expressions for the concatenated code as follows

$$P_l = \langle f_e \rangle \otimes \lambda\Big(\Gamma^{-1}(\rho(\Gamma(P_{l-1})))\Big), \tag{5.19}$$

$$\langle f_e \rangle = \frac{1}{2} \sum_{\substack{i,(w_0,w_1,h_0,h_1)_i,\\ x=0,1}} p_i w_x D_{(w_0,w_1,h_0,h_1)_i} f_{r,0}^{*\otimes h_0} \otimes f_{r,1}^{*\otimes h_1} \otimes f_a^{\otimes(w_0+w_1-1)}, \tag{5.20}$$

$$f_a = \tilde{\lambda}\Big(\Gamma^{-1}(\rho(\Gamma(P_{l-1})))\Big). \tag{5.21}$$

where $\tilde{\lambda}(x) = \frac{\int_0^x \lambda(z)dz}{\int_0^1 \lambda(z)dz}$ is the variable node degree distribution from the node perspective. Since the outgoing message from a variable node towards the BCJR decoder is the summation of all the incoming messages from the check nodes to that variable node, and there is one such message for each variable node, these messages are distributed with respect to $\tilde{\lambda}$ instead of λ. Here, we have considered the inherent cycle-free assumption for the LDPC code, which guarantees the independence of the random variables describing the messages exchanged between the variable and check nodes, and enables us to use the Γ and Γ^{-1} operations over the distributions of the aforementioned random variables [103].

5.4.4 Derivation of the Stability Condition

As mentioned in Section 5.4.1, the average densities are symmetric, therefore instead of looking at the probability of error $\mathcal{P}(P_l)$, we can consider the Bhattacharyya constant of the evolved average densities defined as $\mathcal{B}(P_l) = \int_{-\infty}^{\infty} P_l(x)e^{-x/2}dx$ as a measure of the success of the iterative decoding process. Using the Bhattacharyya constant and the derivations in [116, Page 234], we

can transform the approximate asymptotic density evolution equation into a one-dimensional recursion and obtain the recursive update formula for the Bhattacharyya constant at the variable nodes ($z_l = \mathcal{B}(P_l)$) as

$$z_l \leq \mathcal{B}(\langle f_e \rangle)\lambda\big(1-\rho(1-z_{l-1})\big) = g(z_{l-1}), \tag{5.22}$$

$$\mathcal{B}(\langle f_e \rangle) \leq \sum_{\substack{i,(w_0,w_1,h_0,h_1)_i,\\ x=0,1}} p_i w_{x,i} D_{(w_0,w_1,h_0,h_1)_i} \mathcal{B}^{h_0}(f^*_{r,0})\mathcal{B}^{h_1}(f^*_{r,1})\Big(\tilde{\lambda}\big(1-\rho(1-z_{l-1})\big)\Big)^{w_0+w_1-1}. \tag{5.23}$$

The condition for the fixed point $z_l = 0$ to be locally stable is $\lim_{x\to 0} \frac{\partial g(z)}{\partial z} < 1$. By evaluating the partial derivative of (5.22) we see that the terms with $w_x > 1$ will be equal to zero when $z \to 0$, hence the only terms that remain are for $w_0 = 1, w_1 = 0$ or $w_0 = 0, w_1 = 1$, which correspond to the paths with a single input bit difference. The resulting stability condition is then

$$d\Big(\mathcal{B}(f^*_{r,0}), \mathcal{B}(f^*_{r,1})\Big)\lambda'(0)\rho'(1) < 1 \tag{5.24}$$

where $d\Big(\mathcal{B}(f^*_{r,0}), \mathcal{B}(f^*_{r,1})\Big) = \frac{1}{2} \sum_{\substack{i,(x,1-x,h_0,h_1)_i,\\ x=0,1}} p_i \mathcal{B}^{h_0}(f^*_{r,0})\mathcal{B}^{h_1}(f^*_{r,1})$ is the average directional distance spectrum of the paths with a single input bit difference (either 0 to 1 or 1 to 0), and p_i denotes the percentage of paths with directional distances $(x, 1-x, h_0, h_1)_i$. For the case of a directionally symmetric trellis-based code, since the directional output distances between any pair of correct and erroneous paths with a single input bit difference are the same (h_0, h_1), we simply have $d\Big(\mathcal{B}(f^*_{r,0}), \mathcal{B}(f^*_{r,1})\Big) = \mathcal{B}^{h_0}(f^*_{r,0})\mathcal{B}^{h_1}(f^*_{r,1})$.

Special Case (Transmission over a Symmetric Channel): If the transmission takes place over a symmetric channel, the derived stability condition becomes simpler and it is given by,

$$d(\mathcal{B}(f_r))\lambda'(0)\rho'(1) < 1 \tag{5.25}$$

where $d(\mathcal{B}(f_r)) = \sum_i p_i \mathcal{B}^{h_i}(f_r)$ is the average distance spectrum of the paths with single input difference, and p_i denotes the percentage of paths with output

distance h_i. For the further simplified case of the symmetric trellis-based code since the output distance between any pair of correct and erroneous paths with single input difference is the same h, we simply have $d(\mathcal{B}(f_r)) = \mathcal{B}^h(f_r)$.

5.4.5 Stability Condition for the Joint Decoder

So far, we have analyzed the iterative decoding of a single user decoder, however, in the proposed general coding scheme for DMICs, for some cases we need to jointly decode the users' messages. For instance, when a user transmits a public message, then the second user needs to decode both its own message and the public message of the first user (using a product trellis). With this motivation, we now derive an approximate expression for the densities of the extrinsic LLRs at the output of the BCJR decoder over product trellis in asymptotic regime $\mathcal{P}(f_a) \to 0$. We assume transmission of an arbitrary codeword for the first user denoted by $\mathbf{x}_1^*$, and obtain the modified LLR corresponding to the kth message bit of the first user as

$$\begin{aligned} L_k^* &= \log \frac{P(c_k(\mathbf{x}_1) = c_k(\mathbf{x}_1^*)|\mathbf{y})}{P(c_k(\mathbf{x}_1) = 1 - c_k(\mathbf{x}_1^*)|\mathbf{y})} = \log \frac{\sum\limits_{\mathbf{x}_1, c_k(\mathbf{x}_1)=c_k(\mathbf{x}_1^*)} P(\mathbf{x}_1|\mathbf{y})}{\sum\limits_{\mathbf{x}_1, c_k(\mathbf{x}_1)=1-c_k(\mathbf{x}_1^*)} P(\mathbf{x}_1|\mathbf{y})} \\ &= \log \frac{\sum\limits_{\mathbf{x}_1, c_k(\mathbf{x}_1)=c_k(\mathbf{x}_1^*)} P(\mathbf{y}|\mathbf{x}_1)P(\mathbf{x}_1)}{\sum\limits_{\mathbf{x}_1, c_k(\mathbf{x}_1)=1-c_k(\mathbf{x}_1^*)} P(\mathbf{y}|\mathbf{x}_1)P(\mathbf{x}_1)} \end{aligned}$$

where $c_k(\mathbf{x}_1)$ is the kth bit of the corresponding message to the codeword $\mathbf{x}_1$. Including the second user's codeword $\mathbf{x}_2$ in the conditional probability, and summing over the probability of the second codeword, we can write the previous expression as

$$L_k^* = \log \frac{\sum\limits_{\mathbf{x}_1, c_k(\mathbf{x}_1)=c_k(\mathbf{x}_1^*)} \sum\limits_{\mathbf{x}_2} P(\mathbf{y}|\mathbf{x}_1, \mathbf{x}_2)P(\mathbf{x}_1)P(\mathbf{x}_2)}{\sum\limits_{\mathbf{x}_1, c_k(\mathbf{x}_1)=1-c_k(\mathbf{x}_1^*)} \sum\limits_{\mathbf{x}_2} P(\mathbf{y}|\mathbf{x}_1, \mathbf{x}_2)P(\mathbf{x}_1)P(\mathbf{x}_2)}. \tag{5.26}$$

Assuming that the second user's codeword has been decoded without error $P(x_2 = x_2^*) = 1$, we can simplify L_k as,

$$L_k^* = \log \frac{\sum\limits_{\mathbf{x}_1, c_k(\mathbf{x}_1)=c_k(\mathbf{x}_1^*)} P(\mathbf{y}|\mathbf{x}_1, \mathbf{x}_2^*)P(\mathbf{x}_1)}{\sum\limits_{\mathbf{x}_1, c_k(\mathbf{x}_1)=1-c_k(\mathbf{x}_1^*)} P(\mathbf{y}|\mathbf{x}_2, \mathbf{x}_2^*)P(\mathbf{x}_1)}. \tag{5.27}$$

With the assumption of $\mathcal{P}(f_a) \to 0$, the probability term $P(\mathbf{x}_1) \to 1$ for the correct codeword and $P(\mathbf{x}_1) \to 0$ for all other codewords. In other words, the summations can be approximated by maximum operations asymptotically, and the numerator delivers the correct codeword $\mathbf{x}^*$. Hence

$$\begin{aligned} L_k^* &\simeq \log P(\mathbf{y}|\mathbf{x}_1^*, \mathbf{x}_2^*)P(\mathbf{x}_1^*) - \max_{\mathbf{x}_1, c_k(\mathbf{x}_1)=1-c_k(\mathbf{x}_1^*)} \log P(\mathbf{y}|\mathbf{x}_1, \mathbf{x}_2^*)P(\mathbf{x}_1) \\ &= \min_{\mathbf{x}_1, c_k(\mathbf{x}_1)=1-c_k(\mathbf{x}_1^*)} \log \frac{P(\mathbf{y}|\mathbf{x}_1^*, \mathbf{x}_1^*)P(\mathbf{x}_1^*)}{P(\mathbf{y}|\mathbf{x}_1, \mathbf{x}_2^*)P(\mathbf{x}_1)} \\ &= \min_{\mathbf{x}_1, c_k(\mathbf{x}_1)=1-c_k(\mathbf{x}_1^*)} \left\{ \log \prod_i \frac{P(y_i|x_{1,i}^*, x_{2,i}{}^*)}{P(y_i|x_{1,i}, x_{2,i}{}^*)} \prod_j \frac{P(c_j(\mathbf{x}_1^*))}{P(c_j(\mathbf{x}_1))} \right\}, \end{aligned}$$

where we assume that a priori probabilities of the message bits are independent of each other, i.e., $P(\mathbf{x}_1) = \prod\limits_j P(c_j(\mathbf{x}_1))$.

Note that the only difference with the single user case is due to the conditional probability term being $P(y_i|x_{1,i}, x_{2,i}{}^*)$ instead of $P(y_i|x_i)$. For this case, the conditional probability depends on both the channel and the second user's codeword. For example, if we consider a DMIC with the input-output relationship given by $Y_1 = (X_1 \otimes X_2) \oplus Z_1$, $Y_2 = X_2 \oplus Z_2$, wherever $x_{2,i}{}^* = 1$ the conditional probability $P(y_i|x_{1,i}, x_{2,i}{}^*)$ will be independent of the value of $x_{1,i}$ which means that the difference between $\mathbf{x}_1^*$ and $\mathbf{x}_1$ at the ith bit will not affect L_k^*. Hence, to proceed, we need to determine the number of coincidences of $x_{1,i}{}^* \neq x_{1,i}$ and $x_{2,i}{}^* = 1$, and find the effective distance between $\mathbf{x}_1^*$ and $\mathbf{x}_1$ (for any arbitrary selection of these correct and erroneous codewords) assuming that the second user transmits the codeword $\mathbf{x}_2^*$. From the analysis of the single user case, we know that for the calculation of the stability condition, only the paths with single input difference will appear in the expression, thus determining these coincidences (only for the

paths with a single input bit difference) is feasible. However, the resulting PDF of the L_k^* still needs to be averaged over all codewords of the second user.

Following similar steps as the single user case, the stability condition for this case is finally obtained as

$$d\Big(\mathcal{B}(f_{r,0}^*), \mathcal{B}(f_{r,1}^*)\Big)\lambda'(0)\rho'(1) < 1 \tag{5.28}$$

where $d\Big(\mathcal{B}(f_{r,0}^*), \mathcal{B}(f_{r,1}^*)\Big) = \frac{1}{2} \sum_{\substack{i,(x,1-x,h_0,h_1)_i, \\ x=0,1}} p_i \mathcal{B}^{h_0}(f_{r,0}^*)\mathcal{B}^{h_1}(f_{r,1}^*)$ is the average directional distance spectrum of the paths with a single input bit difference on the *product trellis* of both users' codes. One should note that, the difference between (5.28) and (5.24) is in the definition of the average directional distance spectrum where in the first one it is defined over the product trellis of two codes while in the latter it is over single trellis.

5.5 Code Design Examples

5.5.1 Example 1: One-Sided OR Interference

As the first example of a two-user DMIC, we consider a shared optical channel [100] with one-sided interference, which is an instance of binary-input binary-output ZIC. The input-output relationship for this channel is given by $Y_1 = (X_1 \otimes X_2) \oplus Z_1$, $Y_2 = X_2 \oplus Z_2$ where $\oplus$ and $\otimes$ represent the "XOR" and the "OR" operations, respectively, with Z_1 and Z_2 being the noise samples at receiver 1 and 2 drawn from a Bernoulli distribution with parameters $\epsilon_1 = 0.21$ and $\epsilon_2 = 0.25$, respectively. This model does not satisfy the Markov chain condition for weak interference definition $X_2 - (X_1, Y_2) - Y_1$ [77], however, we can simplify the mutual information condition $I(X_2; Y_1|X_1) \leq I(X_2; Y_2)$ [77] as

$$P(X_1 = 0) \leq \frac{h(\epsilon_2 + q - 2\epsilon_2 q) - h(\epsilon_2)}{h(\epsilon_1 + q - 2\epsilon_1 q) - h(\epsilon_1)} \tag{5.29}$$

where $q = P(X_2 = 1)$ and $h(.)$ is the binary entropy function, and verify that for $P(X_1 = 0) < 0.71$ the condition (5.29) holds, i.e., the example becomes an instance of the weak interference channel by definition in [77, Eq. (23)]. Therefore, motivated by the results of [77], we utilize the simple coding scheme of sending the messages of both users as private and compute a subregion of the HK ARR.

Table 5.1: Label assignment to the branches of 16-state trellis ($M = 4$) using the proposed algorithm.

State/Input								y_{21}	y_{22}	y_{23}	y_{24}
0000/0	0001/1	0100/1	0101/0	1010/0	1011/1	1110/1	1111/0	1000	1000	0111	0111
0000/1	0001/0	0100/0	0101/1	1010/1	1011/0	1110/0	1111/1	0100	0100	1011	1011
0010/0	0011/1	0110/1	0111/0	1000/0	1001/1	1100/1	1101/0	0010	0010	1101	1101
0010/1	0011/0	0110/0	0111/1	1000/1	1001/0	1100/0	1101/1	0001	0000	1110	1111

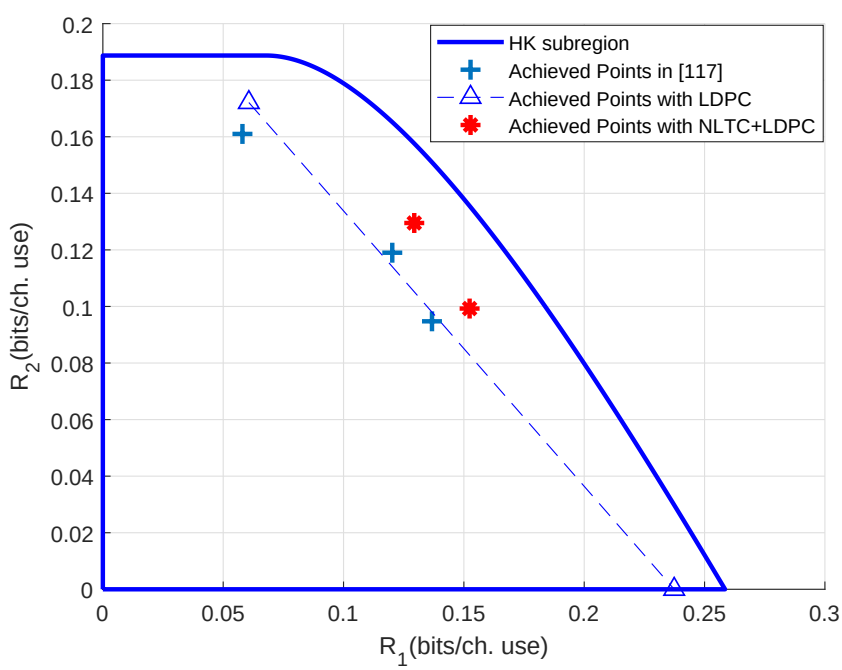

Figure 5.4: Rate region and achieved rate pairs for Example 1.

The achievable HK sub-region is plotted for the considered example in Fig. 5.4. To obtain the largest HK sub-region corresponding to each value of $P(X_2) =$

Table 5.2: Variable degree distribution of the optimized codes for Example 1 with $\epsilon_1 = 0.21$.

p_1, p_2	Msg	Rate	λ_2	λ_3	λ_4	λ_9	λ_{10}	λ_{19}	λ_{20}	λ_{49}	λ_{50}
0.5,0.5	X_1	0.0606	0.5149	0.1849	0.0810	0.0336	0.0946	0.0558	0.0312	0.0037	0.0003
	X_2	0.1721	0.3531	0.2408	0.0673	0.0664	0.1503	0.0300	0.0581	0.0093	0.0247
0.5,0.25	X_1	0.1293	0.3523	0.1713	0.1332	0.1198	0.0294	0.0767	0.0237	0.0612	0.0324
	X_2	0.5180	0.5549	0.0697	0.3754						
0.5,0.1875	X_1	0.1523	0.3662	0.1690	0.1411	0.1092	0.0635	0.0585	0.0281	0.0476	0.0168
	X_2	0.3970	0.3737	0.1608	0.4655						
0.5,0	X_1	0.2374	0.3941	0.2023	0.1478	0.1578	0.0590	0.0206	0.0015	0.0037	0.0132

Table 5.3: Check degree distribution of the optimized codes for Example 1 with $\epsilon_1 = 0.21$.

p_1, p_2	Msg	Rate	ρ_2	ρ_3	ρ_4	ρ_5	ρ_8	ρ_{14}	ρ_{15}
0.5,0.5	X_1	0.0606	0.0125	0.9875					
	X_2	0.1721		0.0063	0.9710				
0.5,0.25	X_1	0.1293		0.0373	0.9488	0.0139			
	X_2	0.5180	0.0004	0.4289	0.04733		0.0006	0.0491	0.4737
0.5,0.1875	X_1	0.1523		0.0581	0.9135	0.0284			
	X_2	0.3970	0.1020	0.3540	0.0401		0.0426	0.0088	0.4525
0.5,0	X_1	0.2374		0.012809	0.944015	0.043176			

$p_2 \in [0, 1]$ we find the optimal value of $P(X_1) = p_1$ by taking the derivative of mutual information $I(X_1; Y_1)$, and equating it to zero. At the end, we take the convex hull of all the subregions and obtain the HK subregion corresponding to use of only private messages.

By calculating the optimal value of p_1 for each $p_2 \in [0, 1]$, we observe that the optimized p_1 is always very close to 0.5, hence we consider the uniform distribution of zeros and ones for user 1 for this example. To enforce the required non-uniform input distribution for user 2, we design the NLTCs delivering the desired distribution of 0's and 1's. Details of the employed trellis codes are given in Table 5.1 with output labels given in columns y_{21} and y_{22}. In each row of the table, the output bits correspond to the input bit u for the current state S. The trellis memory and the number of output bits are both equal to 4, that is, at each section of the trellis, the 1 bit input determines the 4-bit outputs. We then optimize the degree distribution of the LDPC codes (with multiple check node

and variable node degrees).

The optimized degree distributions are given in Tables 5.2 and 5.3. For ones' densities of $p_2 = 0.25$ and 0.1875, the effective rate of the second user's code is the multiplication of the NLTC rate with corresponding LDPC code rate. Fig. 5.4 shows the optimized rate pairs achieved for different input distributions. As noticed, there is a significant improvement over the results of the previous work in [117]. This improvement is obtained by increasing the memory of the trellis, using multiple check node degrees for LDPC codes, and removing the inner trellis based code for the cases of uniform input distribution. According to Fig. 5.4, the optimized codes offer better performance than single user codes used with time sharing for which the boundary can be obtained by connecting two corner points. It is also worthwhile to mention that, the rate pairs $(0.1293, 0.1295)$, $(0.1523, 0.0993)$, which are obtained with a non-uniform distribution cannot be attained with the joint use of linear coding and time sharing, hence there is a definite need for the use of nonlinear codes as pursued here.

Table 5.4: Variable degree distribution of the optimized codes for Example 1 with $\epsilon_1 = 0.1$.

achieved point	Msg	Rate	λ_2	λ_3	λ_4	λ_5	λ_9	λ_{10}	λ_{19}	λ_{20}	λ_{49}	λ_{50}
$*, +$	X_1	0.2543	0.4043	0.2482	0.0987		0.1399	0.0363	0.0274	0.0241	0.0079	0.0131
$*, \triangle$	X_2	0.5180	0.5549	0.0697	0.3754							
$+, \circ$	X_2	0.2422	0.2619	0.4203	0.1729	0.1449						
$\triangle$	X_1	0.3344	0.3478	0.4547	0.0605		0.0567	0.0194	0.0145	0.0034	0.0344	0.0086
$\circ$	X_1	0.3343	0.3043	0.4528	0.0374		0.0771	0.0472	0.0181	0.0149	0.0162	0.0320

Table 5.5: Check degree distribution of the optimized codes for Example 1 with $\epsilon_1 = 0.1$.

achieved point	Msg	Rate	ρ_2	ρ_3	ρ_4	ρ_5	ρ_6	ρ_8	ρ_{14}	ρ_{15}
$*, +$	X_1	0.2543	0.0217	0.8907	0.0876					
$*, \triangle$	X_2	0.5180	0.0004	0.4289	0.04733			0.0006	0.0491	0.4737
$+, \circ$	X_2	0.2422	0.0158	0.4996	0.2774			0.0377	0.0615	0.1080
$\triangle$	X_1	0.3344		0.0225	0.6071	0.3704				
$\circ$	X_1	0.3343		0.0189	0.4980	0.2190	0.2641			

We consider the current example with another set of channel parameters as $\epsilon_1 = 0.1$ and $\epsilon_2 = 0.25$, for which the corresponding HK achievable subregion for

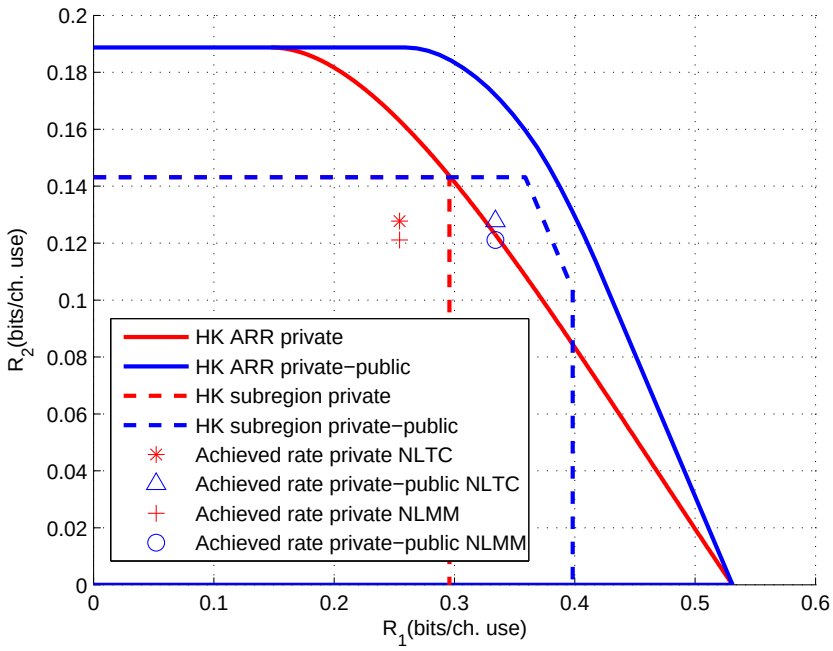

Figure 5.5: Rate region and achieved rate pairs for Example 1 with $\epsilon_1 = 0.1$ and $\epsilon_2 = 0.25$.

both the cases of using only private messages and using private message for first user and public message for the second user is given in Fig. 5.5. It can be seen that for this setup, the HK subregion can be enlarged by utilizing a public message for the second user. For a specific distribution of the users' messages, namely, $p_1 = 0.5$ and $p_2 = 0.25$, the achievable subregion along with the optimized rate pairs are shown in Fig 5.5, which illustrates that by utilizing a more sophisticated version of HK type encoding, namely, private message for one user and public message for the other, we can achieve higher rates compared to the case of using only private messages. Based on this observation we utilize a simplified version of the proposed general coding scheme where the interfering user's message is transmitted as public message and the other user transmits only private message which is illustrated in Fig. 5.6. As shown in this block diagram, both public message of the second user and private message of the first user are decoded in the first user's receiver. A state node decoder iteratively exchanges messages

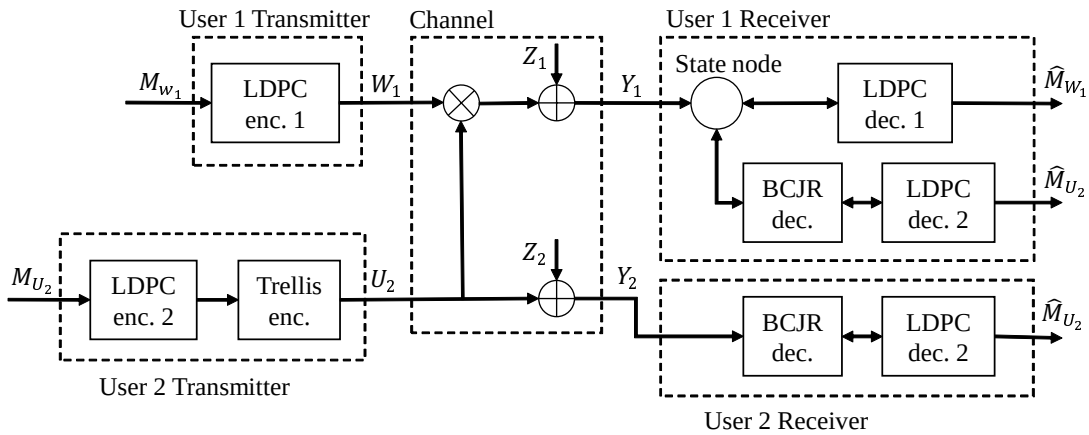

Figure 5.6: Block diagram of the proposed coding scheme for Example 1 with $\epsilon_1 = 0.1$ and $\epsilon_2 = 0.25$.

with LDPC decoder of user 1 and BCJR decoder of user 2. we also consider the reference scheme of using a nonlinear memoryless mapper (NLMM) instead of NLTC and optimizing the outer LDPC codes for this case. The optimal degree distributions for this example are given in Tables 5.4 and 5.5. The achieved rate pairs are depicted in Fig. 5.5 which shows that considering the public message for the second user, higher rate for user 1 can be achieved with both the proposed and reference schemes, and, utilizing the NLTC results in a higher rate for second user compared to the reference scheme.

5.5.2 Example 2: One-Sided AND Interference

As a second example, we consider an instance of one-sided weak interference channel given by $Y_1 = (X_1.Y_2) \oplus Z_1$, $Y_2 = X_2 \oplus Z_2$ where "." is the product operation. Z_1 and Z_2 are the noise samples at receiver 1 and 2 drawn from a Bernoulli distribution with parameters ϵ_1 and ϵ_2, respectively. This model satisfies the Markov chain condition for weak interference [77, Definition 2], namely, $X_2 - (X_1, Y_2) - Y_1$, hence the sum rate capacity [77, Theorem 1] holds, and it can be achieved by treating interference as noise and using only private messages.

We consider an instance of the above channel with noise parameters $\epsilon_1 = 0.15$ and $\epsilon_2 = 0.25$, and calculate the HK sub-region by considering only private messages for both users.

Table 5.6: Variable degree distribution of the optimized codes for Example 2.

p_1, p_2	Msg	Rate	λ_2	λ_3	λ_4	λ_9	λ_{10}	λ_{19}	λ_{20}	λ_{49}	λ_{50}
0.5,0.5	X_1	0.095533	0.523868	0.199662	0.071950	0.076520	0.119350	0.003700	0.000850	0.000910	0.003190
	X_2	0.173089	0.349851	0.250499	0.062660	0.064820	0.145850	0.032120	0.065410	0.002540	0.026250
0.5,0.75	X_1	0.148727	0.362650	0.176620	0.117600	0.139440	0.028560	0.089800	0.007230	0.066030	0.012070
	X_2	0.517044	0.485327	0.114083	0.400590						
0.5,0.8125	X_1	0.161381	0.366155	0.160605	0.133580	0.128990	0.051910	0.043150	0.042440	0.032790	0.040380
	X_2	0.398041	0.355933	0.273207	0.370860						
0.5,1	X_1	0.204304	0.378678	0.190902	0.118990	0.153570	0.048290	0.050350	0.042490	0.000570	0.016160

Table 5.7: Check degree distribution of the optimized codes for Example 2.

p_1, p_2	Msg	Rate	ρ_2	ρ_3	ρ_4	ρ_5	ρ_8	ρ_{14}	ρ_{15}
0.5,0.5	X_1	0.095533	0.002565	0.978053	0.019382				
	X_2	0.173089	0.002510	0.978166	0.019324				
0.5,0.75	X_1	0.148727		0.013686	0.979620	0.006694			
	X_2	0.517044	0.000130	0.401572	0.044785		0.029873	0.034848	0.488791
0.5,0.8125	X_1	0.161381		0.010969	0.925347	0.063684			
	X_2	0.398041	0.097192	0.379362	0.041831		0.002037	0.005181	0.474396
0.5,1	X_1	0.204304		0.004311	0.917350	0.078339			

By [77, Theorem 1] the sum rate capacity is $C_{sum} = \max_{p(x_1)p(x_2)}\{I(X_1;Y_1) + I(X_2;Y_2)\} \simeq 0.307$. In addition the following simple outer bound from [77],

$$\begin{aligned} R_1 &\leq I(X_1;Y_1|X_2), \\ R_2 &\leq I(X_2;Y_2), \\ R_1 + R_2 &\leq I(X_1;Y_1) + I(X_2;Y_2). \end{aligned}$$

can be evaluated for this example which is also shown in Fig. 5.7. Observing that the result of the optimization process for X_1 gives an input distribution very close to uniform, we choose a uniform distribution for the first user. To enforce the non-uniform distributions needed for the second user, we design the trellis codes given in Table 5.1 with output labels y_{23} and y_{24}.

The optimal degree distributions for this example are given in Tables 5.6 and

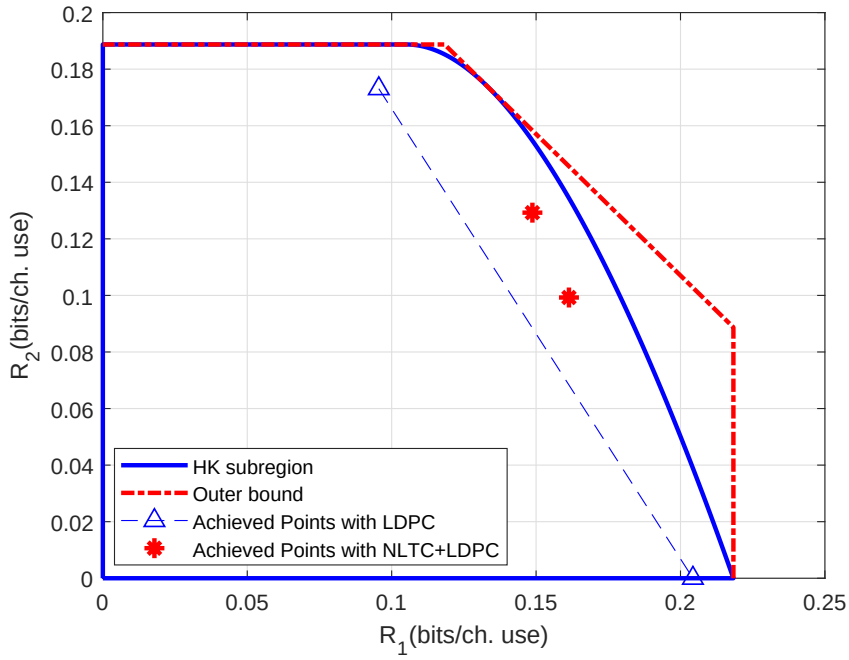

Figure 5.7: Rate region and achieved rate pairs for Example 2.

5.7. Fig 5.7 shows the optimized rate pairs achieved for different degree distributions along with achievable HK subregion and the outer bound. We observe that rate pairs close to the achievable subregion boundaries are obtained which cannot be attained with single user codes or with the use of only LDPC codes with time sharing.

Table 5.8: Channel transition probabilities of Example 3

$p(y_1\|x_1x_2)$	$y_1 = 0$	$y_1 = 1$	$p(y_2\|x_1x_2)$	$y_2 = 0$	$y_2 = 1$
$x_1x_2 = 00$	0.65	0.35	$x_1x_2 = 00$	0.65	0.35
$x_1x_2 = 01$	0.6	0.4	$x_1x_2 = 01$	0.4	0.6
$x_1x_2 = 10$	0.45	0.55	$x_1x_2 = 10$	0.8	0.2
$x_1x_2 = 11$	0.2	0.8	$x_1x_2 = 11$	0.3	0.7

5.5.3 Example 3: Two-Sided Interference

The third example that we consider is an instance of a general two-user DMIC with binary inputs and outputs, and with the channel transition probability given as

$$p(y_1y_2|x_1x_2) = p(y_1|x_1x_2)p(y_2|x_1x_2), \tag{5.30}$$

where $p(y_1|x_1x_2)$ and $p(y_2|x_1x_2)$ are specified in Table 5.8.

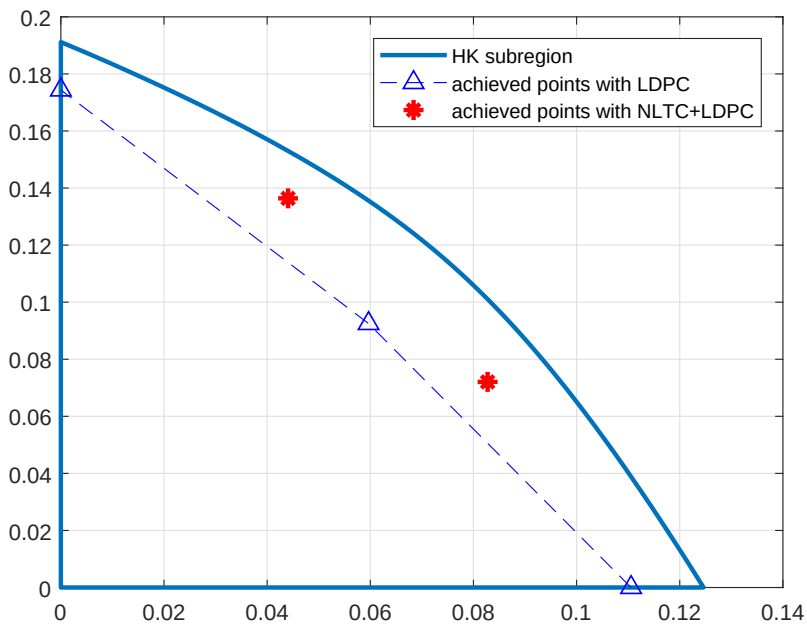

Figure 5.8: Rate region and achieved rate pairs for Example 3

Table 5.9: Variable degree distribution of the optimized codes for Example 3.

p_1, p_2	Msg	Rate	λ_2	λ_3	λ_4	λ_5	λ_9	λ_{10}	λ_{19}	λ_{20}	λ_{49}	λ_{50}
0.5,1	X_1	0.110559	0.524600	0.219120	0.074740		0.073030	0.102140	0.004670	0.001140	0.000540	0.000020
1,0.5	X_2	0.174376	0.382845	0.159305	0.159760		0.096420	0.076520	0.025900	0.017220	0.075790	0.006240
0.5,0.5	X_1	0.059663	0.493890	0.222140	0.052540		0.061960	0.096370	0.007890	0.034620	0.013480	0.017110
	X_2	0.092509	0.494773	0.262927	0.047850		0.032060	0.119730	0.031560	0.008710	0.000980	0.001410
0.5,0.75	X_1	0.082743	0.496704	0.250046	0.044260		0.009440	0.166620	0.018730	0.004610	0.008260	0.001330
	X_2	0.288224	0.301536	0.203664	0.035540	0.459260						
0.75,0.5	X_1	0.176227	0.226072	0.232578	0.030580	0.510770						
	X_2	0.136389	0.367322	0.138428	0.149760		0.110280	0.032280	0.050580	0.076170	0.053370	0.021810

Table 5.10: Check degree distribution of the optimized codes for Example 3.

p_1, p_2	Msg	Rate	ρ_2	ρ_3	ρ_4	ρ_5	ρ_8	ρ_{14}	ρ_{15}
0.5,1	X_1	0.110559	0.002061	0.971365	0.026574				
1,0.5	X_2	0.174376		0.057316	0.911938	0.030746			
0.5,0.5	X_1	0.059663	0.014065	0.945768	0.040166				
	X_2	0.092509	0.004952	0.956397	0.038651				
0.5,0.75	X_1	0.082743	0.006185	0.964730	0.029085				
	X_2	0.288224	0.159902	0.282646	0.051625		0.097479	0.179678	0.228669
0.75,0.5	X_1	0.176227	0.219390	0.278422	0.032670		0.078990	0.178584	0.211944
	X_2	0.136389		0.026075	0.951936	0.021989			

A complete characterization of the HK achievable rate region for this example requires optimization over four random variables with large cardinalities, hence as a simplified version, we consider only private messages and obtain a subregion of HK ARR which is illustrated in Fig 5.8. Note that in this example we used the NLTC from Example 2 with the ones' density of 0.75. The degree distribution of the optimized LDPC codes are given in Table 5.9 and 5.10. The achievable region using the single user codes (inducing uniform distribution for both users), and time sharing between them is shown with a dashed line in this figure. As in the previous examples, it is clear that one can achieve rate pairs that cannot be achieved by linear codes alone by using non-uniform distribution for the inputs.

5.5.4 Finite Length Simulation Results

To study the performance of specific codes from the designed ensemble and verify the estimated threshold of these ensembles, examples of parity check matrices for a block-length of 100k are obtained for the ensembles corresponding to the rate pair (0.1487, 0.1293) with $p_1 = 0.5$ and $p_2 = 0.75$ of Example 2. The parity check matrices are constructed using the tools in [104], which utilizes the random construction method. The resulting bit error rates are depicted in Fig. 5.9 showing that the gap between the decoding threshold values and ϵ values for which small error probability is attained is relatively small which verifies the accuracy of estimated decoding thresholds of the designed codes. Note that while simulating the user 1's code, the parameter ϵ_2 (which effects the interfering signal)

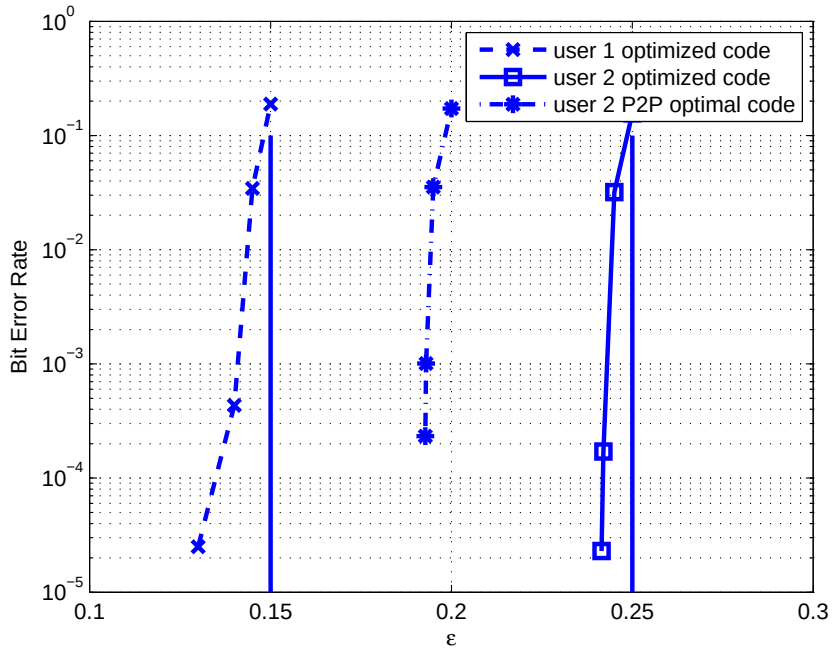

Figure 5.9: BER results of Example 2 with $p_1 = 0.5$ and $p_2 = 0.75$.

is fixed at the value 0.25. Furthermore, for user 2, we consider a P2P optimal LDPC code instead of the optimized outer LDPC code with the same rate, and obtain the corresponding bit error rates. We observe that the optimized code for the specific NLTC significantly outperforms the P2P optimal one.

5.6 Chapter Summary

We have considered the Han-Kobayashi coding scheme by using both public and private messages, and proposed a coding scheme based on a serial concatenation of an NLTC with an outer LDPC code as a solution for different classes of DMICs. By approximate analytical derivations, we have investigated the performance of the proposed iterative decoding algorithm for the concatenated coding scheme in the asymptotic region where the probability of decoding error is close to zero, and based on the analysis, we have derived a stability condition. Furthermore, we

have used an EXIT analysis to design the outer LDPC code in the concatenated coding scheme and utilized the derived stability condition to accelerate the design process.

Our extensive numerical examples demonstrate that the designed codes achieve rate pairs close to the optimal boundary of the HK subregion that cannot be obtained without using nonlinear codes. In addition, the proposed coding scheme for the general instances of DMICs achieve rate pairs that cannot be achieved by using linear codes alone with time sharing and the reference scheme of concatenating LDPC codes with nonlinear memoryless mappers. Furthermore, extensive finite block length simulations verify the accuracy of the estimated thresholds for the designed codes.

Chapter 6

Short Block Length Trellis-Based Codes for Interference Channels

In this chapter, we consider design of short block length codes for GICs with and without fading, which is motivated by the practical applications with decoding delay and complexity constraints. We focus on the application of trellis-based codes for this purpose. The reason is that we can implement optimal decoders for trellis-based codes even in multi-user settings including the case of interference channels, and compute performance bounds in an efficient manner, which facilitates code designs.

The authors in [118] have designed short block length codes for two-user Gaussian multiple access channels (GMACs) employing trellis-based codes showed that the designed codes outperform the P2P optimal ones. The authors in [119, 120] consider the two-user GIC with fixed real channel coefficients and derive error-rate bounds by utilizing the union bound techniques in order to design optimal trellis-based codes with short block lengths, and study their performance via several code design examples. Here, we extend these approaches to the case of GICs with complex coefficients.

The material in this chapter has been submitted to IET Communications [23].

In addition to GICs with fixed complex channel coefficients, we also consider two different fading scenarios, namely, i.i.d. fading and quasi-static fading cases, and develop average union bound expressions on the error rates to obtain a simple performance characterization. We study the tightness of the derived bounds via numerical examples, and provide several error rate performance results for the designed codes. We demonstrate that for GICs with joint maximum likelihood (JML) decoding, the newly designed codes significantly outperform the P2P optimal ones and off-the-shelf LDPC codes with the same block lengths. We also show that, for i.i.d. fading ICs, the best codes obtained by performing code search are also P2P optimal. For the case of quasi-static fading, we derive a simple version of the union bound, however, it is not sufficiently tight for code search purposes. Hence, we also provide a tight performance bound with a higher complexity that is useful for a theoretical assessment of the code performance.

The rest of the chapter is organized as follows. In Section 6.1, we introduce the system model for two-user GICs with and without fading. We review the bounds derived for GICs with real channel coefficients without fading in Section 6.2, and extend them to the complex coefficients case. We utilize these existing methods to derive bounds on the performance of the trellis-based codes for i.i.d. fading and quasi static fading interference channels in Section 6.3. We provide several code design examples in Section 6.4, and finally, we conclude the paper in Section 6.5.

6.1 System Description

Fig. 6.1 illustrates the block diagram of a two-user interference channel with Gaussian noise. Considering receiver i, the length-n received signal vectors can be written as

$$\mathbf{y}_i = \boldsymbol{\alpha}_i \mathbf{c} + \mathbf{z}_i, \quad i = 1, 2, \tag{6.1}$$

where $\mathbf{c}$ denotes the BPSK modulated transmitted codeword matrix as follows

$$\mathbf{c} = \begin{bmatrix} \mathbf{c}_1 \\ \mathbf{c}_2 \end{bmatrix} = \begin{bmatrix} c_{1,1} & c_{1,2} & \dots & c_{1,n} \\ c_{2,1} & c_{2,2} & \dots & c_{2,n} \end{bmatrix}, \tag{6.2}$$

with $\mathbf{c}_1$ and $\mathbf{c}_2$ representing the codewords employed at transmitter 1 and transmitter 2, respectively.

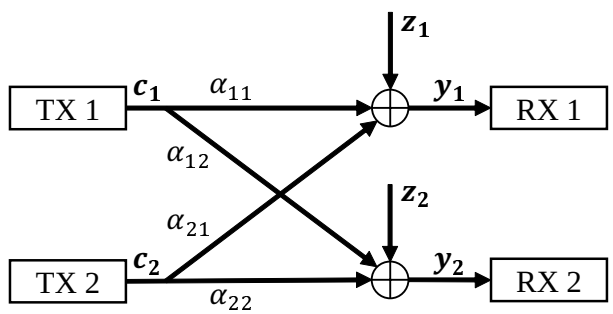

Figure 6.1: Block diagram of a two-user GIC.

The channel gains from the transmitters to the receiver i are denoted as $\boldsymbol{\alpha}_i = [\alpha_{1i}\ \alpha_{2i}]$, where α_{ji} is a complex number (with real and imaginary components α_{ji}^R and α_{ji}^I, respectively) denoting the gain of the channel from the transmitter j to the receiver i. The i.i.d. zero mean complex Gaussian noise samples with variance $\frac{N_0}{2}$ at receiver i are represented by the vector $\mathbf{z}_i$ of length n. For the Gaussian interference channel case, the channel gains are fixed values (and naturally, they are known both at the transmitter and the receiver). We define the SNR and interference-to-noise ratio (INR) at receiver i as

$$SNR_i = \frac{|\alpha_{ii}|^2 P_i}{N_0}, \quad INR_i = \frac{|\alpha_{ji}|^2 P_j}{N_0}, \tag{6.3}$$

where $i, j = 1, 2$, and P_i is the average transmit power per codeword bit at the transmitter i.

For a GIC, based on the interference and signal levels, the interference can be categorized as strong (if $INR_i > SNR_j$), weak (if $SNR_i > INR_j$), or mixed (if $INR_i > SNR_j,\ INR_j < SNR_i$) with $i \neq j$ [69].

We consider two models for fading ICs. In the first one the fading coefficients α_{ji} are modelled as samples of independent zero-mean circularly symmetric complex Gaussian random variables with variance $\frac{\sigma_{ji}^2}{2}$ per dimension that are i.i.d. for each transmission. This case can be considered as fast fading. In the second model, we assume that the fading is slow, and specifically, the fading coefficients are constant throughout each codeword. This case can be considered as quasi-static as it does not offer time diversity. While for the quasi-static case, one can consider the outage probability, we still consider the average error probability as the performance metric as done in the space-time coding literature [121].

For both fast and quasi-static fading scenarios, we assume that perfect CSI is available at the receiver, however, no CSI is available at the transmitter. The SNR and INR at receiver i are defined as

$$SNR_i = \frac{\sigma_{ii}^2}{N_0}, \quad INR_i = \frac{\sigma_{ji}^2}{N_0}, \tag{6.4}$$

with $i, j = 1, 2$.

We consider Joint maximum likelihood (JML) decoding at the receiver side which is the optimal decoding of both messages based on the maximum likelihood criterion and it can be written as

$$(\mathbf{c}_1^{(JML)}, \mathbf{c}_2^{(JML)}) = \underset{(\hat{\mathbf{c}}_1, \hat{\mathbf{c}}_2)}{\arg\min} \ \|\mathbf{y}_i - \alpha_{1i}\hat{\mathbf{c}}_1 - \alpha_{2i}\hat{\mathbf{c}}_2\|^2, \ i = 1, 2, \tag{6.5}$$

where $\|.\|$ denotes the Euclidean norm of the vector, and the minimization is performed over both codebooks.

6.2 Preliminaries

In this section, we go over the performance analysis and code design methods for short block length trellis-based codes developed in [119] for GICs with fixed real channel coefficients. The error-rate bounds have been derived by utilizing

the union bound techniques and the code optimization has been performed by searching for pairs of codes minimizing the corresponding bound.

6.2.1 Gaussian Interference Channel without Fading

For a GIC considering JML decoding and utilizing the union bound technique, the total frame error probability at both receivers is upper-bounded as

$$P_\varepsilon \leq \frac{1}{|\mathcal{C}|} \sum_{\mathbf{c}} \sum_{\hat{\mathbf{c}} \neq \mathbf{c}} \Big(P_{\varepsilon,1}(\mathbf{c}, \hat{\mathbf{c}}) + P_{\varepsilon,2}(\mathbf{c}, \hat{\mathbf{c}}) \Big) \tag{6.6}$$

where $\mathcal{C}$ denotes the set of codeword pairs $\mathbf{c}$, and $|.|$ denotes the cardinality of the set. $P_{\varepsilon,i}(\mathbf{c}, \hat{\mathbf{c}})$ is the pairwise error probability at ith receiver which is the probability that the received signal is closer to another codeword pair $\hat{\mathbf{c}}$ instead of $\mathbf{c}$ when $\mathbf{c}$ is transmitted. $P_{\varepsilon,i}(\mathbf{c}, \hat{\mathbf{c}})$ is expressed as follows

$$P_{\varepsilon,i}(\mathbf{c}, \hat{\mathbf{c}}) = Q\left(\sqrt{\frac{Ed_i^2(\mathbf{c}, \hat{\mathbf{c}})}{2N_0}} \right), \tag{6.7}$$

where $Q(x) = \frac{1}{\sqrt{2\pi}} \int_x^\infty \exp(-\frac{t^2}{2}) dt$, and $Ed_i^2(.,.)$ is the squared Euclidean distance function computed at receiver i, i.e.,

$$Ed_i^2(\mathbf{c}, \hat{\mathbf{c}}) = \boldsymbol{\alpha}_i \mathbf{D}_{\mathbf{c},\hat{\mathbf{c}}} \boldsymbol{\alpha}_i^\dagger$$

where "†" denotes the conjugate transpose and $\mathbf{D}_{\mathbf{c},\hat{\mathbf{c}}}$ represents the codeword difference matrix given by

$$\mathbf{D}_{\mathbf{c},\hat{\mathbf{c}}} = (\mathbf{c} - \hat{\mathbf{c}})(\mathbf{c} - \hat{\mathbf{c}})^\dagger = \begin{bmatrix} d_{11} & d_{12} \\ d_{21} & d_{22} \end{bmatrix}. \tag{6.8}$$

Here we simplify the squared Euclidean distance function for the case of complex coefficients as follows

$$Ed_i^2(\mathbf{c}, \hat{\mathbf{c}}) = |\alpha_{1i}|^2 d_{11} + 2(\alpha_{1i}^R \alpha_{2i}^R + \alpha_{1i}^I \alpha_{2i}^I) d_{12} + |\alpha_{2i}|^2 d_{22},$$

An efficient systematic method is developed to count the multiplicities of different codeword difference matrices $\mathbf{D}_{\mathbf{c},\hat{\mathbf{c}}}$ for all possible correct-erroneous codeword pairs in order to use in the bound computations. We describe the details of this method in the following. Consider a two-user joint trellis diagram with states labeled as (s_1, s_2) with s_i representing the state of the trellis for the code of the ith user. The joint trellis has $n_{s_1} \times n_{s_2}$ states with n_{s_i} denoting the number of states for the ith user's code. To track all possible codeword pairs $(\mathbf{c}, \hat{\mathbf{c}})$, a product trellis diagram with states $(s_1, s_2, \hat{s}_1, \hat{s}_2)$ is formed wherein s_i and $\hat{s}_i$ represent the states of the trellises corresponding to the codes $\mathbf{c}_i$ and $\hat{\mathbf{c}}_i$, respectively. To count the multiplicities of all possible $\mathbf{D}_{\mathbf{c},\hat{\mathbf{c}}}$'s over the joint code of the two users, a state transition matrix $S_{1,2}$ is assigned to the product trellis whose element in the kth row and the lth column is either zero corresponding to the case where the transition from state k to state l is not allowed, or in the form of

$$[S_{1,2}]_{k,l} = D_{11}^{q_{11}^{k,l}} \times D_{12}^{q_{12}^{k,l}} \times D_{22}^{q_{22}^{k,l}}, \quad k, l = 1, ..., (n_{s_1} \times n_{s_2})^2 \tag{6.9}$$

where D_{11}, D_{12}, D_{22} are dummy variables used to list the multiplicities of the different types of errors between two pairs of codewords [121]. The exponent $q_{i,i}^{k,l}$ is the number of indices in which the ith users' correct and erroneous labels corresponding to the transition from state k to state l in product trellis differ from each other. The exponent $q_{i,j}^{k,l}$ with $i \neq j$ is the number of coincidences between the previous indices for ith and jth user. Each of these components are used to compute the contribution of the transition from state k to state l to the corresponding entry of the $\mathbf{D}_{\mathbf{c},\hat{\mathbf{c}}}$.

Tighter bounds are obtained by performing expurgation of the union bound by using a technique developed in [122], which takes into account only simple error events defined as errors associated with the paths that diverge from the correct path through the trellis in only one segment of the trellis diagram. To efficiently count these simple error events, the specific technique given in [121] has been adapted, in which an error state in the product trellis is introduced. The transition to the error state occurs only when the two paths that diverged before merge for the first time. Also, the only possible transition from this state is to itself. Considering L stages of the joint trellis state transitions, the complete

list of possible $\mathbf{D}_{\mathbf{c},\hat{\mathbf{c}}}$ types for the transmitted codewords has been obtained via calculating the Lth power of $S_{1,2}$. Taking the trellis termination into account, the final stages of the state transition matrix considered in the computation has been also modified accordingly [121].

It is argued that the performance of the codes can be ordered based on their performance computed for a sufficiently large (but relatively small) length code and by considering a shorter frame length than the intended design length the computational cost is reduced and the code design process is simplified. Another simplification is performed where the number of terms for each entry of $S_{1,2}$ is restricted to those components (q_{ij}) with magnitudes less than a specific threshold knowing that the omitted terms do not effect the error rate bound considerably [121]. It is noted that, the final computations based on this truncation approach should be considered as approximations rather than being true upper-bounds.

The code design is carried out by searching for the code pair minimizing the upper bound in (6.6).

6.3 Performance Analysis

So far we have reviewed the derivation and systematic calculation of the upper bound on the error probability for the case of GICs without fading from [119]. As we can see from the numerical results in [119], JML decoding has a better decoding performance in all Gaussian channel examples regardless of the interference level, hence we use JML decoding for the fading case as well. We follow the same approach as in Section 6.2.1, and utilize the union bound technique and perform averaging over the fading coefficients to obtain error rate bounds for the fading case. We note that while there are other more sophisticated and improved bounds (such as those based on the Gallager bound [123, 124] and tangential sphere bound [125]), they have higher computational complexities, which makes them unsuitable for the code design purposes, hence they are not explored here.

6.3.1 I.I.D. Fading Interference Channel

We now consider i.i.d. fading with JML decoding and derive the union bound for this case. The channel is neither strong nor weak interference due to fading. Using the union bound, the overall frame error probability under JML decoding can be upper-bounded as,

$$P_\varepsilon \leq P_{\varepsilon,1} + P_{\varepsilon,2}, \tag{6.10}$$

where

$$\begin{aligned} P_{\varepsilon,i} &\leq E_{\boldsymbol{\alpha}_i}\left[\frac{1}{|\mathcal{C}|}\sum_{\mathbf{c}}\sum_{\hat{\mathbf{c}}\neq\mathbf{c}} P_{\varepsilon,i}(\mathbf{c},\hat{\mathbf{c}}|\boldsymbol{\alpha}_i)\right] \\ &= \frac{1}{|\mathcal{C}|}\sum_{\mathbf{c}}\sum_{\hat{\mathbf{c}}\neq\mathbf{c}} E_{\boldsymbol{\alpha}_i}\Big[P_{\varepsilon,i}(\mathbf{c},\hat{\mathbf{c}}|\boldsymbol{\alpha}_i)\Big]. \end{aligned} \tag{6.11}$$

The average pairwise error probability in this case can be upper bounded as

$$\begin{aligned} &E_{\boldsymbol{\alpha}_i}\Big[P_{\varepsilon,i}(\mathbf{c},\hat{\mathbf{c}}|\boldsymbol{\alpha}_i)\Big] = E_{\boldsymbol{\alpha}_i}\left[Q\left(\sqrt{\frac{Ed_i^2(\mathbf{c},\hat{\mathbf{c}})}{2N_0}}\right)\right], \\ &\leq E_{\boldsymbol{\alpha}_i}\left[e^{-\frac{Ed_i^2(\mathbf{c},\hat{\mathbf{c}})}{4N_0}}\right], \\ &= E_{\boldsymbol{\alpha}_i^R}\left[e^{-\sum_{t=1}^{n}\frac{(\alpha_{1i,t}^R)^2 d_{11,t}+(\alpha_{2i,t}^R)^2 d_{22,t}+2\alpha_{1i,t}^R\alpha_{2i,t}^R d_{12,t}}{4N_0}}\right] \\ &\quad\times E_{\boldsymbol{\alpha}_i^I}\left[e^{-\sum_{t=1}^{n}\frac{(\alpha_{1i,t}^I)^2 d_{11,t}+(\alpha_{2i,t}^I)^2 d_{22,t}+2\alpha_{1i,t}^I\alpha_{2i,t}^I d_{12,t}}{4N_0}}\right], \\ &= \left(\prod_{t=1}^{n}\frac{1}{\pi\sigma_{1i}\sigma_{2i}}\int e^{-\frac{\boldsymbol{\alpha}_{i,t}^R\mathbf{D}_t(\boldsymbol{\alpha}_{i,t}^R)^\intercal}{4N_0}}\times e^{-\boldsymbol{\alpha}_{i,t}^R\boldsymbol{\Sigma}^{-1}(\boldsymbol{\alpha}_{i,t}^R)^\intercal}d\boldsymbol{\alpha}_{i,t}^R\right)^2 \\ &= \prod_{t=1}^{n}\left(\frac{8N_0}{\sigma_{1i}\sigma_{2i}\sqrt{(d_{11,t}+\frac{8N_0}{\sigma_{1i}^2})(d_{22,t}+\frac{8N_0}{\sigma_{2i}^2})-d_{12,t}^2}}\right)^2 \\ &= \prod_{t=1}^{n} 8N_0\Big(d_{11,t}\sigma_{1i}^2+d_{22,t}\sigma_{2i}^2+8N_0\Big)^{-1} \end{aligned}$$

where $\mathbf{D}_t$ is the codeword difference matrix at time instant t, i.e., $\mathbf{D}_t = (\mathbf{c}_t -$

$\hat{\mathbf{c}}_t)(\mathbf{c}_t - \hat{\mathbf{c}}_t)^\dagger = \begin{bmatrix} d_{11,t} & d_{12,t} \\ d_{21,t} & d_{22,t} \end{bmatrix}$ and $\mathbf{\Sigma} = E[(\alpha_{i,t}^R)^\intercal \alpha_{i,t}^R] = \begin{bmatrix} \frac{\sigma_{1i}^2}{2} & 0 \\ 0 & \frac{\sigma_{2i}^2}{2} \end{bmatrix}$. In order to count the multiplicities of the codeword difference matrix for all correct-erroneous codeword pairs, we use the same procedure as in Section 6.2.1.

6.3.2 Quasi-Static Fading Interference Channel

In this part, we assume that the fading is slow, and specifically, the fading coefficients are constant throughout each codeword. While it is possible to consider the outage probability for this case, we still consider the average error probability as the performance metric as done in the space-time coding literature [121]. Considering the quasi-static fading IC and using the JML decoding, the union bound on the probability of frame error at both receivers can be written as in (6.10) where the expectation is performed over the distribution of the fading coefficient. The corresponding average pairwise error probability in this case can be bounded as

$$\begin{aligned}
E_{\boldsymbol{\alpha}_i}\Big[P_{\varepsilon,i}(\mathbf{c},\hat{\mathbf{c}}|\boldsymbol{\alpha}_i)\Big] &= E_{\boldsymbol{\alpha}_i}\left[Q\left(\sqrt{\frac{Ed_i^2(\mathbf{c},\hat{\mathbf{c}})}{2N_0}}\right)\right], \\
&\leq E_{\boldsymbol{\alpha}_i}\left[e^{-\frac{Ed_i^2(\mathbf{c},\hat{\mathbf{c}})}{4N_0}}\right], \\
&= E_{\boldsymbol{\alpha}_i^R}\left[e^{-\frac{(\alpha_{1i}^R)^2 d_{11}+(\alpha_{2i}^R)^2 d_{22}+2\alpha_{1i}^R\alpha_{2i}^R d_{12}}{4N_0}}\right] \\
&\quad \times E_{\boldsymbol{\alpha}_i^I}\left[e^{-\frac{(\alpha_{1i}^I)^2 d_{11}+(\alpha_{2i}^I)^2 d_{22}+2\alpha_{1i}^I\alpha_{2i}^I d_{12}}{4N_0}}\right], \\
&= \left(\frac{1}{\pi\sigma_{1i}\sigma_{2i}}\int e^{-\frac{\boldsymbol{\alpha}_i^R \mathbf{D}_{\mathbf{c},\hat{\mathbf{c}}}(\boldsymbol{\alpha}_i^R)^\intercal}{4N_0}} \times e^{-\boldsymbol{\alpha}_i^R \mathbf{\Sigma}^{-1}(\boldsymbol{\alpha}_i^R)^\intercal} d\boldsymbol{\alpha}_i^R\right)^2 \\
&= \left(\frac{1}{\pi\sigma_{1i}\sigma_{2i}}\int e^{-\frac{1}{4N_0}\boldsymbol{\alpha}_i^R \begin{bmatrix} d_{11}+\frac{8N_0}{\sigma_{1i}^2} & d_{12} \\ d_{12} & d_{22}+\frac{8N_0}{\sigma_{2i}^2} \end{bmatrix}(\boldsymbol{\alpha}_i^R)^\intercal} d\boldsymbol{\alpha}_i^R\right)^2
\end{aligned} \tag{6.12}$$

$$= \left(\frac{8N_0}{\sigma_{1i}\sigma_{2i}\sqrt{(d_{11} + \frac{8N_0}{\sigma_{1i}^2})(d_{22} + \frac{8N_0}{\sigma_{2i}^2}) - d_{12}^2}} \right)^2$$

$$= 64N_0^2 \left((d_{11}\sigma_{1i}^2 + 8N_0)(d_{22}\sigma_{2i}^2 + 8N_0) - d_{12}^2\sigma_{1i}^2\sigma_{2i}^2 \right)^{-1}$$

where $\mathbf{D}_{\mathbf{c},\hat{\mathbf{c}}}$ is defined in (6.8) and $\mathbf{\Sigma} = E[(\alpha_i^R)^\intercal \alpha_i^R] = \begin{bmatrix} \frac{\sigma_{1i}^2}{2} & 0 \\ 0 & \frac{\sigma_{2i}^2}{2} \end{bmatrix}$. Using numerical examples, we have observed that although the derived union bound on the error probability under quasi-static fading is much tighter compared to the bound in [126], it is still not tight enough for code design purposes. We note that a similar observation has been made in [121] in the context of space-time trellis codes over a quasi-static fading channel. Therefore, we use the technique proposed in [127] to limit the conditional union bound on the error probability before averaging over the fading coefficient distribution and obtain a new upper bound as

$$P_{\varepsilon,i} \leq E_{\boldsymbol{\alpha}_i} \left[\min \left[1, \frac{1}{|\mathcal{C}|} \sum_{\mathbf{c}} \sum_{\hat{\mathbf{c}} \neq \mathbf{c}} P_{\varepsilon,i}(\mathbf{c}, \hat{\mathbf{c}} | \boldsymbol{\alpha}_i) \right] \right]. \tag{6.13}$$

Obviously, we cannot move the averaging operation inside the min function, hence, (6.13) needs to be calculated either by numerical evaluation of the multi-dimensional integration or by the use of Monte Carlo techniques. Although the bound in (6.13) is tight, due to high complexity of its calculation, it is not a suitable metric for the code design purposes. Therefore, it is provided as a way of theoretical performance characterization.

In order to verify the tightness of these two bounds we consider an example with quasi-static fading IC with $SNR_1 - SNR_2 = 2$ dB, $INR_1 - SNR_2 = 1$ dB, and $INR_2 - SNR_1 = 2$ dB. The simulation and bound results for the optimal P2P convolutional code (5,7)/(7,5) is shown in Fig. 6.2. The result clearly shows that by utilizing the more sophisticated bound in (6.13) we can obtain much a tighter bound on the error probability.

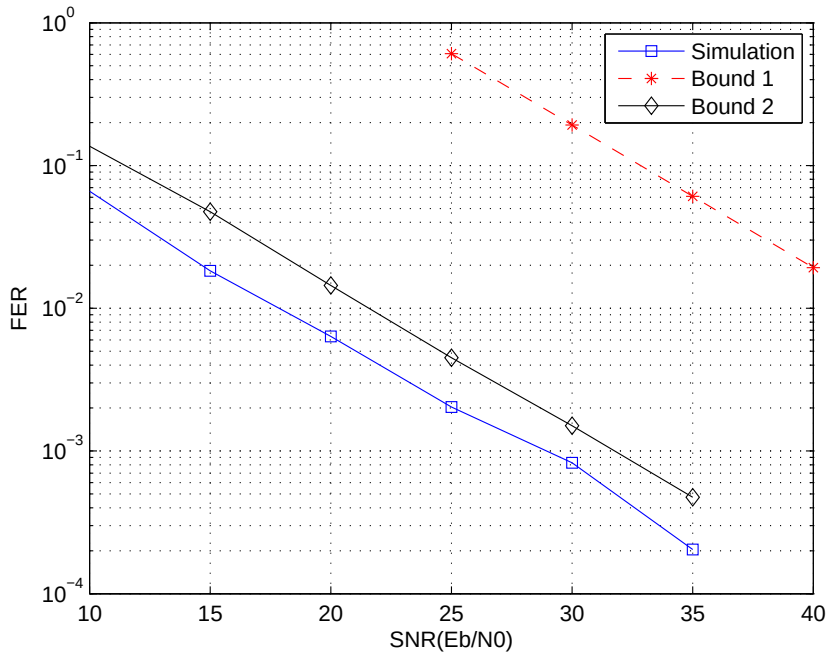

Figure 6.2: Simulation and bound results of the code (5,7)/(7,5) for the quasi-static fading IC with, $SNR_1 - SNR_2 = 1$ dB, $INR_1 - SNR_2 = 2$ dB, and $INR_2 - SNR_1 = 1.5$ dB.

6.4 Code Design Examples

We compare the performance of the optimized trellis-based codes with that of LDPC codes (96.33.964) and (96.33.966) taken from [128] for different cases for several examples. We consider code rates of 1/2 and code block length of $N = 96$. The trellis-based codes are represented in octal form; i.e., $(m_1, n_1)/(m_2, n_2)$ represents the codes adopted for the GIC case where the code (m_i, n_i) represents the convolutional encoder in octal notation for transmitter i. The code optimization is carried out through ordering the codes' performance by computing the approximate bounds in (6.6), and (6.10) for the cases of GIC and i.i.d. fading IC, respectively. To efficiently handle the matrix multiplications and cope with the memory limitations, the number of terms for each entry of the state transition matrix is truncated to 25. In the following unlike [119] for the Gaussian interference channel examples we consider complex channel coefficients.

6.4.1 Gaussian Interference Channel without Fading

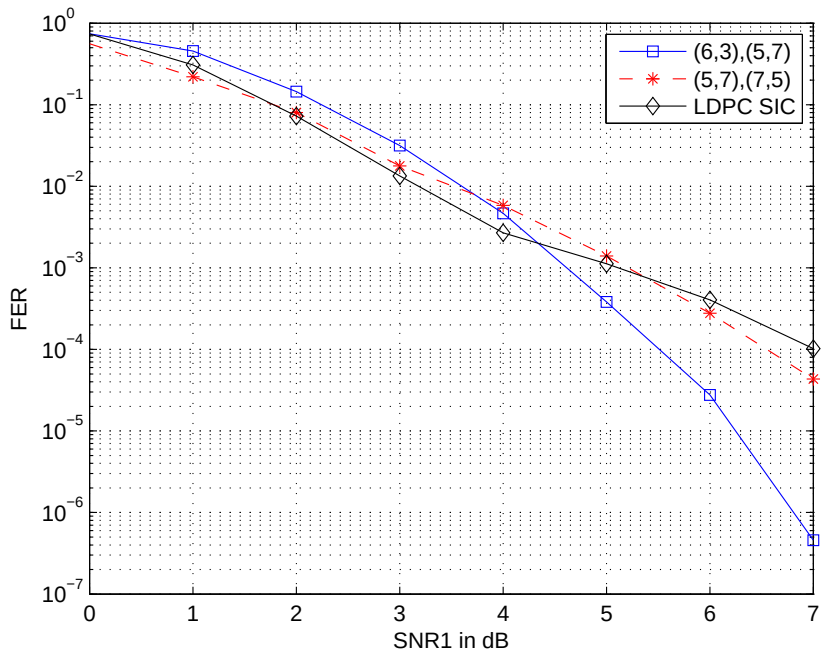

Figure 6.3: Total frame error rate of trellis-based codes employed for a GIC with strong interference, $SNR_1 - SNR_2 = 1$ dB, $INR_1 - SNR_2 = 2$ dB, $INR_2 - SNR_1 = 1.5$ dB, $\angle h_{11} = \angle h_{22} = \frac{\pi}{4}$, and $\angle h_{12} = \angle h_{21} = \frac{\pi}{3}$.

For the first example, we consider a GIC with $SNR_1 - SNR_2 = 1$ dB, $INR_1 - SNR_2 = 2$ dB, $INR_2 - SNR_1 = 1.5$ dB, $\angle h_{11} = \angle h_{22} = \frac{\pi}{4}$, and $\angle h_{12} = \angle h_{21} = \frac{\pi}{3}$. We perform the code design at $SNR_1 = 8$ dB for which $(6,3)/(5,7)$ minimize the upper bound in (6.6). Comparing the result with that of [119], we can see that for the same SNR and INR values depending on the phases of the channel coefficients, different codes might perform better. For comparison purposes, we also consider codes designed for P2P channels. In order to employ the P2P codes for the two-user setup, an *interleaved* scheme is adopted where the same code with different assignment of generator matrices to the output bits are used for different users. That is, for the first user we employ the code $(5,7)$, which has the largest minimum distance among the codes with memory 2. For the second user, we adopt the code $(7,5)$, which obviously is the same code with $(5,7)$ with a different assignment of coded bits. Fig. 6.3 illustrates the decoding results for the trellis-based and LDPC codes employed for this example. The performance of

LDPC codes is simulated using soft interference cancellation (SIC) [88] decoding. It is also evident that while the P2P optimal code and LDPC codes have very close performances the optimized trellis-based code outperforms both.

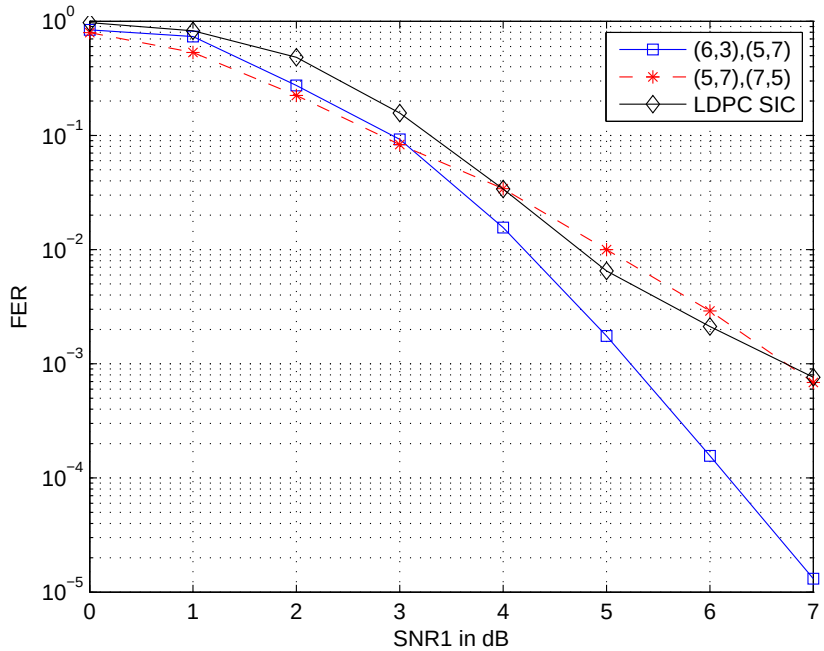

Figure 6.4: Total frame error rate of trellis-based codes employed for a GIC with weak interference, $SNR_1 - SNR_2 = 0.5$ dB, $INR_1 - SNR_2 = -1$ dB, $INR_2 - SNR_1 = -1.5$ dB, $\angle h_{11} = \angle h_{22} = \frac{\pi}{4}$, and $\angle h_{12} = \angle h_{21} = \frac{\pi}{3}$.

As the second example we consider a GIC with $SNR_1 - SNR_2 = 0.5$ dB, $INR_1 - SNR_2 = -1$ dB, $INR_2 - SNR_1 = -1.5$ dB, $\angle h_{11} = \angle h_{22} = \frac{\pi}{4}$, and $\angle h_{12} = \angle h_{21} = \frac{\pi}{3}$. The code design is pursued by minimizing (6.6) at $SNR = 8$ dB over codes with 4 states. The optimization process results in the code pair $(6,3)/(5,7)$. Fig. 6.4 shows the decoding results of the optimized codes along with that of P2P optimal one and off-the-shelf LDPC codes. It is shown that, the optimized codes offer better performance than the P2P codes and LDPC codes.

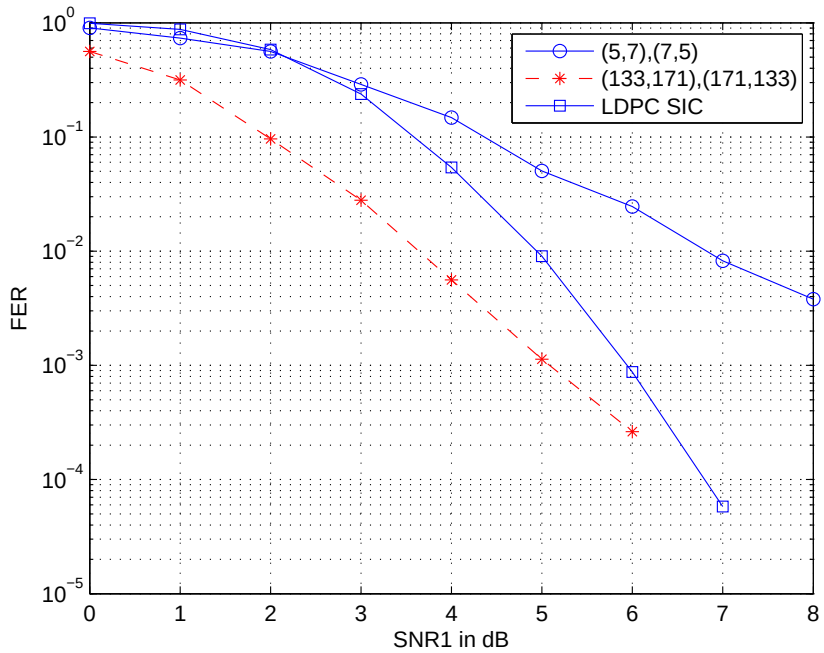

Figure 6.5: Total frame error rate of trellis-based codes employed for an i.i.d. fading IC with $SNR_1 - SNR_2 = 2$ dB, $INR_1 - SNR_2 = 1$ dB, and $INR_2 - SNR_1 = 2$ dB.

6.4.2 I.I.D. Fading Interference Channel

As the first example, we consider an i.i.d. fading IC with $SNR_1 - SNR_2 = 2$ dB, $INR_1 - SNR_2 = 1$ dB, and $INR_2 - SNR_1 = 2$ dB. Code design is performed by minimizing the performance bound in (6.10) at $SNR_1 = 8$ dB over the convolutional codes with memory 2. The minimum value of the upper-bound is achieved for the $(5,7)/(7,5)$ code. We observe that the P2P optimal code among all memory 2 codes is the best one, which suggests that P2P optimal codes perform well in i.i.d. fading scenarios. Fig. 6.5 illustrates the decoding performance of the trellis-based codes and LDPC codes. As it is observed the performance of the optimal convolutional codes with memory 2 is worse than the LDPC codes, however, by increasing the memory of the code and utilizing optimal P2P convolutional code with memory 6, the performance improves and beats that of the LDPC code considerably.

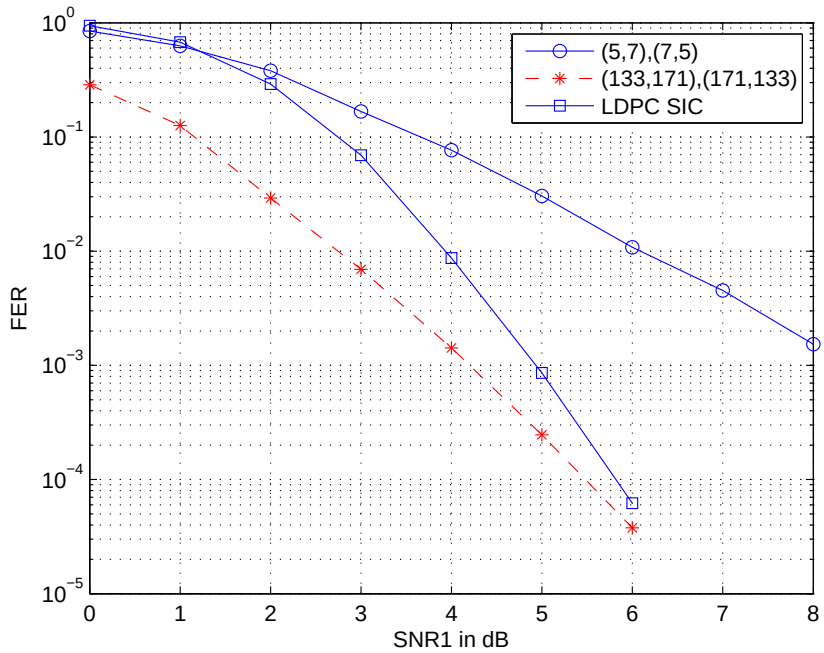

Figure 6.6: Total frame error rate of trellis-based codes employed for an i.i.d. fading IC with $SNR_1 - SNR_2 = 1$ dB, $INR_1 - SNR_2 = 2$ dB, and $INR_2 - SNR_1 = 1.5$ dB.

As another example, code optimization is carried out for an i.i.d. fading IC with $SNR_1 - SNR_2 = 1$ dB, $INR_1 - SNR_2 = 2$ dB, and $INR_2 - SNR_1 = 1.5$ dB. As in the previous example, code design is done targeting an SNR value of $SNR_1 = 8$ dB, that is, the upper-bound is minimized for memory 2 codes at this SNR value. As in the previous example, the $(5,7)/(7,5)$ code minimizes the upper bound in (6.10). Fig. 6.6 demonstrates the decoding results for the codes adopted. The LDPC code performs better than the optimal trellis based code with memory 2, however, we observe that by increasing the memory of the convolutional code we can beat the LDPC code performance. We again attribute the good performance of the LDPC code to the observation that the optimal P2P codes perform well for the i.i.d. fading case.

We also consider an i.i.d. fading IC with $SNR_1 - SNR_2 = 0.5$ dB, $INR_1 - SNR_2 = -1$ dB, and $INR_2 - SNR_1 = -1.5$ dB where the average level of the interference is lower than the signal level. The code design is pursued by

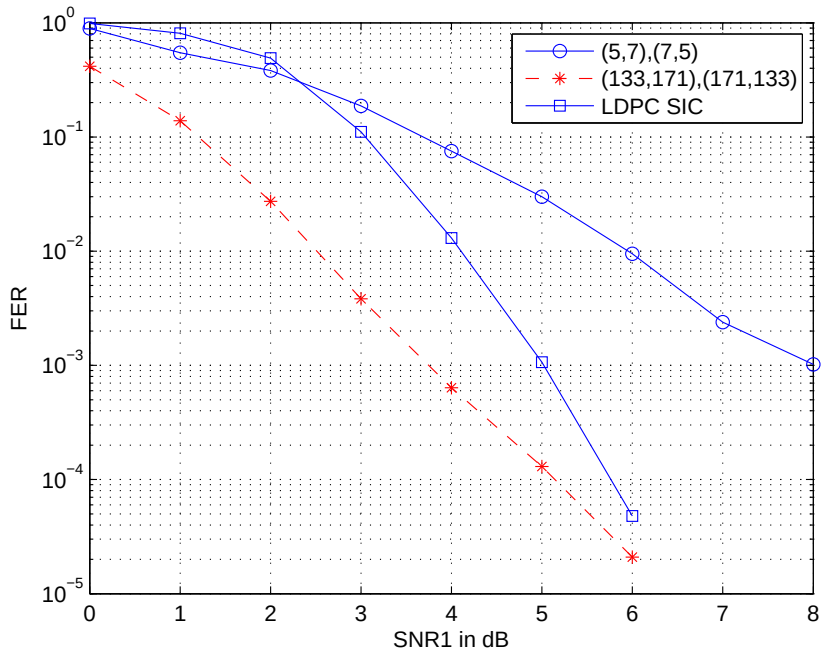

Figure 6.7: Total frame error rate of trellis-based codes employed for an i.i.d. fading IC with $SNR_1 - SNR_2 = 0.5$ dB, $INR_1 - SNR_2 = -1$ dB, and $INR_2 - SNR_1 = -1.5$ dB.

minimizing (6.10) at $SNR = 8$ dB over memory 2 codes. The optimization process results in the code pair $(5,7)/(7,5)$. The performance of the optimized codes is compared against that of the LDPC code. Fig. 6.7 shows the decoding results. We observe that as in the case of previous example while the performance of the LDPC code beats the best trellis-based code with memory 2, a significant gain can be obtained by using a convolutional code of higher memory.

As the final example, code optimization is carried out for an i.i.d. fading IC with $SNR_1 - SNR_2 = -0.75$ dB, $INR_1 - SNR_2 = -1.5$ dB, and $INR_2 - SNR_1 = -0.5$ dB. For this case, $(5,7)/(7,5)$ pair achieve the minimum of the expression in (6.10) considering all the codes with memory 2 where the bounds are computed at $SNR = 8$ dB. For comparison, we also consider an LDPC code and the optimal P2P convolutional code with memory 6. Fig. 6.8 shows the performance of the employed codes demonstrating (as in the previous examples) that the performance of the optimal P2P convolutional code with memory 6 beats the

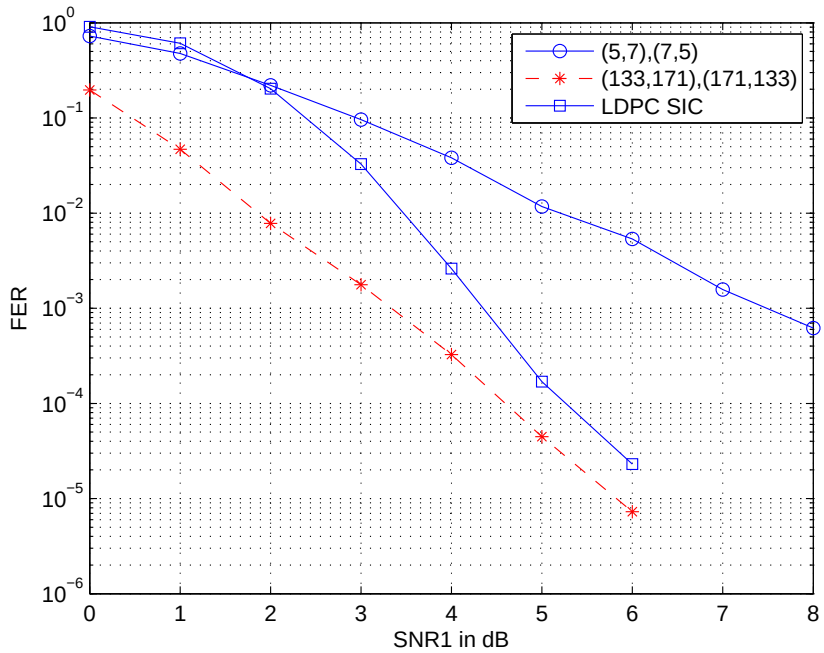

Figure 6.8: Total frame error rate of trellis-based codes employed for an i.i.d. fading IC with $SNR_1 - SNR_2 = -0.75$ dB, $INR_1 - SNR_2 = -1.5$ dB, and $INR_2 - SNR_1 = -0.5$ dB.

other alternatives.

6.5 Chapter Summary

In this chapter, the short block length code design method for the two-user GIC without fading from [119] is extended to the complex channel coefficients case and to fading. Performance bounds based on the union bounding technique have been derived and then they are utilized for designing trellis-based codes. It is shown that for GIC without fading, different codes might offer better performance for the same SNR and INR values (but with different phases of channel coefficients). In addition, it is demonstrated that the optimized trellis based codes for these cases outperform the LDPC codes and P2P codes. The P2P optimal convolutional codes are found to have the best performance for i.i.d. fading ICs and perform superior to the LDPC codes by increasing the memory of the trellis code.

Finally, we note that, for the case of quasi-static fading IC, a tight performance bound has been proposed for theoretical performance characterization, which can be evaluated by using Monte Carlo techniques or numerical multidimensional integration.

Chapter 7

Code Design for Two-User Interference Channels with Energy Harvesting Transmitters

So far, we have considered the two scenarios of energy harvesting communication systems and communication over interference channels separately, and explored different coding solutions for them. We now turn our attention to a scenario where both of these problems is jointly dealt with. To this end, we consider a two-user communication system with energy harvesting transmitters that are equipped with a finite battery operating over a noisy channel. We obtain achievable rate regions considering i.i.d. Shannon strategies at both users while ignoring the memory in the battery state with both single user and joint decoding at the receivers. We design explicit and implementable codes based on concatenation of an NLTC with an outer LDPC code. As in Chapter 4, we first ignore the memory in the battery state and consider a simplified model utilized in the code design. We then take the memory into account and develop a more sophisticated decoding method. We demonstrate the superiority of the newly developed solution over the naive approach via several error rate simulations. Numerical results show that utilizing the proposed scheme, rate pairs close to the optimal boundary of ARR can be obtained.

7.1 System Description

We consider a two-user communication system with energy harvesting transmitters and interference between transmitted signals, referred to as an energy harvesting interference channel (EHIC) (Fig. 7.1). We use the energy harvesting model introduced in [14], where at each time instant an energy packet arrives with probability q independent of the energy arrivals at other time instances, hence we deal with two i.i.d. energy arrival processes (one for each transmitter $E_{ji} \sim$ Bernoulli$(q_j), j \in \{1, 2\}$). We assume that these two processes are independent of each other. The channel inputs X_{ji} are also binary with either zero or one unit energy cost. Each energy harvesting transmitter is equipped with a finite-sized battery for which the battery size is a multiple of the fixed unit of energy harvests (denoted by B_{max}).

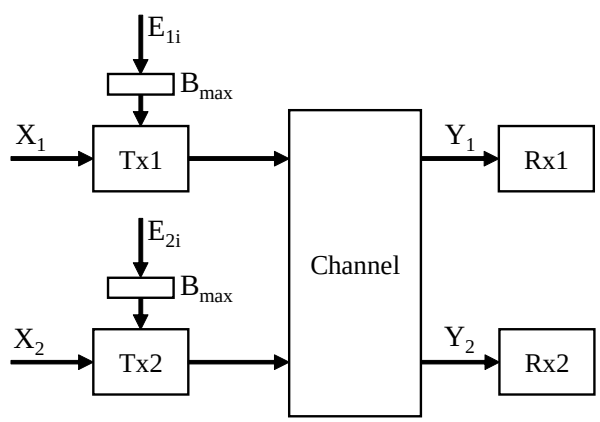

Figure 7.1: System model for a two user energy harvesting interference channel.

By observing the battery state S_{ji}, for each channel use, the transmitter j first transmits a symbol X_{ji}, and then it harvests energy E_{ji} and stores it in its battery if there is space. If the battery is empty, regardless of what the input bit is, $X_{ji} = 0$ is transmitted. The battery state evolves as $S_{ji+1} = \min\{S_{ji} - X_{ji} + E_{ji}, B_{max}\}$, and it is causally known at the transmitter side only. In this model, we have a state dependent channel for which the battery state S_{ji+1} depends on the channel input X_{ji}, energy arrival E_{ji} and the previous battery state, hence it has a finite memory. For the single user energy harvesting communication system, it has been

shown that although i.i.d. Shannon strategy does not yield the channel capacity, it still provides reasonable achievable rates [9, 14]. Hence, we consider the same strategy for the two-user system as well and obtain an ARR.

We consider the encoding scheme with i.i.d. on-off signaling and ones' density ($P(X_{ji} = 1) = p_j$) at the jth user. Since the energy arrivals are i.i.d., the battery state process at each transmitter can be modelled as the same Markov chain as in Fig. 4.1, which is irreducible and aperiodic. Therefore, it has a stationary probability distribution denoted by $\{\pi_{ji}\}_{i=0}^{B_{max}}$ where $\pi_{ji} = P(S_j = i)$ is the steady state probability of the Markov chain being in state i. We obtain

$$\pi_{j0} = \frac{(1-q_j)p_j}{(1-q_j)p_j + q_j \sum_{i=0}^{B_{max}-1} (\frac{q_j(1-p_j)}{p_j(1-q_j)})^i} \tag{7.1}$$

$$\pi_{ji} = \frac{1}{1-q_j}(\frac{q_j(1-p_j)}{p_j(1-q_j)})^i \pi_{j0}, \ i = 1, ..., B_{max}. \tag{7.2}$$

If the receivers ignore the memory in the model, and assume that the battery states are i.i.d. with the state probabilities given above, namely, using NIID [14], the randomness in the battery states in this system model becomes memoryless, i.e., the battery condition operates as a memoryless Z channel with crossover $1 \rightarrow 0$ probability π_{j0}. Therefore, we can utilize a suitable Han-Kobayashi scheme on this simplified model to obtain an achievable rate region for the original problem.

In order to illustrate the above argument, we consider an instance of the discrete memoryless interference channel with energy harvesting transmitters and calculate the achievable rate region with different parameters. For this example the input-output relationship for Channel 1 is given by $Y_1 = (X_1 \otimes X_2) \oplus Z_1$, $Y_2 = X_2 \oplus Z_2$ where $\oplus$ and $\otimes$ represent the "XOR" and the "OR" operations, respectively, with Z_1 and Z_2 being the noise samples at receiver 1 and 2 drawn from a Bernoulli distribution with parameters $\epsilon_1 = 0.21$ and $\epsilon_2 = 0.25$, respectively. The achievable rate subregion using single user decoding at both users for

a specific input distribution (for fixed p_1 and p_2) is given by

$$\begin{aligned}
R_1 &= H_2\Big(p_1(\bar{\pi}_{10}\bar{\epsilon}_1 + \pi_{10}(p_2\bar{\pi}_{20} * \epsilon_1)) + \bar{p}_1(p_2\bar{\pi}_{20} * \epsilon_1)\Big) \\
&\quad - p_1 H_2\Big(\bar{\pi}_{10}\bar{\epsilon}_1 + \pi_{10}(p_2\bar{\pi}_{20} * \epsilon_1)\Big) - \bar{p}_1 H_2\Big(p_2\bar{\pi}_{20} * \epsilon_1\Big), \\
R_2 &= H_2\Big(p_2(\pi_{20} * \epsilon_2) + \bar{p}_2\epsilon_2\Big) - p_2 H_2(\pi_{20} * \epsilon_2) - \bar{p}_2 H_2(\epsilon_2),
\end{aligned}$$

where $\bar{x} = 1 - x$ and $x * y = x(1-y) + (1-x)y$. The ARR corresponding to this scheme is obtained by taking the convex hull of all of the subregions corresponding to different p_1, p_2 values with $0 \leq p_1, p_2 \leq 1$.

The ARRs for single and two unit battery sizes and energy arrival probabilities $q = 0.5$ are shown in Fig. 7.2, which demonstrates that even by using a unit battery at the transmitters we can still achieve a significantly large portion of the ARR obtained with no energy harvesting constraints. The ARRs corresponding to uniform and identically distributed inputs are also shown on the same figure, demonstrating that significant improvements can be gained by allowing nonuniform input distributions for the present setup.

As another example, the ARR for the two-user EH Gaussian interference channel with channel coefficients (from the jth transmitter to the ith receiver) h_{ji}, and noise variance σ_i^2 for $i, j \in \{1, 2\}$ using i.i.d. on-off signaling with $P(X_i = 1) = p_i$, $i = 1, 2$, at the inputs can be obtained as

$$R_i = I(Y_i; X_i) = h(Y_i) - h(Y_i|X_i),$$

where

$$\begin{aligned}
Y_i \sim &\Big(p_i\bar{\pi}_{i0}p_j\bar{\pi}_{j0}\Big)\mathcal{N}(h_{ii} + h_{ji}, \sigma_i^2) \\
&+ \Big(p_i\bar{\pi}_{i0}(1 - p_j\bar{\pi}_{j0})\Big)\mathcal{N}(h_{ii}, \sigma_i^2) \\
&+ \Big((1 - p_i\bar{\pi}_{i0})p_j\bar{\pi}_{j0}\Big)\mathcal{N}(h_{ji}, \sigma_i^2) \\
&+ \Big((1 - p_i\bar{\pi}_{i0})(1 - p_j\bar{\pi}_{j0})\Big)\mathcal{N}(0, \sigma_i^2),
\end{aligned}$$

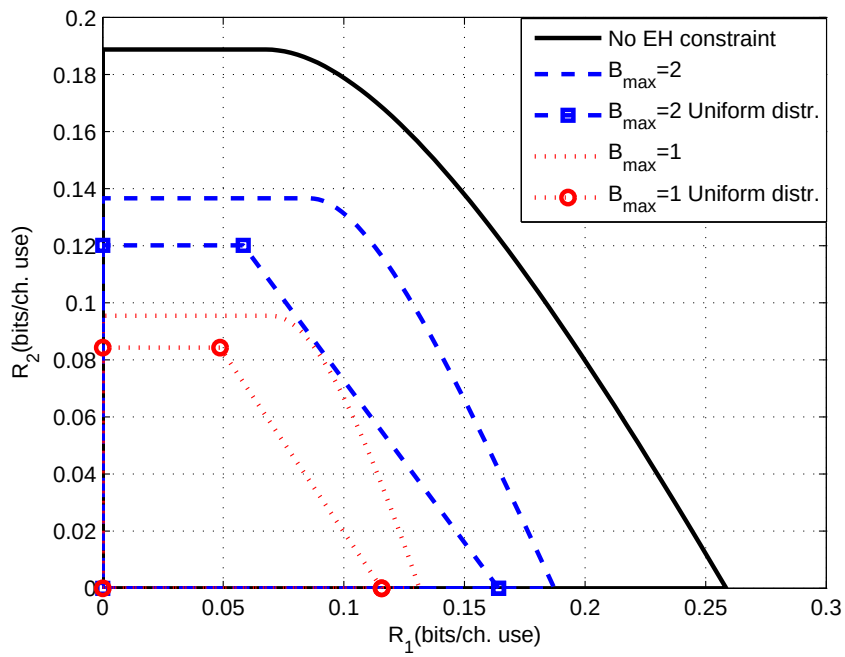

Figure 7.2: The ARR for Channel 1 with two different battery sizes and $q = 0.5$.

and

$$
\begin{aligned}
Y_i|X_i \sim & p_i\Big[\Big(\bar{\pi}_{i0}p_j\bar{\pi}_{j0}\Big)\mathcal{N}(h_{ii}+h_{ji},\sigma_i^2) \\
& + \Big(\bar{\pi}_{i0}(1-p_j\bar{\pi}_{j0})\Big)\mathcal{N}(h_{ii},\sigma_i^2) + \Big(\pi_{i0}p_j\bar{\pi}_{j0}\Big)\mathcal{N}(h_{ji},\sigma_i^2) \\
& + \Big(\pi_{i0}(1-p_j\bar{\pi}_{j0})\Big)\mathcal{N}(0,\sigma_i^2)\Big] \\
& + \bar{p}_i\Big[(p_j\bar{\pi}_{j0})\mathcal{N}(h_{ji},\sigma_i^2) + (1-p_j\bar{\pi}_{j0})\mathcal{N}(0,\sigma_i^2)\Big],
\end{aligned}
$$

and $\mathcal{N}(\mu,\sigma^2)$ denotes the Gaussian PDF with mean μ and variance σ^2.

The SNR and INR for this channel are defined as $\text{SNR}_i = \frac{h_{ii}^2}{2\sigma_i^2}$ and $\text{INR}_i = \frac{h_{ji}^2}{2\sigma_i^2}$, respectively. Fig. 7.3 depicts the ARR for the special case of $q = 0.5$, $SNR_1 = 1$, $SNR_2 = 0$, $INR_1 = 2$ and $INR_2 = 1$. As it can be seen from this figure, by utilizing a nonuniform input distribution, a significantly larger ARR compared to that of uniform inputs can be achieved for this case as well.

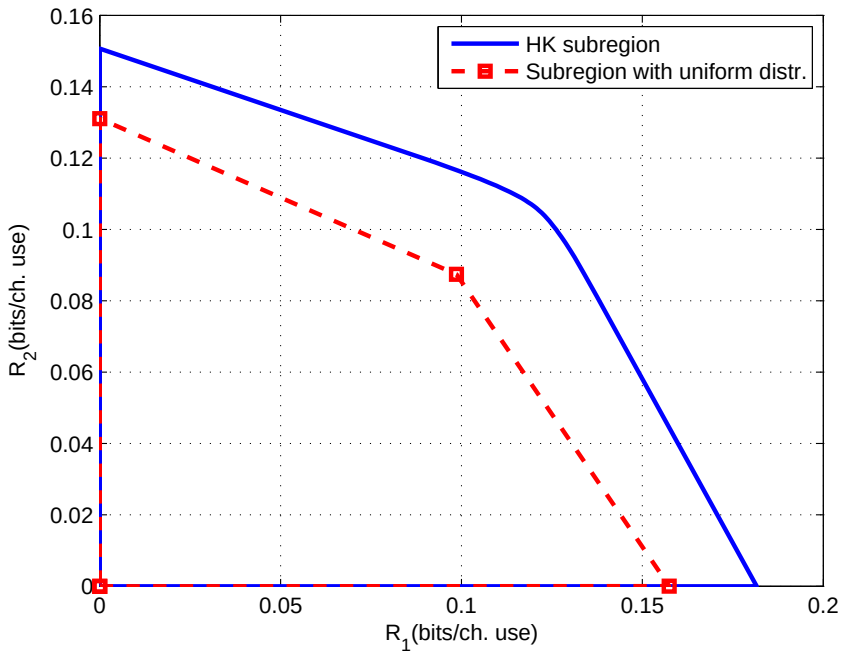

Figure 7.3: The ARR for Gaussian channel case with $q = 0.5$, $SNR_1 = 1$, $SNR_2 = 0$, $INR_1 = 2$ and $INR_2 = 1$.

7.2 Proposed Coding Scheme

As discussed in the previous section, in order to achieve rate pairs on the optimal boundary of the ARRs obtained by using the NIID scheme, specific nonuniform input distributions at the channel inputs need to be employed. To generate the required nonuniform input distribution and also to obtain good error correction performance, as in the previous chapters dealing with the energy harvesting and interference channel setups, we propose concatenation of an outer LDPC code with an inner NLTC as a practical approach. We propose using two different decoding methods at the receiver side, namely single user decoding (SUD) and joint decoding (JD). In cases where decoding of the interfering signal helps with the decoding of the desired signal (i.e., when the use of public messages are beneficial) we utilize the joint decoding method, otherwise we simply employ single user decoding.

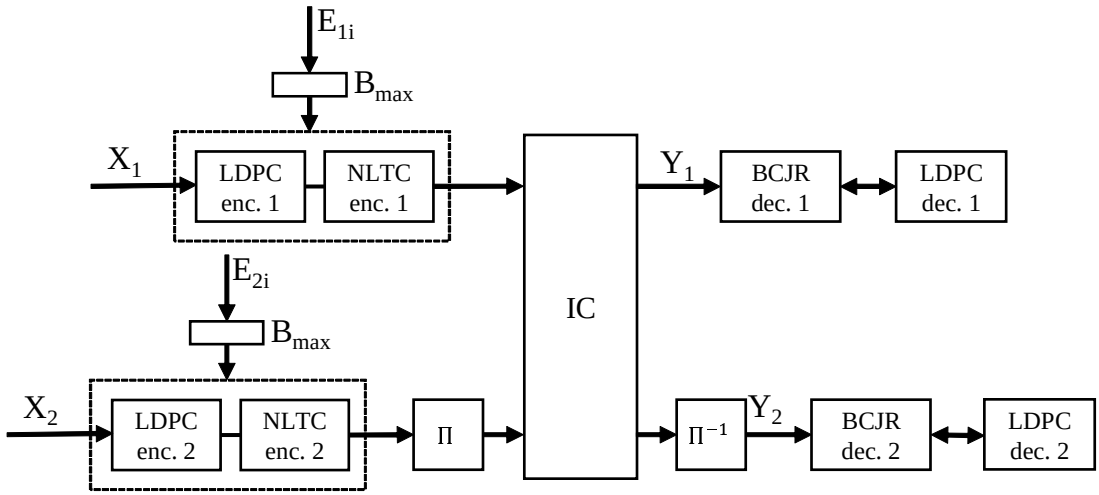

Figure 7.4: Block diagram of the proposed coding scheme.

The block diagram of the proposed coding scheme with SUD is shown in Fig. 7.4. The transmitter side consists of concatenation of an outer LDPC encoder with an inner NLTC. The goal of the inner NLTC is to induce the desired nonuniform distribution at the channel input while providing protection against channel noise. The outer LDPC code is intended to provide error correction capabilities. Each receiver decodes its intended signal while treating interference as noise. However, since the interference from the other user (which is treated as noise) is not i.i.d. (because of having a trellis based code), we utilize an interleaver and de-interleaver just before and right after the channel for one of the users. Fig. 7.5 depicts the block diagram of the proposed coding scheme with joint decoding at the receivers. The difference with the scheme in Fig. 7.4 is that we perform JD of both intended and interfering signals at the receiver side.

As a simple decoding approach, we first ignore the memory in the channel state and consider a channel with i.i.d. states with stationary probabilities given in (7.1). As a result we have a memoryless Z channel with crossover $1 \rightarrow 0$ probability π_{j0} connected to the memoryless noisy interference channel. Then a BCJR algorithm based decoding of both messages over the corresponding product trellis is adopted for the overall channel to compute the log-likelihood-ratios

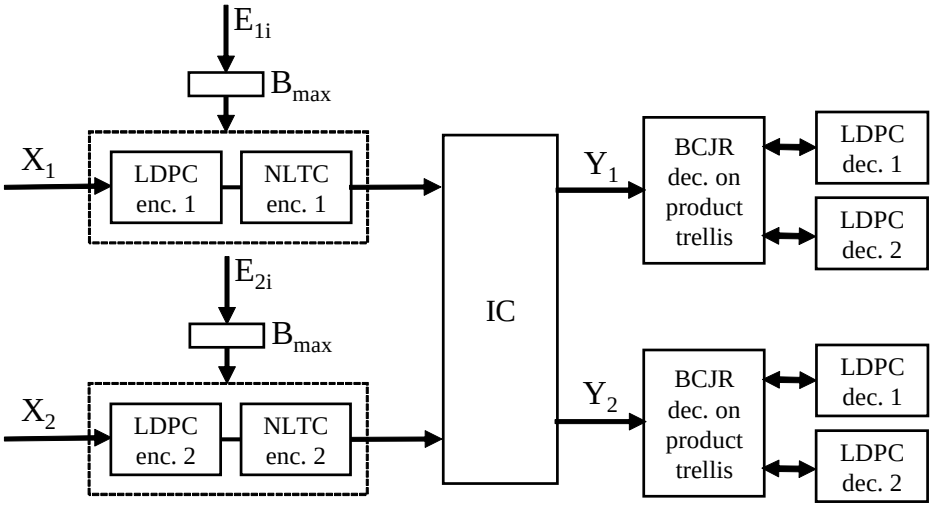

Figure 7.5: Block diagram of the proposed coding scheme.

(LLRs) of the encoded bits to be fed to the LDPC decoders. To improve the decoding performance, the soft outputs of the LDPC decoders are fed back to the BCJR decoder in an iterative fashion as also illustrated in Fig. 7.4. The decoding scheme described above is used for code design purposes in the next section, however, we introduce another (improved) iterative decoding solution in Section 7.2.1 which exploits the memory in the battery state as well.

The specifics of the NLTC and LDPC code design follow the same principles described in Section 4.3.

7.2.1 An Improved Iterative Decoding Algorithm

An improved iterative decoding algorithm can be developed following the same line of arguments as in Section 4.3.3 for the single user decoding scenario. From the product trellis of the two codes, we build an extended trellis by including the battery states of both users at the beginning of each trellis section along with the NLTC states, which expands the size of the product trellis by a factor of $(B_{max}+1)^2$, i.e., for each state in the product trellis, there are $(B_{max}+1)^2$

corresponding states in the extended trellis (one for each pair of battery states). Each transition in the product trellis corresponds to $(B_{max}+1)^2$ transitions in the extended trellis, however, some of these transitions might be invalid depending on the current and the next battery states and the output labels in the product trellis. In this approach, the BCJR decoder operates on the extended trellis and exchanges the soft extrinsic LLRs with the LDPC decoders in an iterative manner. We omit the details of this decoder as it is similar to the one in Section 4.3.3.

7.3 Numerical Examples

As a first example, we consider the two user discrete memoryless interference example in Section 7.1 with unit-sized battery transmitters. The achievable rate subregion considering i.i.d. inputs and single user decoding at both users is shown in Fig. 7.6. We consider a ones' density of $p = 0.25$ for both users and design an NLTC of memory 4 satisfying this constraint while maximizing the minimum distance of the code. The parameters of the designed trellis code is the same as the one given in Table 4.2.

The achievable rate subregion using i.i.d. inputs with a ones' density of $p = 0.25$ is also shown in this figure. Considering the specific designed NLTC and utilizing the numerical methods in [129], we calculate the achievable rates for both of the users with single user decoding. We illustrate the resulting achievable rate subregion in Fig. 7.6 as well, which clearly shows the advantage of using an NLTC instead of nonuniform i.i.d. inputs. In the next step, by fixing the inner NLTC, the outer LDPC codes are designed by maximizing the rate of the code for which the resulting degree distributions are given in Table 7.1. The achieved rate pair for this example is (0.07831,0.09705).

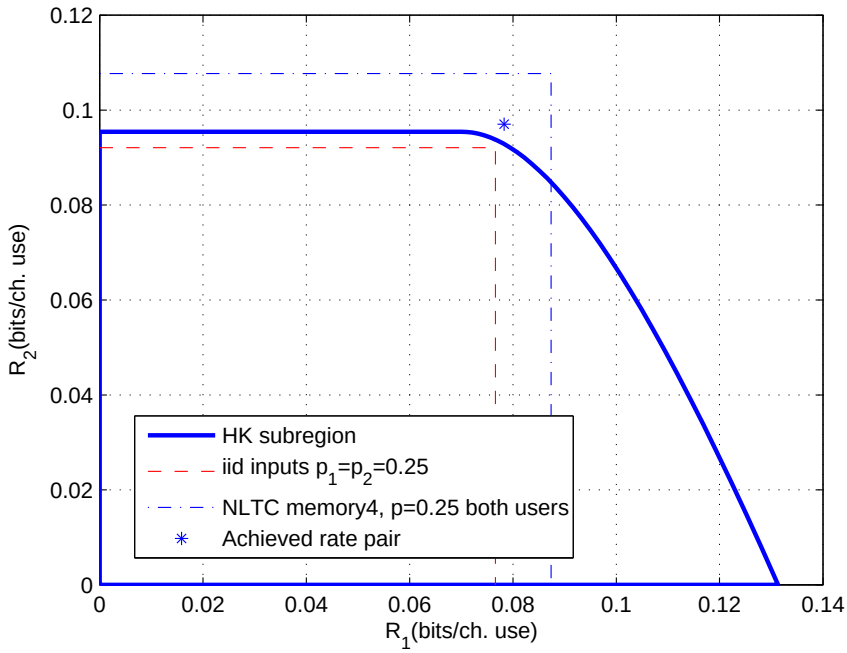

Figure 7.6: Achievable rate subregions and the achieved rate pair using the proposed coding scheme with single user decoding for Example 1.

To study the performance of the specific codes from the designed ensemble, parity check matrices for a block-length of 10k are obtained using the tools in [104] where the length-4 cycles are removed for improved performance. Parity check matrices for P2P optimal LDPC codes with same rate as the overall rate of the concatenated coding scheme are also obtained. The selected codes are simulated over Channel 1 for which the resulting bit error rates are depicted in Fig. 7.7. The BER simulation results show that the sample codes exhibit a waterfall behavior close to the estimated thresholds, and they significantly outperform the P2P alternatives. In particular, for the first user, which is prone to interference, the performance gain is more significant. Furthermore, the superior performance of the improved decoding scheme compared to the simple one (by about an order of magnitude in the same crossover probability) can be observed from the simulation results.

As a second example, we consider the same channel as in the previous example

Table 7.1: Optimized degree distribution of the outer LDPC codes for Example 1.

	λ_2	λ_3	λ_4	λ_5		
User 1	0.251016	0.235664	0.046370	0.466950		
User 2	0.219598	0.286582	0.025020	0.468800		
	ρ_2	ρ_3	ρ_4	ρ_8	ρ_{14}	ρ_{15}
User 1	0.134175	0.271975	0.029495	0.144806	0.220355	0.199195
User 2	0.073385	0.299035	0.001771	0.121574	0.247337	0.256898

Table 7.2: Label assignment to the branches of 4-state trellis ($M = 2$) for the designed NLTC.

State/Input		Output
00/0	01/1	0001
00/1	01/0	0010
10/0	11/1	0100
10/1	11/0	1000

with the only difference that $\epsilon_1 = 0.15$ (referred as Example 2), and utilize both single user decoding and joint decoding at the first user's receiver. The ARRs corresponding to the NIID scheme with both decoding schemes are depicted in Fig. 7.8, which clearly shows that using a public message for the second user and performing joint decoding at the first user's receiver improves the achievable subregion significantly. Again we consider a ones' density of $p = 0.25$, however, in order to reduce the complexity, in the joint decoder we design an NLTC of memory 2. Table 7.2 shows the details of the designed NLTC. We optimize the outer LDPC codes for both decoding schemes, resulting in the rate pairs of (0.1101,0.0933) and (0.1353,0.09333) for SUD and JD, respectively (see Table 7.3 for the resulting degree distributions). The achieved rate pairs are shown in Fig. 7.8, which demonstrates that by using the proposed approach with joint decoding we can achieve rate pairs that cannot be achieved with single user decoding alone.

As a third and final example, we consider a two-user EH Gaussian interference channel with $q = 0.5$, $SNR_1 = 1$, $SNR_2 = 1$, $INR_1 = 0.5$ and $INR_2 = 0.5$

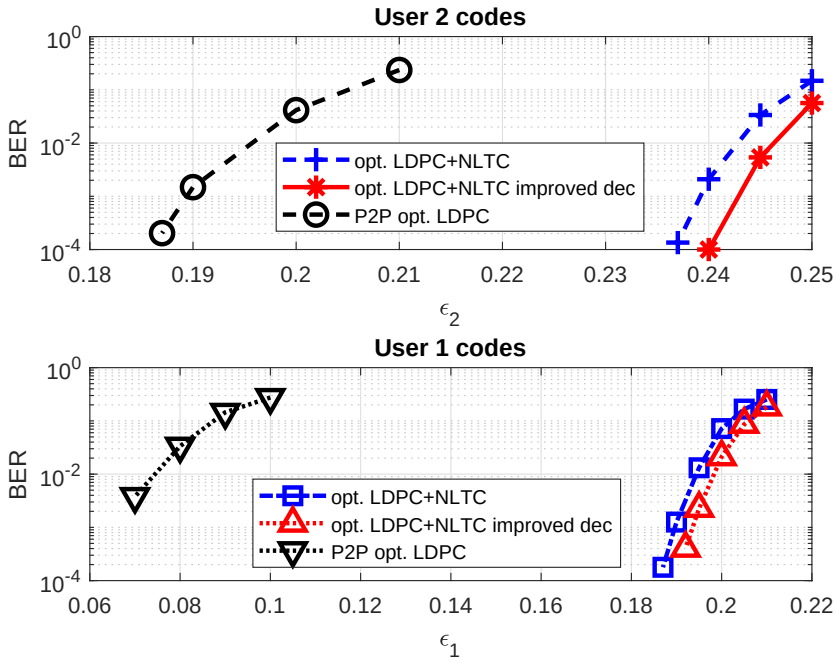

Figure 7.7: Bit error rate performance of the designed codes with simple and improved decoding approaches and that of the P2P optimal LDPC codes.

(Example 3). We obtain the achievable rate subregion for this channel utilizing SUD with i.i.d. inputs as depicted in Fig. 7.9. The subregions with i.i.d inputs with ones' density of $p = 0.25$, and with specific NLTC in Table 4.2 are also shown in this figure. The results demonstrate that utilizing the NLTC instead of i.i.d. inputs results in a larger achievable rate subregion. Designing the outer LDPC for the specific NLTC, we achieve a rate pair of $R_1 = R_2 = 0.1406$. Since the channel is symmetric the same code works for both of the users. Degree distribution of the designed code is given in Table 7.4.

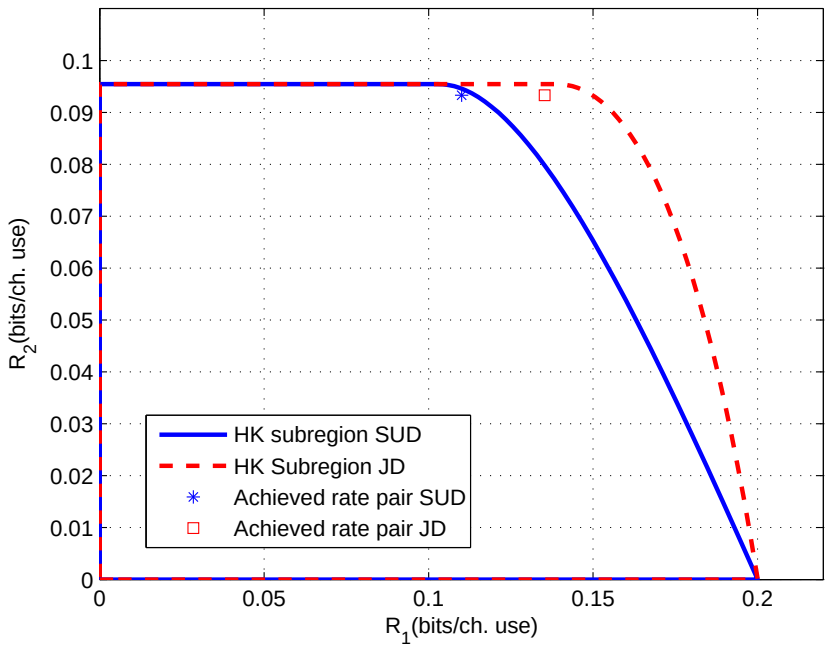

Figure 7.8: Achievable rate subregions and the achieved rate pair using the proposed coding scheme with single user decoding and joint decoding.

Table 7.3: Optimized degree distribution of the outer LDPC codes for Example 2.

	λ_2	λ_3	λ_4	λ_5			
User 1(SUD)	0.206124	0.296626	0.030490	0.466760			
User 1(JD)	0.247980	0.533610	0.139760	0.078650			
User 2	0.237414	0.111726	0.038380	0.612480			
	ρ_2	ρ_3	ρ_4	ρ_5	ρ_8	ρ_{14}	ρ_{15}
User 1(SUD)	0.000848	0.305336	0.064133		0.140212	0.243930	0.245541
User 1(JD)	0.005507	0.138682	0.048959	0.281425	0.155395	0.027638	0.342395
User 2	0.010801	0.296790	0.118995		0.118142	0.276270	0.179002

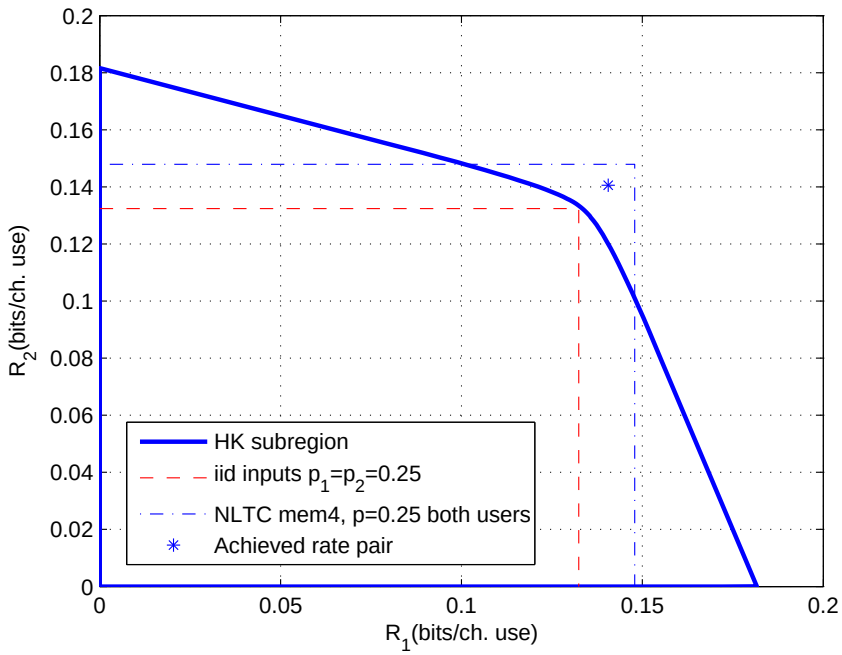

Figure 7.9: Achievable rate subregions and the achieved rate pair using the proposed coding scheme for Example 3.

Table 7.4: Optimized degree distribution of the outer LDPC codes for Example 3.

	λ_2	λ_3	λ_4	λ_5		
User 1 and 2	0.610905	0.007875	0.001550	0.379670		
	ρ_2	ρ_3	ρ_4	ρ_8	ρ_{14}	ρ_{15}
User 1 and 2	0.002293	0.302971	0.079697	0.071308	0.216830	0.326903

7.4 Chapter Summary

In this chapter, we have considered a two-user interference channel with energy harvesting transmitters with finite batteries. For both cases of DMICs and GICs, we have obtained achievable rate regions based on HK coding with i.i.d. on-off signaling for both single user and joint decoding. We proposed a practical coding solution utilizing a serially concatenated coding scheme. Furthermore, we developed a decoding method utilizing the memory in the system to the two-user joint decoding case (extending the approach in Section 4.3.3), and we have shown that employing the designed codes, we can achieve rate pairs close to the information theoretic achievable rate region boundaries via several numerical examples.

Chapter 8

Summary and Conclusions

In this dissertation, we study the design of LDPC codes, trellis-based codes and their concatenation for different energy harvesting communication systems and interference channel scenarios. We first examine the code design for these setups separately, and then consider a joint formulation, which is a two user interference channel with energy harvesting transmitters, and provide a practical coding solution.

We start with the problem of code design for joint energy and information transfer. We propose a coding scheme based on concatenation of a nonlinear trellis code with an outer LDPC code for this set-up. In order to design the NLTCs, we provide an algorithm based on maximizing the minimum distance of the code. Also, we obtain necessary and sufficient conditions for catastrophicity of nonlinear trellis codes; and, in order to avoid such catastrophic codes, we connect each designed NLTC to a corresponding linear convolutional code. This allows for the use of simpler conditions for checking for the catastrophicity of the designed NLTCs. Furthermore, we employ EXIT charts to design the outer LDPC codes while fixing the inner NLTCs by utilizing the LDPC EXIT functions for that part and performing Mote Carlo simulations for the BCJR decoder. We provide several design examples and evaluate their performance, which indicate that the designed codes operate at about 0.8 dB away from the information theoretic limits, and

they outperform both regular LDPC codes and the optimized irregular LDPC codes for AWGN channels when used with NLTCs for joint energy and information transfer. In order to have a practical code design, we employ small degrees in both check and variable nodes, however, we expect that by using larger degrees, the gap to the information theoretic limits can be decreased. Furthermore, our results show that the designed codes significantly outperform the alternative of using classical linear block codes with time switching and the reference scheme of concatenating LDPC codes with nonlinear memoryless mappers.

As another line of investigation, the code design for a binary energy harvesting communication system over noisy channels is studied. Considering naive i.i.d. Shannon strategies, the achievable rates for an arbitrary finite size battery are obtained and a concatenated coding solution consisting of an inner NLTC and an outer LDPC code is proposed. At the receiver side, two decoding approaches are studied. The first one ignores the memory in the battery state, while the second one incorporates this memory into the trellis resulting in an extended trellis description for the system. For both cases, the BCJR decoder iteratively exchanges soft information with the LDPC decoder. To design the outer LDPC code, the first decoding scheme is utilized as it is simpler. Through several numerical examples for different channel models, it is illustrated that the newly designed codes outperform the alternatives of using P2P optimal codes and the reference scheme of utilizing nonlinear memoryless mappers with specifically optimized LDPC codes.

We also examine the code design principles for DMICs. We consider the Han-Kobayashi coding scheme by using both public and private messages, and propose a coding approach based on a serial concatenation of an NLTC with an outer LDPC code as a solution for different classes of DMICs. By approximate analytical derivations, we investigate the performance of the iterative decoder in the asymptotic regime where the probability of decoding error is close to zero, and based on that, we derive a stability condition for the concatenated coding scheme. Furthermore, we use an EXIT analysis to design the outer LDPC code, and utilize the derived stability condition to accelerate the design process. Our extensive numerical examples demonstrate that the designed codes achieve rate

pairs close to the optimal boundary of the HK subregion that cannot be obtained without using nonlinear codes. In addition, the proposed coding scheme for the general instances of DMICs achieves rate pairs that cannot be achieved by using linear codes alone with time sharing, and the reference scheme of concatenating an LDPC code with nonlinear memoryless mappers. Finite block length simulations verify the accuracy of the estimated thresholds for the designed codes.

We also study the problem of short block length code design for the two-user GIC with and without fading. We take the proposed approach in [119] and extend it to the complex channel coefficients case and to the fading scenario. We derive performance bounds based on the union bounding technique, and utilize them for designing trellis-based codes. We show that for GIC without fading, different codes might offer better performance for the same SNR and INR values when the channels are different. In addition, we demonstrate that the optimized trellis based codes for these cases outperform the LDPC codes and P2P optimal trellis based codes. We find that the P2P optimal convolutional codes have the best performance for i.i.d. fading ICs, and they outperform the LDPC codes by increasing the code memory. Finally, for the case of quasi-static fading IC, we find a tight performance bound, which can be evaluated by using Monte Carlo techniques or via a numerical multidimensional integration.

In the last part of the thesis, we investigate the code design principles for a multiuser energy harvesting communication system. We consider a two-user interference channel with energy harvesting transmitters and utilize the schemes that have been developed in the earlier chapters to propose a practical coding solution to this problem. We calculate achievable rate regions using the HK scheme with all private and all public messages. For the cases where utilizing the public messages provides a larger ARR, we use public messages for the interfering users, and perform joint decoding at the receiver of the user experiencing interference. Through numerical examples, we illustrate that using the proposed method, rate pairs close to the optimal boundary of the achievable rate subregion can be obtained.

As possible extensions of the work developed in this thesis, we cite several

research directions. In the case of joint energy and information transfer, in this thesis, we assume binary on-off signaling. This can be extended to other signal constellation with different energy levels among its constellation points, e.g., pulse amplitude modulation (PAM) and QAM. Next possible extension is to generalize the NLTC design algorithm for higher rates ($R = \frac{k}{n}$ and $k \leq 2$) so that we can design codes with rates higher than 0.5. Yet another direction is to use other types of constrained codes such as RLL codes instead of the NLTC in the concatenated coding scheme, and compare the results with the present solutions. It is also interesting to explore short block length code designs and lower complexity decoders for joint energy and information transfer applications, which would be necessary considering the delay constraints and energy requirements in decoding. Investigating this problem in an interference scenario and utilizing the beneficial side of interference for the energy transfer is another aspect that requires attention.

There are interesting extensions of the present work in the area of energy harvesting communications as well. For instance, by considering different assumptions on the availability of energy arrival information (e.g., causal or non-causal information at both transmitter and receiver), the corresponding achievable rates and decoding methods can be investigated. In this dissertation, we did not consider the energy requirements for encoding of the messages in the energy harvesting transmitter, which is an important practical constraint and should be studied further. Furthermore studying energy harvesting communications with other channel models, e.g., inter-symbol interference (ISI) channels and frequency selective fading is also of interest.

Despite its practical importance, explicit and implementable code design for multi-user scenarios, especially for interference channels, is still not very well examined, hence further investigations using different practical codes are required. In addition, short block length code designs with SWIPT and EH for both single user and multi-user communications setups need further investigations.

Bibliography

[1] X. Lu, P. Wang, D. Niyato, D. I. Kim, and Z. Han, "Wireless networks with RF energy harvesting: A contemporary survey," *Commun. Surveys Tuts.*, vol. 17, pp. 757–789, Secondquarter 2015.

[2] L. R. Varshney, "Transporting information and energy simultaneously," in *Proc. IEEE Int. Symp. Information Theory (ISIT)*, pp. 1612–1616, July 2008.

[3] P. Grover and A. Sahai, "Shannon meets Tesla: Wireless information and power transfer," in *Proc. IEEE Int. Symp. Information Theory (ISIT)*, pp. 2363–2367, June 2010.

[4] A. M. Fouladgar, O. Simeone, and E. Erkip, "Constrained codes for joint energy and information transfer," *IEEE Trans. Commun.*, vol. 62, pp. 2121–2131, June 2014.

[5] A. Tandon, M. Motani, and L. Varshney, "On code design for simultaneous energy and information transfer," in *Proc. Information Theory Applications Workshop (ITA)*, pp. 1–6, Feb. 2014.

[6] A. Tandon, M. Motani, and L. R. Varshney, "Subblock-constrained codes for real-time simultaneous energy and information transfer," *IEEE Trans. Inf. Theory*, vol. 62, pp. 4212–4227, July 2016.

[7] O. Ozel and S. Ulukus, "Achieving AWGN capacity under stochastic energy harvesting," *IEEE Trans. Inf. Theory*, vol. 58, pp. 6471–6483, Oct. 2012.

[8] O. Ozel and S. Ulukus, "AWGN channel under time-varying amplitude constraints with causal information at the transmitter," in *Conf. Rec. 45th Asilomar Conf. on Signals, Systems and Computers (ASILOMAR)*, pp. 373–377, Nov. 2011.

[9] W. Mao and B. Hassibi, "On the capacity of a communication system with energy harvesting and a limited battery," in *Proc. IEEE Int. Symp. Information Theory (ISIT)*, pp. 1789–1793, July 2013.

[10] W. Mao and B. Hassibi, "Capacity analysis of discrete energy harvesting channels," *IEEE Trans. Inf. Theory*, vol. 63, pp. 5850–5885, Sept. 2017.

[11] Y. Dong and A. Ozgur, "Approximate capacity of energy harvesting communication with finite battery," in *Proc. IEEE Int. Symp. Information Theory (ISIT)*, pp. 801–805, June 2014.

[12] V. Jog and V. Anantharam, "An energy harvesting AWGN channel with a finite battery," in *Proc. IEEE Int. Symp. Information Theory (ISIT)*, pp. 806–810, June 2014.

[13] D. Shaviv, P. M. Nguyen, and A. Ozgur, "Capacity of the energy-harvesting channel with a finite battery," *IEEE Trans. Inf. Theory*, vol. 62, pp. 6436–6458, Nov. 2016.

[14] K. Tutuncuoglu, O. Ozel, A. Yener, and S. Ulukus, "Binary energy harvesting channel with finite energy storage," in *Proc. IEEE Int. Symp. Information Theory (ISIT)*, pp. 1591–1595, July 2013.

[15] K. Tutuncuoglu, O. Ozel, A. Yener, and S. Ulukus, "Improved capacity bounds for the binary energy harvesting channel," in *Proc. IEEE Int. Symp. Information Theory (ISIT)*, pp. 976–980, June 2014.

[16] A. Bennatan, S. Shamai, and A. R. Calderbank, "Soft-decoding-based strategies for relay and interference channels: Analysis and achievable rates using LDPC codes," *IEEE Trans. Inf. Theory*, vol. 60, pp. 1977–2009, Apr. 2014.

[17] S. Sharifi, A. K. Tanc, and T. M. Duman, "On LDPC codes for Gaussian interference channels," in *Proc. IEEE Int. Symp. Information Theory (ISIT)*, pp. 1992–1996, June 2014.

[18] S. Sharifi, A. K. Tanc, and T. M. Duman, "Implementing the Han-Kobayashi scheme using low density parity check codes over Gaussian interference channels," *IEEE Trans. Commun.*, vol. 63, pp. 337–350, Feb. 2015.

[19] M. Dabirnia and T. M. Duman, "Nonlinear code design for joint energy and information transfer," in *Proc. IEEE Int. Conf. Communications (ICC)*, pp. 4247–4252, June 2015.

[20] M. Dabirnia and T. M. Duman, "On code design for joint energy and information transfer," *IEEE Trans. Commun.*, vol. 64, pp. 2677–2688, June 2016.

[21] M. Dabirnia and T. M. Duman, "Code design for binary energy harvesting channel," in *Proc. IEEE Int. Symp. Information Theory (ISIT)*, pp. 1127–1131, June 2017.

[22] M. Dabirnia, A. K. Tanc, S. Sharifi, and T. M. Duman, "Code design for discrete memoryless interference channels." *submitted to* IEEE Trans. Commun., 2017.

[23] M. Dabirnia, S. Sharifi, A. K. Tanc, and T. M. Duman, "Short block length trellis-based codes for interference channels." *submitted to* IET Communications, 2017.

[24] H. J. Visser and R. J. M. Vullers, "RF energy harvesting and transport for wireless sensor network applications: Principles and requirements," *Proc. IEEE*, vol. 101, pp. 1410–1423, June 2013.

[25] H. Nishimoto, Y. Kawahara, and T. Asami, "Prototype implementation of ambient RF energy harvesting wireless sensor networks," in *Proc. IEEE Sensors*, pp. 1282–1287, Nov. 2010.

[26] S. Bi, C. K. Ho, and R. Zhang, "Wireless powered communication: opportunities and challenges," *IEEE Commun. Mag.*, vol. 53, pp. 117–125, Apr. 2015.

[27] L. Liu, R. Zhang, and K. C. Chua, "Wireless information transfer with opportunistic energy harvesting," *IEEE Trans. Wireless Commun.*, vol. 12, pp. 288–300, Jan. 2013.

[28] A. Ozcelikkale, T. McKelvey, and M. Viberg, "Wireless information and power transfer in MIMO channels under rician fading," in *Proc. IEEE Int. Conf. on Acoustics, Speech and Signal Processing (ICASSP)*, pp. 3187–3191, Apr. 2015.

[29] R. Zhang and C. K. Ho, "MIMO broadcasting for simultaneous wireless information and power transfer," *IEEE Trans. Wireless Commun.*, vol. 12, pp. 1989–2001, May 2013.

[30] J. Xu, L. Liu, and R. Zhang, "Multiuser MISO beamforming for simultaneous wireless information and power transfer," *IEEE Trans. on Signal Process.*, vol. 62, pp. 4798–4810, Sept. 2014.

[31] D. Li, C. Shen, and Z. Qiu, "Two-way relay beamforming for sum-rate maximization and energy harvesting," in *Proc. IEEE Int. Conf. Communications (ICC)*, pp. 3115–3120, June 2013.

[32] D. Li, C. Shen, and Z. Qiu, "Sum rate maximization and energy harvesting for two-way af relay systems with imperfect CSI," in *Proc. IEEE Int. Conf. on Acoustics, Speech and Signal Processing*, pp. 4958–4962, May 2013.

[33] A. ozcelikkale and T. M. Duman, "Linear precoder design for simultaneous information and energy transfer over two-user MIMO interference channels," *IEEE Trans. Wireless Commun.*, vol. 14, pp. 5836–5847, Oct. 2015.

[34] J. Park and B. Clerckx, "Joint wireless information and energy transfer in a two-user MIMO interference channel," *IEEE Trans. Wireless Commun.*, vol. 12, pp. 4210–4221, Aug. 2013.

[35] C. Shen, W. C. Li, and T. H. Chang, "Wireless information and energy transfer in multi-antenna interference channel," *IEEE Trans. on Signal Process.*, vol. 62, pp. 6249–6264, Dec 2014.

[36] S. Lee, L. Liu, and R. Zhang, "Collaborative wireless energy and information transfer in interference channel," *IEEE Trans. Wireless Commun.*, vol. 14, pp. 545–557, Jan. 2015.

[37] L. Liu, R. Zhang, and K. C. Chua, "Secrecy wireless information and power transfer with MISO beamforming," *IEEE Trans. on Signal Process.*, vol. 62, pp. 1850–1863, Apr. 2014.

[38] D. W. K. Ng, E. S. Lo, and R. Schober, "Robust beamforming for secure communication in systems with wireless information and power transfer," *IEEE Trans. Wireless Commun.*, vol. 13, pp. 4599–4615, Aug. 2014.

[39] M. R. A. Khandaker and K. K. Wong, "Robust secrecy beamforming with energy-harvesting eavesdroppers," *IEEE Wireless Commun. Lett.*, vol. 4, pp. 10–13, Feb. 2015.

[40] X. Chen, D. W. K. Ng, and H. H. Chen, "Secrecy wireless information and power transfer: challenges and opportunities," *IEEE Wireless Commun.*, vol. 23, pp. 54–61, Apr. 2016.

[41] A. Ozcelikkale, T. McKelvey, and M. Viberg, "Simultaneous information and power transfer with transmitters with hardware impairments," in *Proc. Int. Symp. on Wireless Communication Systems (ISWCS)*, pp. 114–118, Sept. 2016.

[42] X. Xu, A. Ozcelikkale, T. McKelvey, and M. Viberg, "Simultaneous information and power transfer under a non-linear RF energy harvesting model," in *Proc. IEEE Int. Conf. Communications Workshops (ICC Workshops)*, pp. 179–184, May 2017.

[43] B. Gurakan, O. Ozel, J. Yang, and S. Ulukus, "Energy cooperation in energy harvesting wireless communications," in *Proc. IEEE Int. Symp. on Information Theory (ISIT)*, pp. 965–969, July 2012.

[44] B. Gurakan, O. Ozel, J. Yang, and S. Ulukus, "Energy cooperation in energy harvesting communications," *IEEE Trans. Commun.*, vol. 61, pp. 4884–4898, Dec. 2013.

[45] B. Gurakan, O. Ozel, J. Yang, and S. Ulukus, "Two-way and multiple-access energy harvesting systems with energy cooperation," in *Conf. Rec. of the 46th Asilomar Conf. on Signals, Systems and Computers (ASILOMAR)*, pp. 58–62, Nov. 2012.

[46] B. Gurakan, O. Ozel, J. Yang, and S. Ulukus, "Energy cooperation in energy harvesting two-way communications," in *Proc. IEEE Int. Conf. Communications (ICC)*, pp. 3126–3130, June 2013.

[47] K. Tutuncuoglu and A. Yener, "Multiple access and two-way channels with energy harvesting and bi-directional energy cooperation," in *Proc. Information Theory and Applications Workshop (ITA)*, pp. 1–8, Feb. 2013.

[48] K. Tutuncuoglu and A. Yener, "Cooperative energy harvesting communications with relaying and energy sharing," in *Proc. IEEE Information Theory Workshop (ITW)*, pp. 1–5, Sept. 2013.

[49] A. M. Fouladgar and O. Simeone, "Information and energy flows in graphical networks with energy transfer and reuse," *IEEE Wireless Commun. Lett.*, vol. 2, pp. 371–374, Aug. 2013.

[50] P. Popovski, A. M. Fouladgar, and O. Simeone, "Interactive joint transfer of energy and information," *IEEE Trans. Commun.*, vol. 61, pp. 2086–2097, May 2013.

[51] X. Zhou, R. Zhang, and C. K. Ho, "Wireless information and power transfer: Architecture design and rate-energy tradeoff," *IEEE Trans. Commun.*, vol. 61, pp. 4754–4767, Nov. 2013.

[52] J. Yang and S. Ulukus, "Optimal packet scheduling in an energy harvesting communication system," *IEEE Trans. Commun.*, vol. 60, pp. 220–230, Jan. 2012.

[53] K. Tutuncuoglu and A. Yener, "Optimum transmission policies for battery limited energy harvesting nodes," *IEEE Trans. Wireless Commun.*, vol. 11, pp. 1180–1189, Mar. 2012.

[54] O. Ozel, K. Tutuncuoglu, J. Yang, S. Ulukus, and A. Yener, "Transmission with energy harvesting nodes in fading wireless channels: Optimal policies," *IEEE J. Sel. Areas Commun.*, vol. 29, pp. 1732–1743, Sept. 2011.

[55] C. K. Ho and R. Zhang, "Optimal energy allocation for wireless communications with energy harvesting constraints," *IEEE Trans. on Signal Process.*, vol. 60, pp. 4808–4818, Sept. 2012.

[56] C. Huang, R. Zhang, and S. Cui, "Optimal power allocation for outage probability minimization in fading channels with energy harvesting constraints," *IEEE Trans. Wireless Commun.*, vol. 13, pp. 1074–1087, Feb. 2014.

[57] J. Yang and S. Ulukus, "Optimal packet scheduling in a multiple access channel with energy harvesting transmitters," *Journal of Communications and Networks*, vol. 14, pp. 140–150, Apr. 2012.

[58] J. Yang, O. Ozel, and S. Ulukus, "Broadcasting with an energy harvesting rechargeable transmitter," *IEEE Trans. Wireless Commun.*, vol. 11, pp. 571–583, Feb. 2012.

[59] M. A. Antepli, E. Uysal-Biyikoglu, and H. Erkal, "Optimal packet scheduling on an energy harvesting broadcast link," *IEEE J. Sel. Areas Commun.*, vol. 29, pp. 1721–1731, Sept. 2011.

[60] O. Ozel, J. Yang, and S. Ulukus, "Optimal broadcast scheduling for an energy harvesting rechargeable transmitter with a finite capacity battery," *IEEE Trans. Wireless Commun.*, vol. 11, pp. 2193–2203, June 2012.

[61] O. Ozel, J. Yang, and S. Ulukus, "Optimal transmission schemes for parallel and fading Gaussian broadcast channels with an energy harvesting rechargeable transmitter," *Computer Communications*, vol. 36, no. 12, pp. 1360 – 1372, 2013.

[62] O. Ozel, K. Shahzad, and S. Ulukus, "Optimal scheduling for energy harvesting transmitters with hybrid energy storage," in *Proc. IEEE Int. Symp. on Information Theory (ISIT)*, pp. 1784–1788, July 2013.

[63] C. Huang, R. Zhang, and S. Cui, "Throughput maximization for the Gaussian relay channel with energy harvesting constraints," *IEEE J. Sel. Areas Commun.*, vol. 31, pp. 1469–1479, Aug. 2013.

[64] K. Huang, "Throughput of wireless networks powered by energy harvesting," in *Conf. Rec. of the 45th Asilomar Conf. on Signals, Systems and Computers (ASILOMAR)*, pp. 8–12, Nov. 2011.

[65] O. Orhan and E. Erkip, "Optimal transmission policies for energy harvesting two-hop networks," in *46th Annu. Conf. on Information Sciences and Systems (CISS)*, pp. 1–6, Mar. 2012.

[66] O. Orhan and E. Erkip, "Throughput maximization for energy harvesting two-hop networks," in *Proc. IEEE Int. Symp. on Information Theory (ISIT)*, pp. 1596–1600, July 2013.

[67] B. Varan and A. Yener, "The energy harvesting two-way decode-and-forward relay channel with stochastic data arrivals," in *Proc. IEEE Global Conf. on Signal and Information Processing (GlobalSIP)*, pp. 371–374, Dec. 2013.

[68] O. Orhan, D. Gündüz, and E. Erkip, "Energy harvesting broadband communication systems with processing energy cost," *IEEE Trans. Wireless Commun.*, vol. 13, pp. 6095–6107, Nov. 2014.

[69] A. E. Gamal and Y.-H. Kim, *Network Information Theory.* first ed.

[70] T. Han and K. Kobayashi, "A new achievable rate region for the interference channel," *IEEE Trans. Inf. Theory*, vol. 27, pp. 49–60, Jan. 1981.

[71] H. Sato, "On the capacity region of a discrete two-user channel for strong interference (corresp.)," *IEEE Trans. Inf. Theory*, vol. 24, pp. 377–379, May 1978.

[72] M. Costa and A. E. Gamal, "The capacity region of the discrete memoryless interference channel with strong interference (corresp.)," *IEEE Trans. Inf. Theory*, vol. 33, pp. 710–711, Sept. 1987.

[73] R. Benzel, "The capacity region of a class of discrete additive degraded interference channels (corresp.)," *IEEE Trans. Inf. Theory*, vol. 25, pp. 228–231, Mar. 1979.

[74] N. Liu and S. Ulukus, "The capacity region of a class of discrete degraded interference channels," *IEEE Trans. Inf. Theory*, vol. 54, pp. 4372–4378, Sept. 2008.

[75] A. E. Gamal and M. Costa, "The capacity region of a class of deterministic interference channels (corresp.)," *IEEE Trans. Inf. Theory*, vol. 28, pp. 343–346, Mar. 1982.

[76] H. F. Chong and M. Motani, "The capacity region of a class of semideterministic interference channels," *IEEE Trans. Inf. Theory*, vol. 55, pp. 598–603, Feb. 2009.

[77] F. Zhu and B. Chen, "Capacity bounds and sum rate capacities of a class of discrete memoryless interference channels," *IEEE Trans. Inf. Theory*, vol. 60, pp. 3763–3772, July 2014.

[78] H. Sato, "On degraded Gaussian two-user channels (corresp.)," *IEEE Trans. Inf. Theory*, vol. 24, pp. 637–640, Sept. 1978.

[79] G. Kramer, "Outer bounds on the capacity of Gaussian interference channels," *IEEE Trans. Inf. Theory*, vol. 50, pp. 581–586, Mar. 2004.

[80] R. H. Etkin, D. N. C. Tse, and H. Wang, "Gaussian interference channel capacity to within one bit," *IEEE Trans. Inf. Theory*, vol. 54, pp. 5534–5562, Dec. 2008.

[81] A. S. Motahari and A. K. Khandani, "Capacity bounds for the Gaussian interference channel," in *Proc. IEEE Int. Symp. on Information Theory (ISIT)*, pp. 250–254, July 2008.

[82] M. A. Maddah-Ali, A. S. Motahari, and A. K. Khandani, "Communication over MIMO X channels: Interference alignment, decomposition, and performance analysis," *IEEE Trans. Inf. Theory*, vol. 54, pp. 3457–3470, Aug. 2008.

[83] V. R. Cadambe and S. A. Jafar, "Interference alignment and degrees of freedom of the k-user interference channel," *IEEE Trans. Inf. Theory*, vol. 54, pp. 3425–3441, Aug. 2008.

[84] A. Roumy and D. Declercq, "Characterization and optimization of ldpc codes for the 2-user gaussian multiple access channel," *EURASIP J. Wireless Commun. Networking*, vol. 2007, p. 074890, June 2007.

[85] A. Amraoui, S. Dusad, and R. Urbanke, "Achieving general points in the 2-user gaussian mac without time-sharing or rate-splitting by means of iterative coding," in *Proc. IEEE Int. Symp. Inf. Theory,*, pp. 334–, July 2002.

[86] A. Sanderovich, M. Peleg, and S. Shamai, "Ldpc coded MIMO multiple access with iterative joint decoding," *IEEE Trans. Inf. Theory*, vol. 51, pp. 1437–1450, Apr. 2005.

[87] T. W. Sun, R. D. Wesel, M. R. Shane, and K. Jarett, "Superposition turbo TCM for multirate broadcast," *IEEE Trans. Commun.*, vol. 52, pp. 368–371, Mar. 2004.

[88] P. Berlin and D. Tuninetti, "LDPC codes for fading Gaussian broadcast channels," *IEEE Trans. Inf. Theory*, vol. 51, pp. 2173–2182, June 2005.

[89] A. Amraoui and G. K. S. Shamai, "Coding for the mimo broadcast channel," in *Proc. IEEE Int. Symp. Information Theory (ISIT)*, pp. 296–296, June 2003.

[90] M. Uppal, V. Stankovic, and Z. Z. Xiong, "Code design for MIMO broadcast channels," *IEEE Trans. Commun.*, vol. 57, pp. 986–996, Apr. 2009.

[91] Z. Zhang and T. M. Duman, "Capacity-approaching turbo coding and iterative decoding for relay channels," *IEEE Trans. on Commun.*, vol. 53, pp. 1895–1905, Nov. 2005.

[92] Z. Zhang and T. M. Duman, "Capacity-approaching turbo coding for half-duplex relaying," *IEEE Trans. Commun.*, vol. 55, pp. 1895–1906, Oct. 2007.

[93] J. Hu and T. M. Duman, "Low density parity check codes over wireless relay channels," *IEEE Trans. Wireless Commun.*, vol. 6, pp. 3384–3394, Sept. 2007.

[94] A. K. Tanc, T. M. Duman, and C. Tepedelenlioglu, "Design of LDPC codes for two-way relay systems with physical-layer network coding," *IEEE Commun. Lett.*, vol. 17, pp. 2356–2359, Dec. 2013.

[95] A. Vem, Y. C. Huang, K. R. Narayanan, and H. D. Pfister, "Multilevel lattices based on spatially-coupled LDPC codes with applications," in *Proc. IEEE Int. Symp. on Information Theory (ISIT)*, pp. 2336–2340, June 2014.

[96] L. Lin, X. Ma, C. Liang, X. Huang, and B. Bai, "An information-spectrum approach to the capacity region of the interference channel," *Entropy*, vol. 19, no. 6, 2017.

[97] S. B. Wicker, *Error Control Systems for Digital Communication and Storage.* second ed.

[98] T. M. Cover and J. A. Thomas, *Elements of Information Theory.* second ed.

[99] M. Franceschini, G. Ferrari, R. Raheli, and A. Curtoni, "Serial concatenation of LDPC codes and differential modulations," *IEEE J. Sel. Areas Commun.*, vol. 23, pp. 1758–1768, Sept. 2005.

[100] M. Griot, A. Vila Casado, W.-Y. Weng, H. Chan, J. Wang, and R. Wesel, "Nonlinear trellis codes for binary-input binary-output multiple-access channels with single-user decoding," *IEEE Trans. Commun.*, vol. 60, pp. 364–374, Feb. 2012.

[101] J. P. Odenwalder, *Optimal Decoding of Convolutional Codes.* PhD thesis, Dept. of Syst. Sci., Univ. California. Los Angeles, L.A., CA, 1970.

[102] R. Storn and K. Price, "Differential evolution – a simple and efficient heuristic for global optimization over continuous spaces," *Journal of Global Optimization*, vol. 11, pp. 341–359, Dec 1997.

[103] T. Richardson, M. Shokrollahi, and R. Urbanke, "Design of capacity-approaching irregular low-density parity-check codes," *IEEE Trans. Inf. Theory*, vol. 47, pp. 619–637, Feb. 2001.

[104] [Online]. Available http://itpp.sourceforge.net/4.3.1/.

[105] G. Bocherer and R. Mathar, "Operating LDPC codes with zero shaping gap," in *Proc. IEEE Information Theory Workshop*, pp. 330–334, Oct. 2011.

[106] S. ten Brink, "Convergence behavior of iteratively decoded parallel concatenated codes," *IEEE Trans. Commun.*, vol. 49, pp. 1727–1737, Oct. 2001.

[107] J. Hagenauer, "The EXIT chart - introduction to extrinsic information transfer in iterative processing," in *12th European Signal Processing Conf.*, pp. 1541–1548, Sept. 2004.

[108] J. Hou, P. H. Siegel, L. B. Milstein, and H. D. Pfister, "Capacity-approaching bandwidth-efficient coded modulation schemes based on low-density parity-check codes," *IEEE Trans. Inf. Theory*, vol. 49, pp. 2141–2155, Sept. 2003.

[109] B. Xie, M. Griot, A. I. V. Casado, and R. D. Wesel, "Optimal transmission strategy and explicit capacity region for broadcast Z channels," *IEEE Trans. Inf. Theory*, vol. 54, pp. 4296–4304, Sept. 2008.

[110] U. Bhat, D. Fertonani, and T. M. Duman, "New capacity-achieving encoding schemes for degraded binary broadcast channels," in *Proc. IEEE Global Telecommunications Conf. (GLOBECOM)*, pp. 1–5, Dec. 2010.

[111] B. Xie, T. A. Courtade, and R. D. Wesel, "Optimal encoding for discrete degraded broadcast channels," *IEEE Trans. Inf. Theory*, vol. 59, pp. 1360–1378, Mar. 2013.

[112] L. Wang and E. Sasoglu, "Polar coding for interference networks," in *Proc. IEEE Int. Symp. on Information Theory (ISIT)*, pp. 311–315, June 2014.

[113] M. Zheng, C. Ling, W. Chen, and M. Tao, "A New Polar Coding Scheme for the Interference Channel," *ArXiv e-prints*, 2016. [Online]. Available: http://arxiv.org/abs/1608.08742.

[114] M. Mondelli, R. Urbanke, and S. H. Hassani, "How to achieve the capacity of asymmetric channels," in *52nd Annual Allerton Conference on Communication, Control, and Computing (Allerton)*, pp. 789–796, Sept. 2014.

[115] L. Schmitt and H. Meyr, "On the asymptotics of density evolution for iterative (turbo) decoding," in *43th Annu. Allerton Conf. on Communication, Control, and Computing (Allerton)*, pp. 2187–2196, Sept. 2005.

[116] T. Richardson and R. Urbanke, *Modern coding Theory.* first ed.

[117] S. Sharifi, A. K. Tanc, and T. M. Duman, "LDPC code design for binary-input binary-output z interference channels," in *Proc. IEEE Int. Symp. Information Theory (ISIT)*, pp. 1084–1088, June 2015.

[118] A. Ozcelikkale and T. M. Duman, "Short length trellis-based codes for Gaussian multiple-access channels," *IEEE Signal Process. Lett.*, vol. 21, pp. 1177–1181, Oct. 2014.

[119] S. Sharifi, *On Code Design for Interference Channels.* PhD thesis, Arizona State University, Arizona, 8 2015.

[120] S. Sharifi, M. Dabirnia, A. K. Tanc, and T. M. Duman, "Short block length code design for interference channels," in *Proc. IEEE Int. Symp. on Information Theory (ISIT)*, pp. 1909–1913, July 2016.

[121] A. Stefanov and T. M. Duman, "Performance bounds for space-time trellis codes," *IEEE Trans. Inf. Theory*, vol. 49, pp. 2134–2140, Sept. 2003.

[122] S. Verdu, "Maximum likelihood sequence detection for intersymbol interference channels: A new upper bound on error probability," *IEEE Trans. Inf. Theory*, vol. 33, pp. 62–68, Jan. 1987.

[123] T. M. Duman and M. Salehi, "New performance bounds for turbo codes," *IEEE Trans. Commun.*, vol. 46, pp. 717–723, June 1998.

[124] I. Sason and S. Shamai, "Performance analysis of linear codes under maximum-likelihood decoding: A tutorial," *Foundations and Trends in Communications and Information Theory*, vol. 3, no. 1–2, pp. 1–222, 2006.

[125] G. Poltyrev, "Bounds on the decoding error probability of binary linear codes via their spectra," *IEEE Trans. Inf. Theory*, vol. 40, pp. 1284–1292, July 1994.

[126] K. D. P. Dharmawansa and R. M. A. P. Rajatheva, "On the pairwise error probability bounds of STTC over Nakagami-m fading channels," in *Proc. IEEE Int. Conf. Communications (ICC)*, vol. 5, pp. 2927–2931 Vol. 5, May 2005.

[127] E. Malkamaki and H. Leib, "Evaluating the performance of convolutional codes over block fading channels," *IEEE Trans. Inf. Theory*, vol. 45, pp. 1643–1646, Jul 1999.

[128] D. MacKay. Encyclopedia of sparse graph codes. [Online]. Available: http://www.inference.phy.cam.ac.uk/mackay/codes/data.html.

[129] D. M. Arnold, H. A. Loeliger, P. O. Vontobel, A. Kavcic, and W. Zeng, "Simulation-based computation of information rates for channels with memory," *IEEE Trans. Inf. Theory*, vol. 52, pp. 3498–3508, Aug. 2006.